NUCLEAR STRUCTURE STUDIES IN THE Ge–As REGION

Értekezés a doktori (PhD) fokozat megszerzése érdekében

a ..... tudományában

Irta: ..... okleveles .....

Készült a Kossuth Lajos Tudományegyetem ..... programja

(..... alprogramja) keretében

Témavezető: Dr. .....

és Dr. .....

Elfogadásra javaslom: 199.... ....

Jelölt a doktori szigorlatot 199.... ....-n eredményesen letette:

a bizottság elnöke: Dr. ..... .

Az értekezést bírálóként elfogadásra javaslom:

Dr. ..... .

Dr. ..... .

Jelölt az értekezést 199.... ....-n sikeresen megvédte:

A védési bizottság elnöke: Dr. ..... .

D e b r e c e n - 1997

Dorottya Sohler

NUCLEAR STRUCTURE STUDIES IN THE Ge–As REGION

Doctoral (PhD) dissertation

Supervisors:

Tibor Fényes
and
Zsolt Dombrádi

MTA ATOMKI

Debrecen

1997

Contents

Chapter 1

Introduction

Nuclei in the A≈60-80 mass region display a rich variety of complex phenomena, which are a challenging testing ground for our understanding of transitional nuclei. The investigated As and Ge nuclei lie between closed shells, they contain 4-5 valence protons and 5-10 valence neutrons. The large number of the valence nucleons can give rise to deformation of these nuclei [1], which can be described in the framework of the liquid drop model. Addition of a proton or neutron to the even-even core can result in further deformation via polarization. The relatively large values of the quadrupole moments ($Q_{2_1^+}$≈0.8-0.9 eb) of even-even Ge nuclei suggest the presence of deformation in this mass region. Recently, several experiments have been carried out to reveal the structure of these nuclei. In the case of even-even Ge isotopes band structures were found [2]. Further experimental investigations in this mass region evidenced the coexistence of oblate and prolate deformed states with rapid transitions between them [3, 4]. The existencee of similar structural features can also be expected in light Ge and As nuclei according to the predictions of EXCITED VAMPIR calculations [5, 6].

On the other hand, from the shell model point of view the nuclei in the A≈60-80 mass region are not expected to have pronounced deformation, as most of the valence orbits ($2p_{1/2}, 2p_{3/2}, 1f_{5/2}$) have short radii and therefore deformation driving quadrupole force is weak. Thus, the nucleons on these orbits can only weakly polarize the core and no strong directional correlation between protons and neutrons will develope in these nuclei. This idea is supported by the fact that in even-even Ge isotopes the energy of the 2_1^+ state is ≈1 MeV, which is high, compared to similar values of deformed nuclei. In addition, the band structures of the even-even Ge nuclei show quasivibrational characteristics, with high phonon energies.

These interesting double features of the nuclei with A≈60-80 mass number reflect

the competition between the collective and single-particle degrees of freedom in these nuclei. The interacting boson [7, 8], interacting boson-fermion [9, 10] and interacting boson-fermion-fermion models [11] are capable of treating a large variety of even-even, odd and odd-odd nuclei. Their special strength is in description of nuclei lying in transitional regions. They are expected to give good results also for the Ge–As region. That is why we have chosen them for the description of the structure of nuclei investigated in this project.

It is worth mentioning that in the Ga-Se region occurence of the SU(5) limit of the U(6/12) supersymmetry is predicted, but the discussion of this question is out of range of the present study.

In order to study the above phenomena, including the supersymmetry, a program was started at the nuclear spectroscopy group of the Institute of Nuclear Research (ATOMKI) in Debrecen. The aim of the program was the investigation of the structure of As and Ga nuclei. The experimental work was motivated by the fact, that the level schemes of the investigated nuclei were known very scantily. In addition, the new, consistent data obtained in this project can also be employed in the other fields of nuclear physics, e.g. nuclear astrophysics, studies of nuclear reactions. The beams of the Debrecen isochronous cyclotron enabled excitation both of particle and collective states and the selective production of the desired nucleus, as well as the low background radiations made easier the identification of the γ rays. The high resolution, high efficiency Ge(HP) detectors and unique superconducting magnetic electron spectrometer, constructed in the ATOMKI, assured good possibility for complex γ- and electron-spectroscopic in-beam studies.

The nuclei, investigated in the framework of this program, are shown in Fig. 1.1. The Ga nuclei were studied by J. Timár et al. [12, 13, 14, 15], the ^{70,74,76}As nuclei by Zs. Podolyák et al. [16], A. Algora et al. [17] and Z. Gácsi et al. [18], respectively. As a part of this project I have investigated the structure of ^{68,72,73}As and ^{65}Ge. The ^{72,73}As nuclei were studied in Debrecen via $(p, n\gamma)$ reaction, while the ^{68}As and ^{65}Ge lying further from the line of stability were investigated via the ^{12}C(^{58}Ni,$xpyn$) reaction at Risø, Denmark with the NORDBALL setup on the basis of the collaboration with the Royal Institute of Technology, Stockholm. A part of

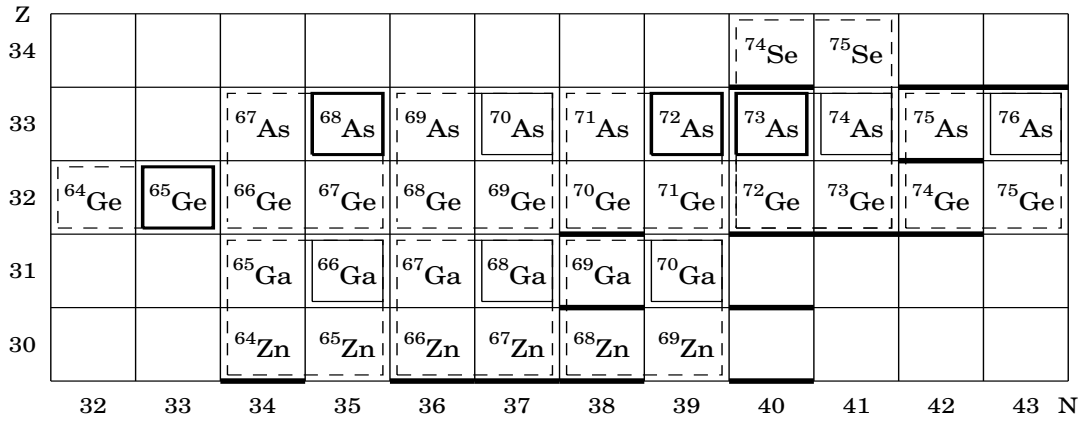

Figure 1.1: *Nuclei, investigated in the program at the nuclear spectroscopy group of the ATOMKI, are indicated in thin, solid frames. Nuclei, studied by me in this project, are marked with thick frames. Sign of isotope in dotted frame: theoretical calculations, Z: atomic, N: neutron numbers, underlining with a thick line: stable nucleus.*

the data analysis was performed at Stockholm. The analysis of $\gamma\gamma$-coincidence data for ^{73}As was carried out by Zs. Podolyák.

In the present dissertation I give account on the experimental techniques and methods employed in chapter II. Chapters III and IV contain the results obtained in Debrecen for ^{72}As and ^{73}As, respectively. Chapters V and VI are devoted to the description of the results obtained on ^{68}As and ^{65}Ge in the NORDBALL experiment. The summary of the results is presented in chapter VII.

Chapter 2

Experimental techniques and methods

2.1 The Debrecen setup

In the present section I give a detailed overview of the circumstances of the measurements, the experimental setups and the evaluation techniques of the γ-ray spectra from the ^{72,73}As experiments.

I studied both ^{72}As and ^{73}As nuclei via (p,nγ) reaction using in-beam γ- and electron-spectroscopic methods with a special emphasis on the determination of spins and parities of the levels. One of the most important features of the (p,n) reaction is that the angular momentum transferred to the bombarded nucleus is small. Since the spin and parity value of the ground state of the even-even ^{72}Ge is 0^+ [19], only the low-spin states up to I=6 spin value were excited in ^{72}As nucleus. The spin-parity of the ground state of ^{73}Ge is $9/2^+$ [20], therefore the states of ^{73}As were populated in the spin-window 1/2-15/2. The (p,n) reaction is not selective, both collective and single-particle states are excited.

2.1.1 Accelerators, detectors and targets

The ^{72}As and ^{73}As experiments were performed at the Nuclear Research Institute of the Hungarian Academy of Sciences (ATOMKI) in Debrecen based on the accelerator facilities of the institute. The targets were bombarded with proton beams of the 103 cm MGC-20E type compact isochronous cyclotron at bombarding energies higher than 3 MeV. For the bombarding energies lower than 3 MeV the Van de Graaff electrostatic accelerator was used.

By these accelerators light charged particles, e.g. protons, deuterons, ^{3}He^{++} ions and α particles, can be accelerated. The cyclotron allows of accelerating protons in the energy range 3-20 MeV and it provides a beam current of 50 μA at the maximum

energy. At the Van de Graaff generator the energy of a proton beam can be varied between 0.5 MeV and 4.8 MeV with a maximum current 5–10μA. Both the cyclotron and the Van de Graaff generator have the advantageous property that the energy spread of the external beam is relatively small. Namely, it is less than 0.3 % and 0.05% for the cyclotron and the Van de Graaff generator, respectively. This makes possible the precise tuning of the beam energy what is needed for a detailed study of the level schemes. Varying the energy of the beam we could control the excitation energies of the studied nucleus.

The single and coincidence γ spectra were collected using coaxial Ge(HP) detectors with efficiency 20% and 25% relative to that of a 7.5 cm x 7.5 cm cylindrical NaI(Tl) detector. The energy resolution of the spectrometer was better than 2.2 keV at 1332 keV. In order to reduce the intensity of the contaminating radiation coming from the activated parts of the devices the detectors were surrounded by Pb and Cu absorbers.

In the γ- and e^--spectroscopic measurements for ^{72}As I used targets of thickness $\sim$0.5 and $\sim$0.2 mg/cm^2 and isotopically enriched to 98%. For the case of ^{73}As the target material was enriched to 86% and the corresponding thickness values were $\sim$0.3 and $\sim$0.8 mg/cm^2. The targets were prepared by evaporating GeO_2 (^{72}As) and metallic Ge (^{73}As) onto carbon backing foils of 40 μg/cm^2 thickness. For reliable assignment of γ rays not only the γ spectra of the ^{72}Ge+p and ^{73}Ge+p, but the ^{74}Ge+p and ^{76}Ge+p reactions were also measured and analysed.

2.1.2 Determination of the energy and intensity of the γ rays

In (p,n) reaction the final nuclei were populated up to about 1 MeV excitation energy. The states produced deexcite via radiating γ photons, since their excitation energies are not enough to emit charged particles or neutrons. The energy and the intensity of these γ rays can be determined by measuring single γ-ray spectra. The γ-ray spectra of odd and odd-odd nuclei are very complicated even at low excitation energies due to their high level densities. In order to separate the transitions having similar energies, and to detect the weak γ rays a spectrometer with good resolution and high efficiency was needed.

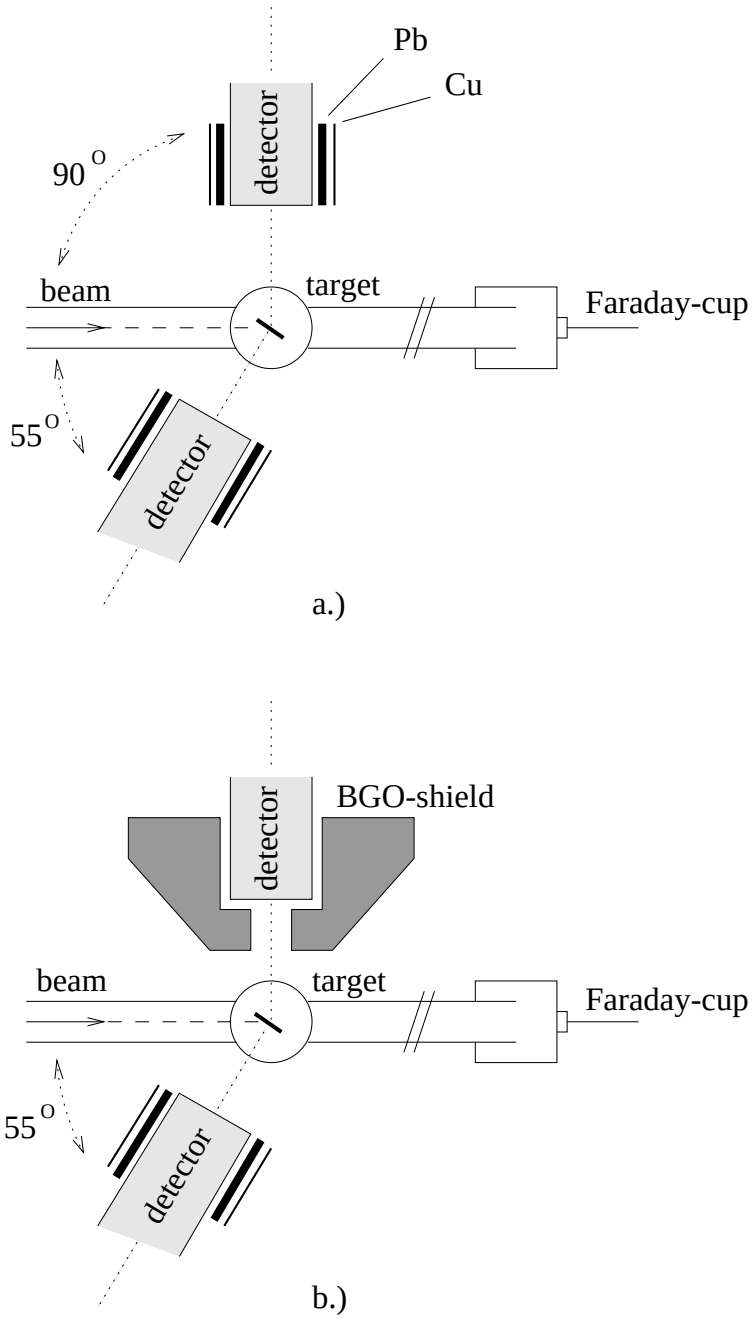

Figure 2.1: *Geometrical arrangement of detectors at single γ spectrum measurements.*

For the determination γ-ray energies the detectors were placed at 90^o to the beam direction in order to eliminate the shift of the peaks due to the Doppler-effect. The distance of 15 cm between the detectors and the target was enough to avoid generation of sumpeaks. The arrangement of the single γ-spectra measurements can be seen in Fig. 2.1 a.).

In single γ measurements standard ORTEC and Canberra electronic units were used: the signals from the detectors were amplified by a preamplifier and a linear amplifier of type ORTEC 572 and they were evaluated in a multichannel analyser based on a 4k PCA Nucleus Card.

The determination of the energies of the γ rays was done in several steps: at first, the "in-beam" spectrum was measured together with standard γ sources. Using the γ rays of the sources as calibration lines the exact energies of the strongest γ lines of the studied nucleus were obtained. At this step the nonlinearity of the electronic units was also taken into account. In the other "in-beam" spectra these strongest γ rays with known exact energy values were applied as calibration lines. For the calibration of the γ lines below and above 200 keV ^{133}Ba and ^{152}Eu sources were used, respectively. In the low-energy region the X rays of these sources also served as calibration lines.

In order to reduce the background rising from the escape of Compton scattered γ rays the γ spectrum of ^{72}As was also measured using Ge(HP) detector equipped with anti-Compton shield consisted of bismuth germanate (BGO=$Bi_4Ge_3O_{12}$) scintillators. The Ge(HP) detector was placed at 90° as in the previous measurement shown in Fig. 2.1 b.). In the Compton-suppressed spectra the photo peak-background ratio was four times larger than in those collected without anti-Compton shields. Analysing these spectra it was possible to assign exact energy values even to weak γ rays.

The block diagram of the electronic circuit used in anti-Compton measurement is shown in Fig. 2.2. The signals coming from the Ge(HP) detector through a preamplifier (PA) were shaped and amplified in a linear amplifier (LA) of type ORTEC 572 and they were transmitted directly to the multichannel analyser (MCA) which consisted of a 4k PCA Nucleus Card. In order to produce a gate signal when both the Ge(HP) detector and the BGO shield fired at the same time, the analog signals from the Ge(HP) detector and the BGO crystals (BGO) going through a photomultipliers (PM) were shaped and amplified in timing filter amplifiers (TFA) of type ORTEC 472. After that, these signals were recognized in the constant fraction discriminator (CFD) of type CANBERRA 1428A and connected to the

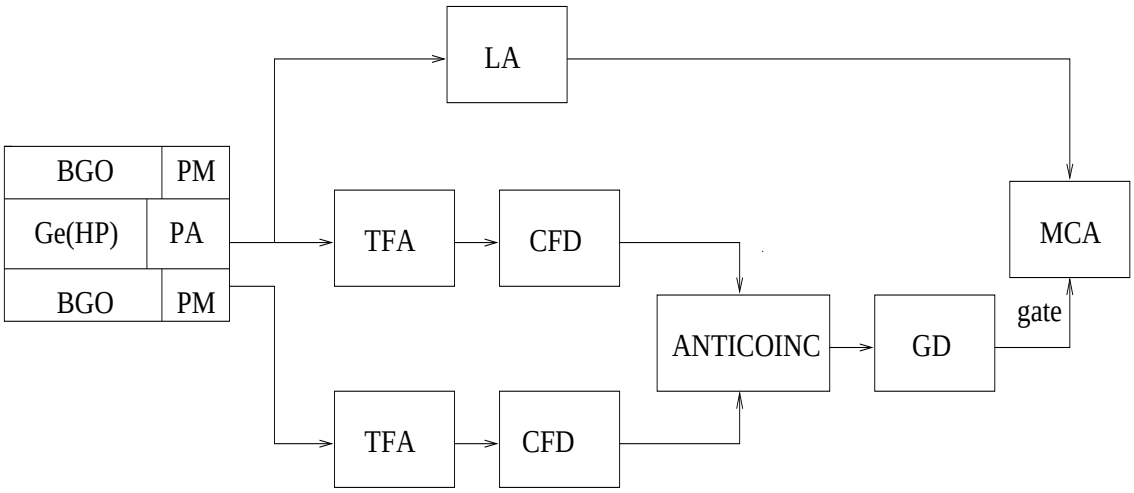

Figure 2.2: *Block diagram of the electronics used in the single γ spectra measurements applied BGO shielded Ge(HP) detector.*

anticoincidence unit (ANTICOINC) of type Phillips Scientific 756. This logic unit produced a veto signal which was transmitted through a signal generator-delay unit (GD) to the MCA in order to inhibit the detection of the escaped γ rays. This spectrometer made possible to decrease not only the intensity of the Compton-scattered γ rays but that of the escape peaks created in the pair creation process in the Ge crystals.

For intensity measurements the detectors were placed at 55° to the beam direction (see in Fig. 2.1) in order to minimalize the change of the γ-ray intensities due to the effect of the angular distribution of transitions. For the calibration of efficiency, the detectors and the standard sources, ^{133}Ba and ^{152}Eu, were put in the same geometry as the detectors and the target were placed in the "in-beam" measurements. Dividing the peak areas with the relative efficiency obtained at the given γ-energy the relative intensities of the γ rays were extracted.

In order to unambiguously identify the γ rays background spectra were collected, as well as spectra of the contaminating ^{A}Ge(p,nγ)^{A}As reactions at the same bombarding energies at which the energy and intensity measurements were done. Spectra measured in few 100 keV steps were also recorded to decide whether a γ ray belongs to the studied reaction or not.

During the analysis of the γ-ray spectra I used the FGM computer code [21] to

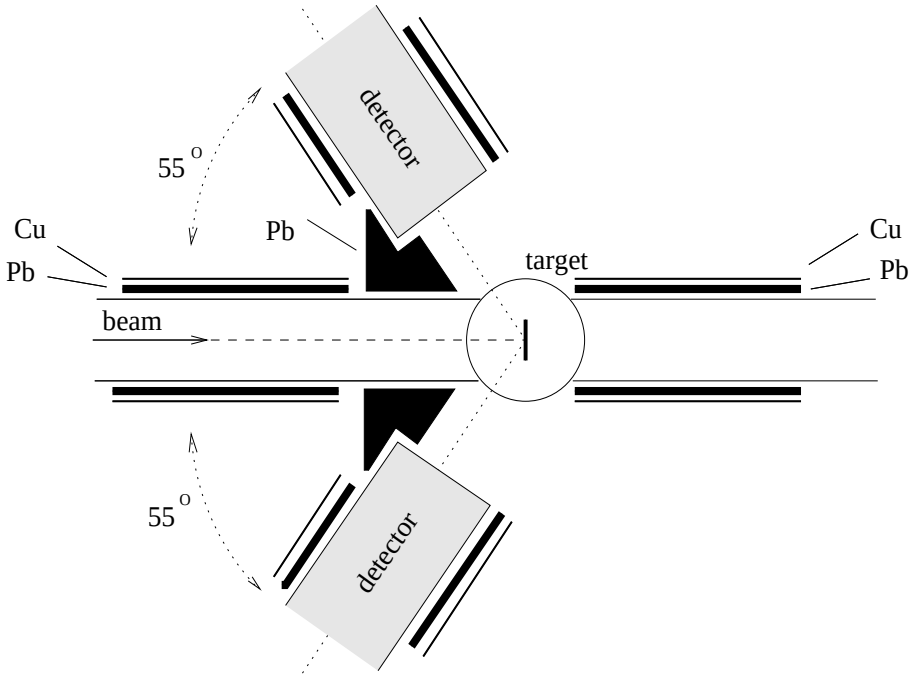

Figure 2.3: *Geometry for the in-beam $\gamma\gamma$ coincidence experiments.*

determine the positions and the areas of the peaks, and the energies of the γ rays from the position values. The intensities of the transitions were extracted with the help of the PKL code.

2.1.3 $\gamma\gamma$-coincidence measurements

To construct a level scheme the $\gamma\gamma$ coincidence relations are indispensable because they show which γ transitions belong to the same cascade. In addition, since in the studied level schemes most of the levels were decaying and populated via several branches the $\gamma\gamma$ coincidence measurements made possible to determine the exact position of γ transitions in many cases. These measurements were also used to improve the resolution of the detection system resolving the overlaps of the peaks as the one-dimensional single spectra which contain several hundreds of γ rays were spread into two dimensions.

The coincidence experiments were performed with two Ge(HP) detectors for ^{72}As nucleus and with four Ge(HP) detectors for ^{73}As nucleus. The 4-detector measurements do not belong to the subject of my thesis thus they will not be discussed here. In the 2-detector measurements the detectors were placed at 55°

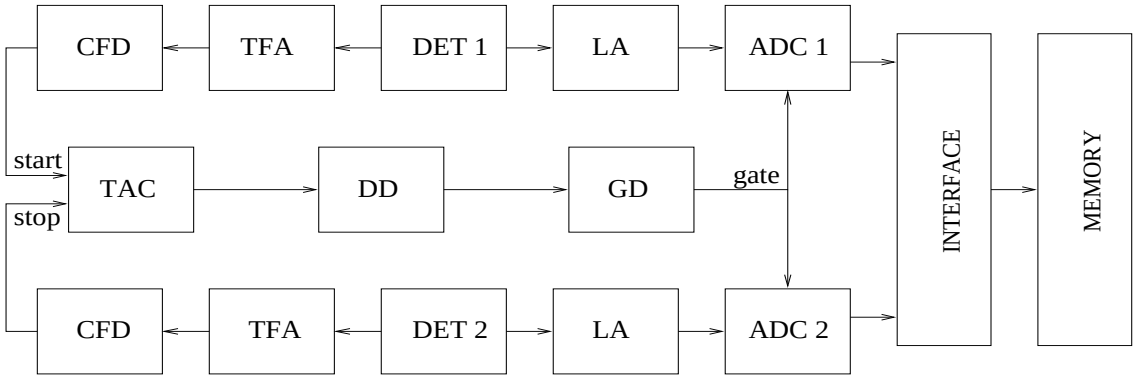

Figure 2.4: *Block diagram of the electronics used in the coincidence measurements.*

relative to the beam direction as shown in Fig. 2.3. The sides of the detectors were shielded with copper sheets to suppress the X rays. Lead absorbents were placed between the detectors to prevent the crosstalk. The distance between the target and the detectors was chosen to be 4 cm, which corresponds to the possible closest geometry. This ensures the proper ratio of real–chance coincidence events and the good detection efficiency increasing the solid angle of the detectors. This geometry resulted in the occurence of sumpeaks which was taken into account during the analysis.

The block diagram of the electronic circuit with the used standard CAMAC and NIM units is presented in Fig. 2.4. The signals for the energy analysis from the Ge(HP) detectors (DET1, DET2) were shaped and amplified in preamplifiers (PA) and linear amplifiers (LA) type ORTEC 572. The analog signals were processed further by analog-to-digital converters with 8k channels (ADC1, ADC2) type Silena 7420/G. The signals for timing from the detectors were amplified and shaped in timing-filter-amplifiers (TFA) type ORTEC 474, and they were recognized in constant-fraction-discriminators (CFD) type Canberra 2126Q to generate start and stop signals for the time to amplitude converter (TAC) type ORTEC 567 . The signal obtained from the TAC was checked in the fats discriminator (DD) type ATOMKI CAM. 4.26-82 in which the time window was set. The generated gate signal was sent through a signal generator and delay unit (GD) type ORTEC 8010 to the ADCs to allow or to veto the acception of the energy signals. The data from

the ADCs were read out by the CAMAC interface and each data belonging to the same coincidence event was written event by event into the CAMAC memory in list mode. Finally the data were stored on magnetic tape by means of the TPA 11/440 computer. The width of the time window was set to be 60 ns for ^{72}As and 50 ns for ^{73}As and time resolution of the set-up was $\approx$10 ns.

From the measured data a two dimensional symmetrized $\gamma\gamma$ coincidence matrix was built with the DATAP computer code [22]. LINGAT [23] and GATES codes were used to produce gate spectra in order to gain information to coustruct the level scheme.

2.1.4 Internal conversion electron measurements

I determined the multipolarities of the transitions in ineternal conversion electron measurements and from them I deduced the parities of the states. In the following I present the theoretical background and the experimental technique of these measurements.

Electronic transitions between nuclear excited states are partly converted to internal conversion electron. The energy of the intarnal conversion electron is written as

$$E_{e^-}(\kappa) = E_\gamma - B_\kappa$$

where E_{e^-}, E_γ and $B_{K,L,M}$ are the electron energy, the transtion energy and the electron binding energy, respectively. The symbol κ stands for the electron orbit characterized by the K, L, M, ... letters. The ratio of the conversion electron emission intensity I_{e^-} to the γ emission intensity I_γ is given by the internal conversion coefficient (ICC) denoted by α.

$$I_{e^-}(\kappa, E_\gamma, L^\tau) = \alpha(\kappa, E_\gamma, L^\tau) I_\gamma(E_\gamma, L^\tau).$$

L^τ is the transition multipolarity with $\tau = E$ being the electric transition and $\tau = M$ being the magnetic transition. The α conversion coefficient depends on the transition multipolarity, the transition energy and the atomic number of the nucleus. Deducing the experimental α coefficients by measuring both conversion

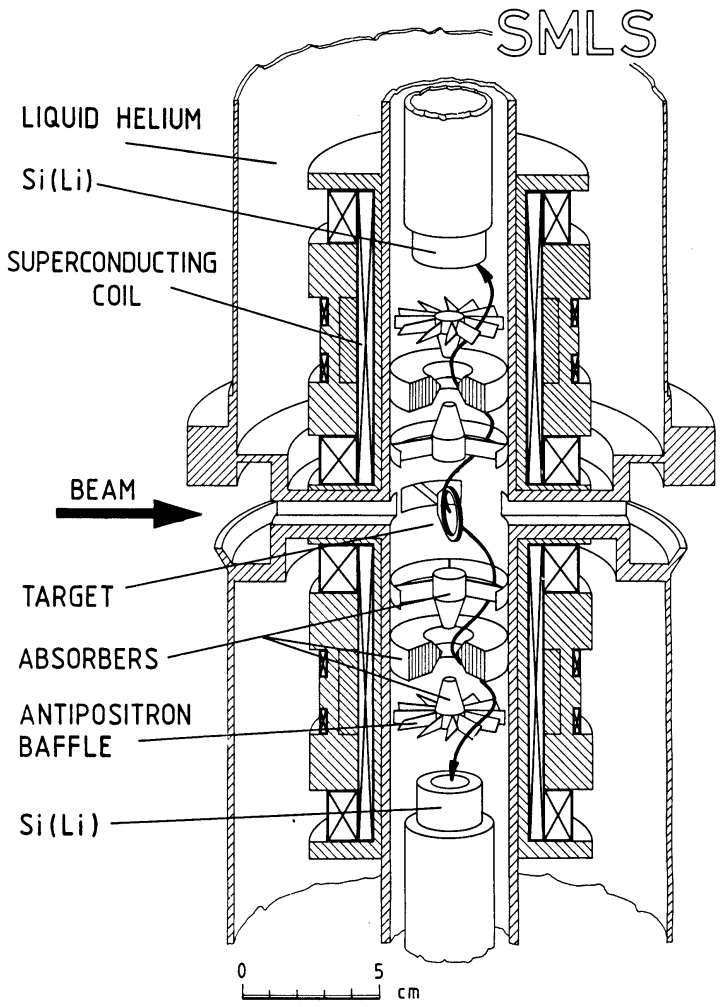

Figure 2.5: *A sectional drawing of the superconducting magnet transporter spectrometer (SMLS).*

electrons and γ rays and comparing these values to the theoretical curves [25], a sensitive tool is obtained used for assignment of the multipolarity of the transitions. As $\alpha_K > \alpha_L > \alpha_M$, the α_K values can be determined with the smallest errors.

If the L^τ transition multiplarity is known, the spin and parity values of the initial and final states can be deduced applying the following selection rules:

$$|J_i - J_f| \leq L \leq J_i + J_f$$

$\pi_i/\pi_f = (-1)^L$ if τ being electric transition and

$\pi_i/\pi_f = (-1)^{L+1}$ if τ being magnetic transition.

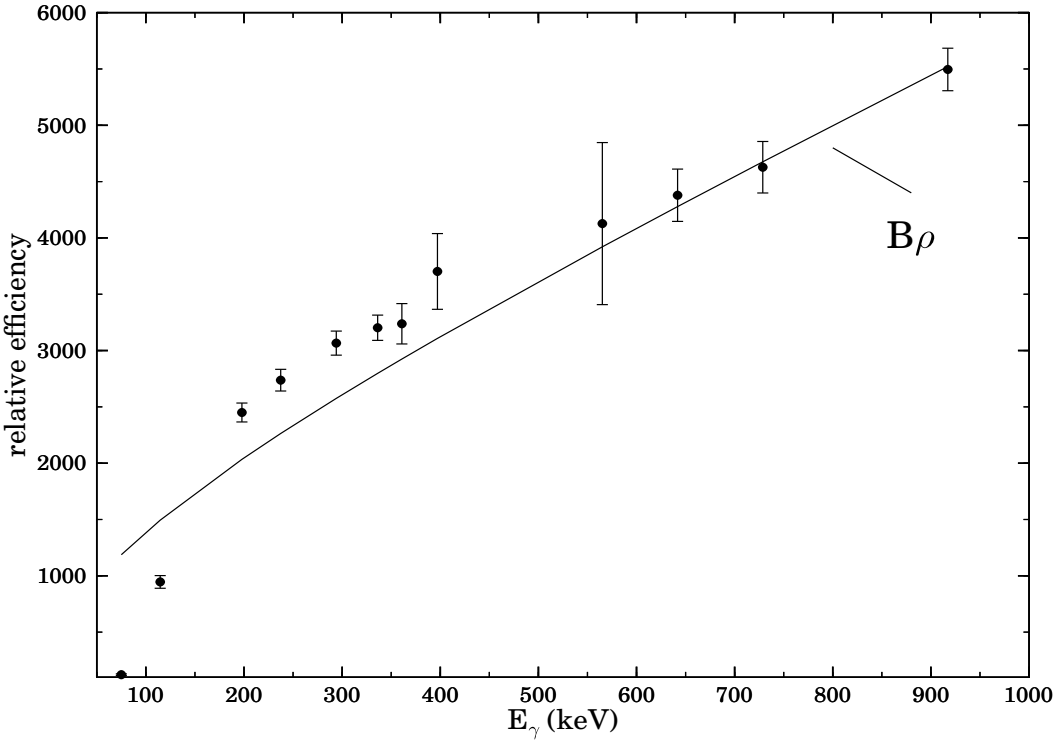

Figure 2.6: *Efficiency of the SMLS measured with* ^{133}Ba *and* ^{152}Eu *sources is compared to the* $B\rho$ *curve.*

Conversion electron spectra were measured in-beam with the Superconducting Magnetic Lens plus Si(Li) Spectrometer (SMLS) [24] developed at the ATOMKI. As it can be seen on the schematic view of the spectrometer in Fig. 2.5 the target is bombarded with a horizontally incident beam. By means of superconducting magnets a strong, homogeneous, vertical field is generated which turns the emitted internal conversion electrons in helical orbits to the Si(Li) detectors. The resolution of the detectors, which are placed at 9 cm under and above the target, is ~2.2 keV (at 917 keV) and the transmission of the spectrometer is 10% (for two detectors). In order to produce high vacuum (10^{-7} bar) the vacuum vessel is cooled by the surrounding liquid helium and liquid nitrogen vessels.

At a given magnetic field the quadrupole lenses transport only a certain part of the emitted electrons from the target to the detectors. Sweeping periodically the magnetic field the relative efficiency curve of the spectrometer is proportional to Bρ

curve characterizes the efficiency of electron spectrometers:

$$B\rho = \sqrt{(E_{e^-}/m_o c^2 + 1)^2 - 1}$$

where E_{e^-} is the kinetic energy and $m_o c^2$ is the rest energy of the electron. The efficiency of the spectrometer calibrated with ^{133}Ba and ^{152}Eu sources is compared to the Bρ curve in Fig. 2.6. The difference at low energy (<100 keV) between the efficiency and the Bρ curves is caused by increasing the deadtime of the spectrometer because of the background due to the δ electron radiation which consists of atomic electrons ejected by projectiles.

In order to reduce the background the scattered particles, X and γ rays are absorbed by the baffles made of tungsten. Further background reduction due to the X rays from structural materials is achieved by using backing foils and frames of the target made of light materials as aluminium and carbon. Paddle-wheel-shaped antipositron baffle systems are applied to weaken the positron radiation rises during the β decay taken place in the target.

The block scheme of the electric circuit used in conversion electron measurements is shown in Fig. 2.7. The signal from the Si(Li) detector (DET) and the preamlifier (PA) was shaped and amplified in the linear amplifier (LA) type ORTEC 572 and sent to the multichannel analyser (MCA) based on a 4k PCA Nucleus Card. The sweeped magnetic field was produced by the power supply (PS) controlled by the electromechanical programmer (PROG). In order to reduce further the background due to γ rays and scattered electrons only those analog signals were allowed to be converted to which belonging energy fitted into the transferred momentum window. For this purpose the signal of the programmer was sent to the so-called Bρ unit (Bρ $\rightarrow$E) which provided signals (E and δE) proportional to the energy and the width of the momentum window. The differential discriminator (DD) type ATOMKI CAM. 4.26-81 compared the analog signal coming from the detector to the E and δE signals and provided gate signal for the multichannel analyser.

Taking into account the available γ-ray angular distribution coefficients for the studied nuclei, the solid angle correction factors, and the normalized direction-particle coefficients, the effect of the angular distribution of electrons was estimated on the measured internal conversion coefficients. The results showed that this effect

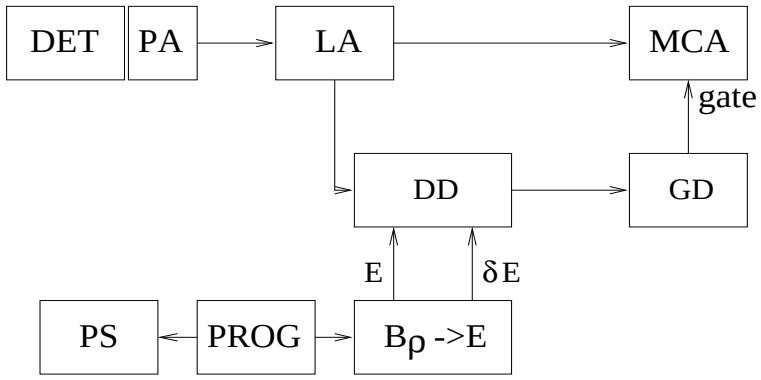

Figure 2.7: *Block diagram of the electronics used in the internal converse electron measurements.*

was much less than the statistical uncertainty of the ICCs.

2.1.5 Hauser-Feshbach analysis

As a result of a detailed γ- and $\gamma\gamma$-coincidence spectroscopic measurements the low spin level scheme of the stuided nuclei can be considered nearly complete below 1 MeV excitation energy. Thus in (p,n) reaction the cross sections for the neutron groups feeding the levels can be deduced from transition intensities, since the cross section of a level is proportional to the differency of the intensity of the transitions populating and depopulating it. To obtain the transition intensities, the γ-ray intensities must be corrected for internal conversion.

On the other hand the σ_{level} values are calculated by using the CINDY computer code [26] based on the statistical compound-nucleus theory, with spin-orbit interaction and the Moldauer level-width fluctuation correction, if necessary. The transmission coefficients for the incoming and outgoing particles are calculated using the optical model sets given by Perey and Perey [27], based on the results of Perey [28] for protons and Wilmore and Hodgson [29] for neutrons. In addition the neutron channels, the (p,p') and (p,γ) channels are also taken into account in the calculation.

In order to assigne spin values to the states, experimental cross sections are compared to the theoretical ones after normalization by using excited states with

known spin values. In spite of the Hauser-Feshbach analysis is not selective for parities and some of the calculated curves lie close to each other, combining the method with multipolarity measurements unambiguous spin values can be assigned to the states.

2.2 The NORDBALL experiment

The ^{68}As and ^{65}Ge nuclei were studied in heavy-ion induced reaction, since they are far from the stability line thus they can not be populated via light-ion induced reactions.

In heavy-ion induced fusion reaction highly excited compound nuclei with large angular momenta are produced and after evaporation of particles neutron deficient nuclei are populated. The lifetime of the compound nucleus is long enough for the excitation energy to be shared among the nucleons. The highly excited compund nucleus cools down by evaporating neutrons, protons, α particles and γ rays. Particle emission is possible when the excitation energy is more than the binding energies for the particles. The evaporated neutron carries away about 8 MeV energy and 1-2 $\hbar$ units angular momentum. The charged particles must be emitted with higher energies to overcome the Coulomb barrier, thus this process produces residual nuclei with lower excitation enegies. If the excitation energy is not high enough to evaporate particles, the remaining excitation energy and angular momentum are dissipated by the series of electromagnetic transitions. After the particle emission the residual nuclei are still excited high above the yrast line and the level density is large. These states decay mainly by statistical cascades of E1 transitions until the yrats line is reached. Close to the yrast line the level density is lower and discrete γ rays can be resolved. Since the compound nucleus ^{70}Se produced in this experiment is neutron deficient the emitted particles are dominated by protons in order to being the residual nucleus forwards the stability line.

In fusion evaporation reaction usually around 20-30 different residual nuclei are pupolated far from the stability line with cross sections between 1 and 100 mb. In order to observe and identify γ rays belong to final nuclei populated with low cross

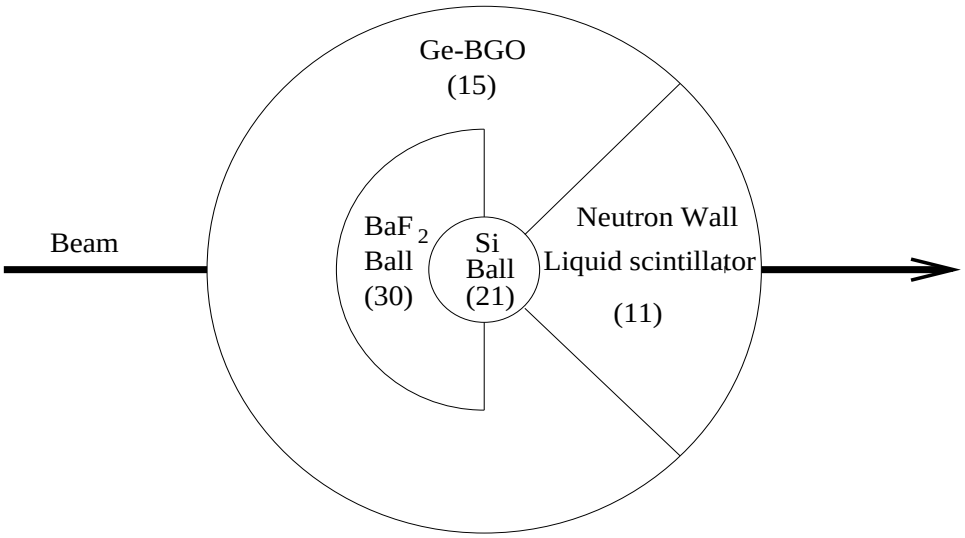

Figure 2.8: *The schematic view of the NORDBALL experiment set-up.*

section, detector array with high efficiency and selectivity is needed. In the present experiment a technique based on detection of γ rays in coincidence with evaporated charged particles and neutron was used to select the reaction channels.

The experiment was performed at the Tandem Accelerator Laboratory of the Niels Bohr Institute in Denmark. A 1.5 mg/cm^2 thick ^{12}C target, evaporated onto a 23 mg/cm^2 Au backing, was bombarded by a ^{58}Ni beam with an energy of 261 MeV. The emitted particles and γ rays were detected with the NORDBALL detector array of γ-ray detectors [30, 31] equipped with a γ-ray calorimeter (Inner Ball), a charged particle detector system (Silicon Ball) [32] and a neutron detector assambly (Neutron Wall) [33]. The schematical view of the experimental set-up is shown in Fig. 2.8.

2.2.1 Detectors

The NORDBALL

The NORDBALL multi-detector array consisted of 15 high purity Ge detectors surrounded by anti-Compton shields. Each shield was made of 6 BGO scintillator crystals mounted together. The number of Ge detectors was less than that of the basic NORDBALL configuration (20) in order to provide enough room for the neutron wall. The energy resolution of the individual Ge detectors was between 1.8 and 3 keV at an enegy of 1332 keV and their efficiency varied between 20% and 40% rel-

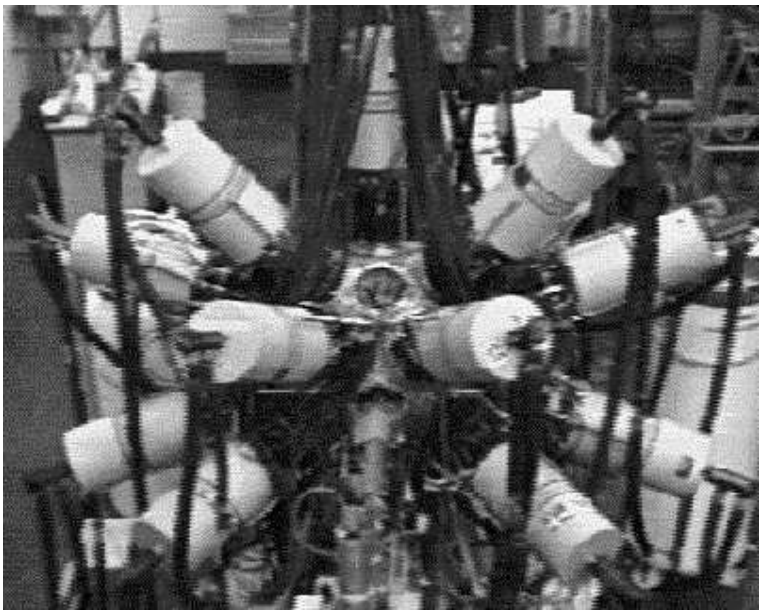

Figure 2.9: *The photo of the NORDBALL multi-detector assambly.*

Table 2.1: Angular positions of the Ge detectors in NORDBALL with respect to the beam axis.

Ring	θ	ϕ				
I	142.6°	54°,	126°,	198°,	270°,	342°
II	100.9°	54°,	126°,	198°,	270°,	342°
III	79.1°	18°,	90°,	162°,	234°,	306°

ative to the efficiency of a 3"×3" NaI(Tl) crystal. The total photo-peak efficiency of the whole array was ∼1%. The photo of the NORDBALL multi-detector assambly is shown in Fig. 2.9.

The Ge detectors formed three rings at the angles of 79°, 101° and 143° relative to the beam direction and they were placed symmetrically around the target. The angular position of the Ge detectors are shown in Table 2.1.

The Inner Ball

The γ-ray calorimeter composed of 30 BaF_2 scintillators covering the backward 2π hemisphere. The inner ball had a total γ-ray detection efficiency of about 40% at 1 MeV. As the BaF_2 crystals possess excellent timing properties the signals from the BaF_2 detectors provided the time reference for all other signals. After careful

time matching of the individual BaF_2 detectors, the time resolution of the whole γ-ray calorimeter was of the order of 1 ns. The inner ball also supplied information about the total γ-ray multiplicity and sum-energy, which are related to the initial spin and excitation energy of the residual nucleus, respectively. This information could be used as a tool to distinguish between different final nuclei.

The Silicon Ball

In a compund nucleus reactions leading to neutron deficient nuclei charged particle channels are open. Therefore the charged particle identification is crucial for unambiguous assigment of γ rays to a certain residual nucleus.

In the present experiment the emitted light charged particles were detected in a silicon ball consisted of 21 ΔE type Si detectors [32], covering a solid angle of about 90% of 4π. The Si ball has been designed to fit into the space inside the BaF_2 inner ball. The Si detectors were placed on a frame with an inner diameter of about 5 cm. The average distance between the Si detectors and the target was about 2.5 cm. In a heavy-ion reaction the evaporated particles concentrate to the forward angles, hence the silicon wafers covering the most forward faces of the frame were split into several parts in order to decrease the probability of multiple hits.

Each of the Si detector element has been covered with an absorber foil to stop the elastically scattered beam particles. The absorbers were thick enough to stop these particles, but thin enough to let through a large fraction of the evaporated protons and α particles.

Protons and α particles were distinguished according to the energy deposit in the detectors. The efficiency of the Si-ball was approximately 60% for detection of protons and about 40% for α particles. In charged particle energy spectra for the detectors placed at forward angles the proton peak situated at lower energies was well separated from the broad high-energy bump corresponding to the α particles. At larger detector angles the α bump moved towards the proton peak and almost dissappeared under the proton peak in the most backward detector. This effect caused that some of the α particles were misinterpreted as protons. Also a small fraction of the events connected to the emission of 2 protons were interpreted as a

1α event because both protons hit the same detector.

The Neutron Wall

In the NORDBALL detector system a neutron wall gave information about the emitted neutrons. The wall consisted of 11 detectors filled with an organic scintillator liquid of type BC501. The detectors occupied five hexagonal and six pentagonal positions in the forward hemisphere of the NORDBALL frame covering a solid angle of about 1π. The distance between the scintillators and the target was 18 cm. Neutron and γ-ray signals were separated off-line by means of a combined time-off-flight and pulse shape discrimination technique [34, 35]. The neutron detection efficiency was $\sim$22%.

Although the combined discrimination technique improves the neutron-γ separation as compared to puls shape discrimination alone, about 0.8% of the events not connected to neutron emission were missassigned for neutrons. In addition, the detection of the neutrons scattered between the detectors led to an overlap between the $1n$ and $2n$ channels.

Data acquisition system

Standard CAMAC and NIM electronics were used to process the signals from the detectors and to provide a trigger for the data acquisition system. An event was recorded on magnetic tape if at least two γ rays were detected in the Ge detectors with a maximum time difference of 80 ns and at least one γ ray in the BaF_2 calorimeter, or at least one Ge detector and one BaF_2 crystal fired in coincidence with at least one neutron detected in the liquid scintillators. The events were packed into large data blocks and subsequently sent via an optical links to a VAX 8650 computer for monitoring and for storing on high-density EXABYTE tapes.

2.2.2 Data analysis

$\gamma\gamma$- coincidence analysis

Standard ^{133}Ba and ^{152}Eu sources were used for energy and efficiency calibration of the Ge detectors. With the energy calibration information the Ge detectors were gain

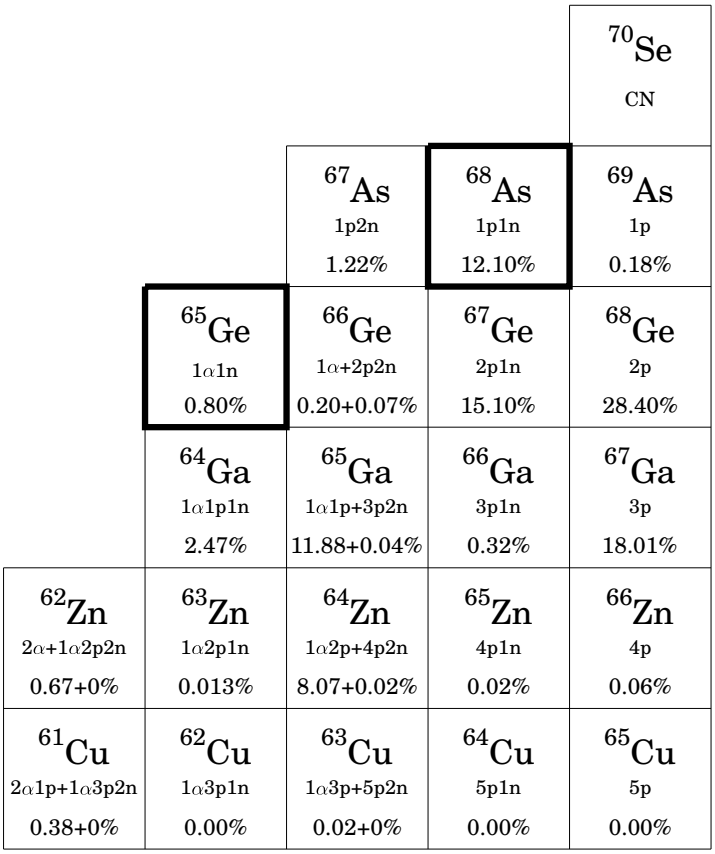

Figure 2.10: *The population pattern obtained for the $^{58}Ni + ^{12}C$ reaction at 261 MeV.*

matched and gain corrected, and after several presorts the data were compressed.

In order to construct level schemes a total of about 120 million coincidence events were collected and then sorted into a set of prompt $\gamma\gamma$ matrices of the size of 4096×4096 channels by requiring different conditions on the number of detected charged particles and neutrons. The contaminating γ lines due to the incomplete particle identification were eliminated by using a successive subtraction technique [36]. A number of $\gamma\gamma$ matrices were also sorted for the angular distribution analysis, as well as prompt-delayed and delayed-delayed $\gamma\gamma$ matrices for the time analysis. The particle gated matrices were analysed in detail using standard gating techniques with help of the RADWARE software package [37].

Transitions belonging to 22 residual nuclei were identified in the present experiment. The obtained population pattern following the ^{58}Ni + ^{12}C reaction is shown

in Fig. 2.10. The observed relative experimental yields for different final nuclei, deduced from the intensities of the strong γ rays in the particle gated $\gamma\gamma$ coincidence projections, are also shown in Fig. 2.10. The yields are corrected for the particle-detection efficiency. The yield of the studied nuclei were estimated: about 10% of the events belonged to the $1p1n$ channel leading to ^{68}As, and less than 1% of the events connected to the $1\alpha 1n$ channel leading to ^{65}Ge.

Angular distribution analysis

The multipolarities of the γ rays were obtained by means of a simplified $\gamma\gamma$ correlation analysis. The coincidence events were sorted into two $\gamma\gamma$ matrices with the following angle combinations: (143°)×(all angles) and (79° + 101°)×(all angles), where the first is the x-axis and then the y-axis is given. By setting equal gates on the y-axis in both matrices two coincidence spectra representing the angles (143°) and (79° + 101°) were constructed. Then the $R = I_\gamma(143°)/[I_\gamma(79°)+I_\gamma(101°)]$ intensity ratios were deduced from the fitted peak intensities to determine the angular momentum transferred by the γ rays.

According to theoretical estimations on the NORDBALL geometry R∼1.5 corresponded to stretched quadrupole, ΔJ=0 dipole or ΔJ=1 mixed M1/E2 transitions, while the R∼0.8 value to stretched dipole or ΔJ=0 highly mixed M1/E2 transitions [38]. R∼1.2-1.3 values were reasonable for ΔJ=0,1 mixed M1/E2 transitions, R∼0.4-0.6 corresponded to ΔJ=1 mixed M1/E2 transitions. These R values were in agreement with the angular distribution ratios obtained for transitions with known multipolarity from different nuclei populated in the present reaction. In order to reduce the error of the R values, average values of the intensisy ratios were determined by using several stronger γ rays as gating transitions. In spite of that the multipolarities were assigned ambiguously to the transitions, in many cases the same state was populated and depopulated via different decay paths, which helped in solving this problem.

Chapter 3

Structure of ^{72}As

3.1 Earlier studies

In the electron capture decay of ^{72}Se only the 46 keV 1_1^+ state of ^{72}As is populated (Cumming and Johnson [39], Hübner [40]), the other ^{72}As excited levels can be studied through nuclear reactions. The investigation of (p,nγ) reaction by Mordechai et al. [41], Bertschat et al. [42], Kimura et al. [43], and Ten Brink et al. [44], as well as (α,xnpγ) and different heavy ion reactions by Mariscotti et al. [45], Raghavan et al. [46] and Döring et al. [47] extended our knowledge on the level scheme of ^{72}As considerably. Nevertheless unambiguous spin-parity values have been assigned only to four levels of ^{72}As in the last Nuclear Data Sheets evaluation (Chou and King [48]). The former studies are summarized in Table 3.1.

3.2 Experimental results

The γ-ray spectra of the ^{72}Ge(p,nγ)^{72}As reaction were measured at E_p =5.75, 5.96, 6.01, 6.16, 6.21, and 6.41 MeV energy and with ~4 nA proton beam intensity. After the energy and efficiency calibration of γ spectrometers with ^{133}Ba and ^{152}Eu sources, the energies of intensive 45.90(5), 167.80(4), 242.52(3) and 344.17(3) keV ^{72}As internal calibration lines [48] have been reproduced within experimental errors.

The internal conversion electron spectra were carried out using 5.96 and 6.16 MeV energy and 550 nA intensity proton beams. Typical γ-ray and internal conversion electron spectra are shown in Fig. 3.1. The α_K internal conversion coefficients (ICC) obtained from the different electron spectra agreed within experimental errors. The ICCs, the deduced and formerly known multipolarities are also given in Table 3.2.

Table 3.1: Summary of the former experimental studies of the structure of ^{72}As

Reference *	Reaction	Techniques, detectors	Measurements	Results
Cumming (1958) [39]	decay of ^{72}Se	NaI(Tl) scintillators	E_γ, I_γ, I_{ce}, $T_{1/2}$	ICC, K/L ratio for the 46 keV transition, deduced J^π assignment only for the first excited state, measured $T_{1/2}$ and logft values for this state
Hübner (1965) [40]	decay of ^{72}Se	NaI(Tl) scintillators	$T_{1/2}$	J^π assignment only for the first excited state, $T_{1/2}$ determined for this state
Mordechai (1974) [41]	^{72}Ge(p,nγ)^{72}As, E_p=5.1-6.2 MeV	in-beam techniques, Ge(Li) detectors and NaI scintillators	E_γ, I_γ, σ(E,Eγ,θ), $\gamma\gamma$-coinc	16 transitions identified and placed in the level scheme, energy thresholds for these γ rays determined, $\gamma\gamma$-coinc relations for 2 transitions, angular distribution of 2 γ rays measured, deduced 13 levels, unambiguous J^π assignments only for 3 states
Bertschat (1975) [42]	^{72}Ge(p,nγ)^{72}As, E_p=5.2-6.0 MeV	in-beam and time of flight techniques, Ge(Li) detector and NaI(Tl) scintillators	E_γ, I_γ, σ(E,Eγ), $\gamma\gamma$-coinc, $\gamma\gamma$-delay, $\varphi\gamma(\theta$,H,t), $T_{1/2}$, g	11 transitions identified and placed in the level scheme, energy thresholds for these γ rays determined, $\gamma\gamma$-coinc relations only for 3 transitions, Hauser-Feshbach analysis for 2 levels, unambiguous J^π assignments only for 3 states, $T_{1/2}$ and g factor of the 213 keV state measured
Kimura (1976) [43]	^{72}Ge(p,nγ)^{72}As, E_p=5.0-6.3 MeV	in-beam techniques, Ge(Li) detectors, sector field double focusing β-ray spectrometer	E_γ, I_γ, σ(E,Eγ), I_{ce}	44 transitions identified and placed in the level scheme, energy thresholds for these γ rays deduced, ICCs determined for 14 γ rays, Hauser-Feshbach analysis for 12 levels, the level scheme contains 26 levels below 800 keV with 14 unambiguous J^π assignments, γ-branching given

Table 3.1: continued

Reference *	Reaction	Techniques, detectors	Measurements	Results
Ten Brink (1979) [44]	^{72}Ge(p,nγ)^{72}As, E_p=6.5-14 MeV	in-beam techniques, planar Ge and Ge(Li) detectors	E_γ, I_γ, σ(E,Eγ,θ), $\gamma\gamma$-coinc, $T_{1/2}$	86 transitions identified and placed in the level scheme, which contains 52 levels below 1308 keV only with 2 unambiguous J^π assignments, A_2, A_4 factors deduced for 36 γ rays, $T_{1/2}$ measured for 5 states, Hauser-Feshbach analysis for 2 levels
Mariscotti (1976) [45]	^{70}Ge(α,npγ)^{72}As, ^{72}Ge(α,3npγ)^{72}As E_α=30-55 MeV	in-beam techniques, Ge(Li) detectors	E_γ, I_γ, σ(E,Eγ,θ,t), $\gamma\gamma$-coinc	16 transitions identified and placed in the high spin level scheme, A_2, A_4 factors deduced for 7 transitions, excitation functions of 13 γ rays measured, $T_{1/2}$ determined for 3 states, unambiguous J^π assignments deduced for 3 states, γ-branching given
Raghavan (1977) [46]	^{59}Co(^{16}O,2pn)^{72}As, $E_{^{16}O}$=53-56 MeV	in-beam techniques, planar Ge(Li) detector, NaI(Tl) scintillator	$T_{1/2}$	$T_{1/2}$ and g factor of isomeric states at 213 keV and 561 keV measured, unambiguous J^π assignments given for 3 levels
Döring (1994) [47]	^{59}Co(^{19}F,αpn)^{72}As, $E_{^{19}F}$=55 MeV, ^{65}Cu(^{12}C,αn)^{72}As, $E_{^{12}C}$=50 MeV	in-beam techniques, BGO-shielded Ge(HP) detectors	E_γ, I_γ, $\gamma\gamma$-coinc	high spin level scheme up to 6.1 MeV deduced with 26 states and 39 transitions placed in it, angular correlation coefficients determined for 21 γ rays, unambiguous J^π assignments deduced for 6 levels, $T_{1/2}$ measured for 6 states
Chou, King (1994) [48]				compilation

* Only the first author is indicated in this column.

The theoretical curves and experimental ICCs of the ^{72}As transitions are presented in Fig. 3.2. The experimental ICCs were normalized by using the theoretical α_K internal conversion coefficient [25] of the 309.78 keV E2 $4^- \rightarrow 2^-$ transition of ^{72}As [43]. With this normalization the conversion coefficients of the 105 keV M1(E1), 214 keV E1, 226 keV M1, 243 keV M1+E2, 344 keV M1, 468 keV M1, and 520 keV M1 ^{72}As transitions obtained by Kimura et al. [43] were reproduced within experimental errors.

The $\gamma\gamma$-coincidence measurements were performed at 6.1 and 6.5 MeV bombarding proton energies. The measurements were repeated at greater detector-target distances to avoid unwanted sumpeak effects. Approximately 9 million $\gamma\gamma$-coincidence events were recorded on magnetic tapes. After creation of symmetrized, two-dimensional coincidence matrices and a standard gating procedure, more than 150 gate spectra were evaluated. Due to the large enrichment of the targets and the good statistics of the $\gamma\gamma$-coincidence measurements, most of the γ rays were identified unambiguously. If the γ ray was unresolved or small in singles spectra, the energy was determined from the gate spectra. The energies, relative intensities, and $\gamma\gamma$-coincidence relations of the γ rays assigned to ^{72}As are listed in Table 3.2. Typical $\gamma\gamma$-coincidence spectra are shown in Fig. 3.3.

3.3 Level scheme of ^{72}As

The construction of the level scheme was based mainly on the $\gamma\gamma$-coincidence relations, but the energy and intensity balance of transitions was also taken into account. The low- and high-energy parts of the proposed level scheme are presented in Figs. 3.4 and 3.5, respectively. All γ rays, listed in Table 3.2, have been placed in the scheme. The multipolarities of transitions and γ-ray branching ratios (with errors) are given in the level scheme after the transition energies. These branching ratios are weighted averages of values obtained at different bombarding energies. Many of them are new, the others show good agreement with the corresponding data of Kimura et al. [43] and Ten Brink et al. [44].

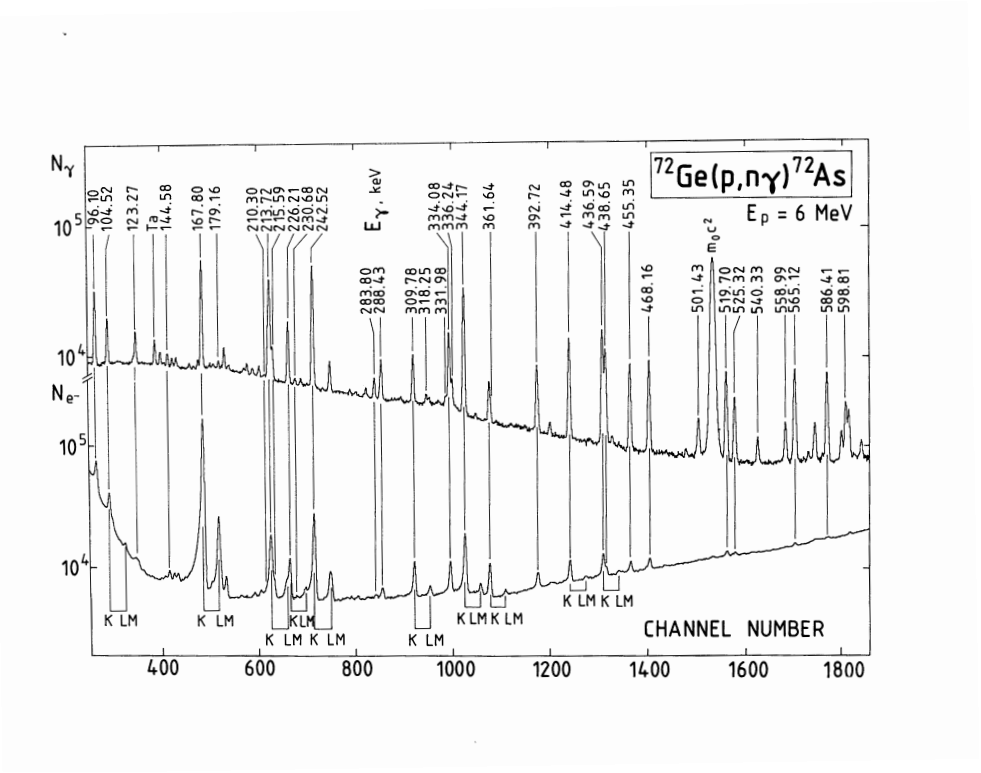

Figure 3.1: *Typical γ-ray and internal conversion electron spectra of the $^{72}Ge(p,n\gamma)^{72}As$ reaction. The energies of γ rays are given only at the strongest ^{72}As γ transitions.*

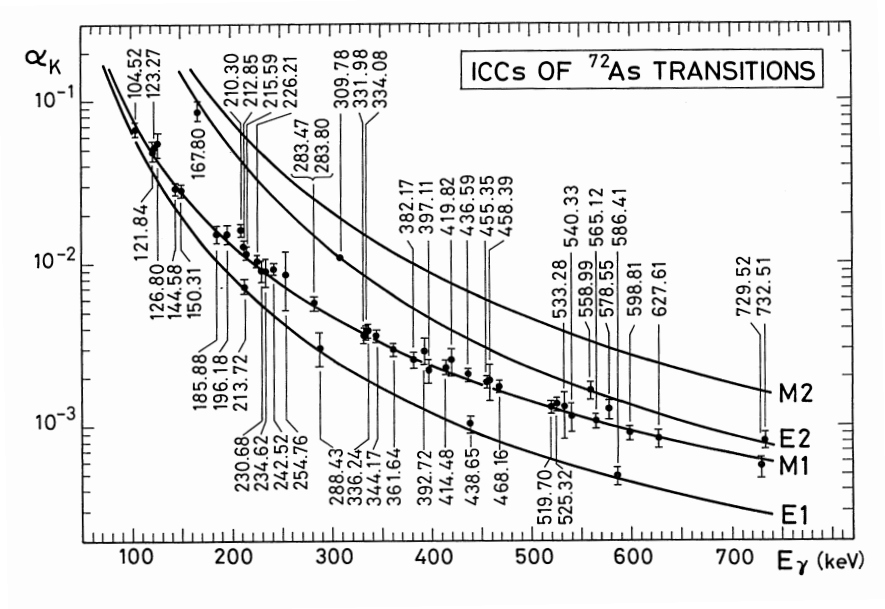

Figure 3.2: *Experimental internal conversion coefficients (ICC) of the ^{72}As transitions (data with error bars) as a function of γ-ray energy. Curves show theoretical results [18].*

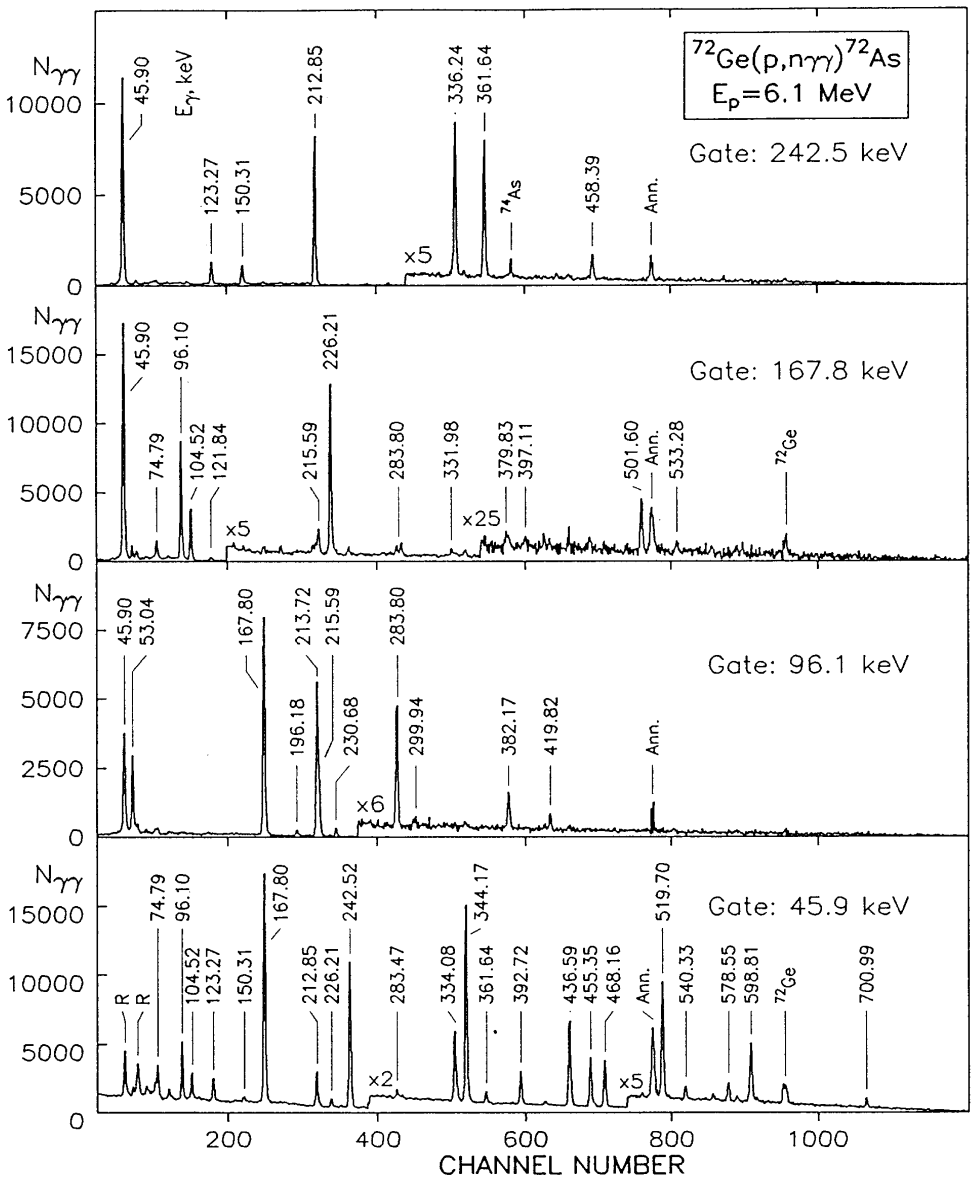

Figure 3.3: *Typical $\gamma\gamma$-coincidence spectra of the $^{72}Ge(p,n\gamma)^{72}As$ reaction. The background was subtracted. The $N_{\gamma\gamma}$ scales correspond to the first parts of the spectra.*

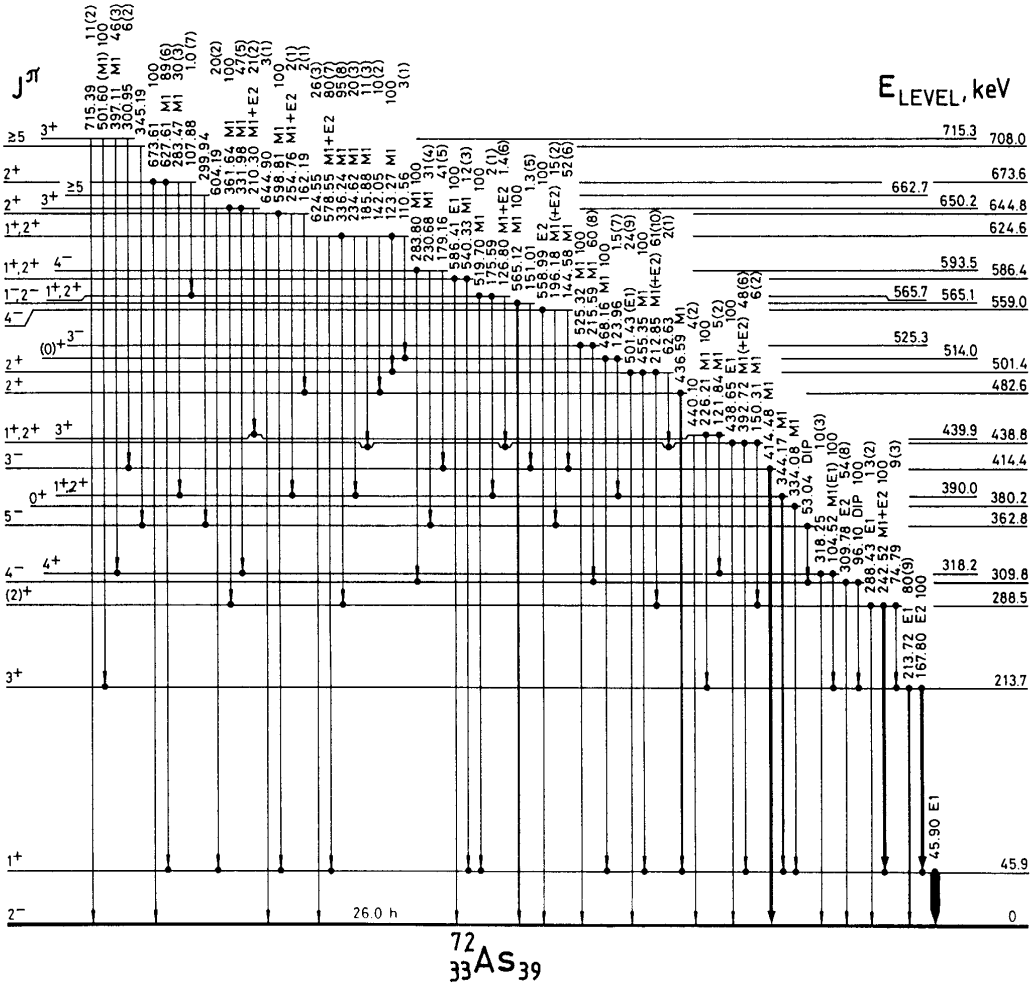

Figure 3.4: *Low-energy part of the proposed level scheme of* ^{72}*As. Solid circles at the ends of arrows indicate* $\gamma\gamma$*-coincidence relations. Behind the* γ*-ray energies and multipolarities relative* γ*-branching ratios (and their errors) are given. Dip. means dipole transition. The multipolarities were taken from Table 2.1.*

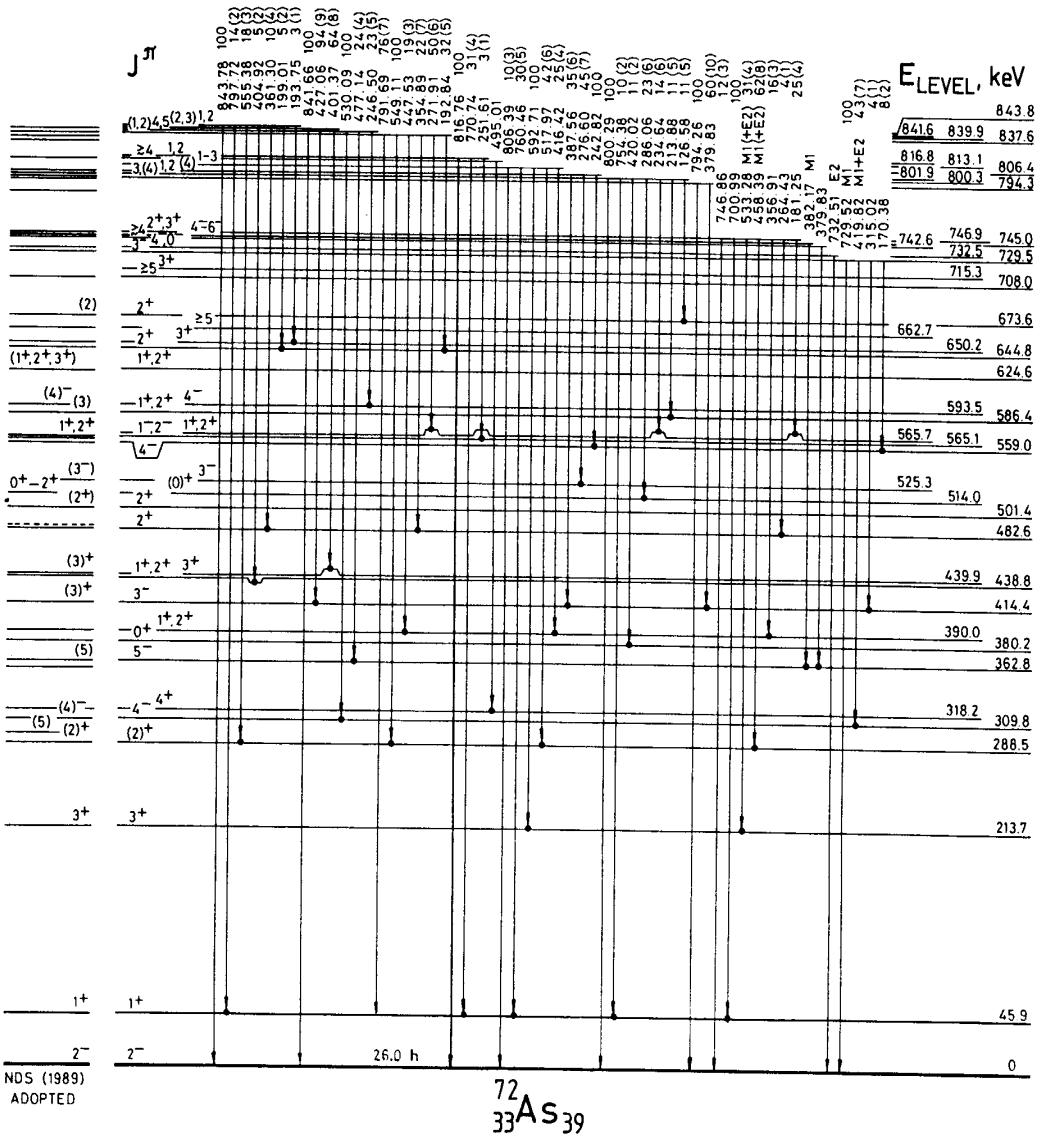

Figure 3.5: *High-energy part of the proposed level scheme of* ^{72}*As. Adopted levels of the Nuclear Data Sheets evaluation (King [41]) are shown on the left side. Further explanation see in caption of Fig. 3.4.*

Table 3.2: Energy, intensity, internal conversion coefficient, multipolarity and coincidence relations of γ rays of the ^{72}Ge(p,nγ)^{72}As reaction at 6.2 MeV proton energy. New γ rays compared with the compilation of King [10] are marked with N and Dip means dipole transition.

E_γ	I_γ		ICC measurements				Coincident γ rays
(keV)	(relative)		$10^4\alpha_K$	Multip. of γ ray	Former results		E_γ (keV)
45.90(5)	4125(949)				E1	[39, 40]	53, 75, 96, 105, 108, 111, 123.3, 150, 168, 212.8, 216, 226, 234.62, 242.5, 255, 283.5, 334, 336, 344, 361.6, 393, 437, 455, 458, 468, 501.6, 520, 540, 549, 579, 599, 604, 628, 701, 754, 760, 771, 798
53.04(7)	135(27)				Dip	[44]	46, 96, 168, 196, 213.7, 231, 299.9, 310, 382, 477
62.63(6)	7.4(13)	N					439
74.79(6)	103(17)						46, 123.3, 168, 213.7, 336, 361.6,
96.10(15)	458(55)				Dip	[43]	46, 53, 168, 196, 213.7, 216, 231, 242.5, 283.8, 299.9, 345, 382, 419.8, 530
104.52(6)	231(28)		666(57)	M1(E1)	M1(E1)	[43]	46, 122, 168, 213.7, 332, 397,495
107.88(10)	1.5(5)	N					176, 520
110.56(10)	4.2(7)	N					46, 468
121.84(10)	14.0(12)		485(56)	M1			46, 105, 168,210, 213.7,
123.27(7)	131(10)		517(45)	M1	M1+E2	[43]	46, 75, 168, 212.8, 213.7, 242.5, 288, 455, 501.4
123.96(20)	5.3(7)	N					286, 344
126.58(10)	14.3(76)	N					283.4, 344, 628, 674
126.80(10)	6.3(6)	N	550(95)	M1+E2			46, 150, 168, 242.5, 393, 439
142.05(5)	13.8(74)	N					46, 437
144.58(5)	57.2(42)		290(26)	M1			414
150.31(10)	24.2(22)	N	283(27)	M1			46, 75, 126.8, 168, 186, 242.5, 288

Table 3.2: continued

E_γ (keV)	I_γ (relative)		ICC measurements $10^4\alpha_K$	Multip. of γ ray	Former results	Coincident γ rays E_γ (keV)
151.01(10)	8.2(9)	N				414
162.19(9)	6.6(7)	N				437
167.80(4)	1000(69)		859(75)	E2	E2,M2 [43]	46, 53, 63, 75, 96, 105, 122, 123.3, 126.8, 150, 210, 212.8, 216, 226, 231, 246, 283.8, 332, 336, 345, 379.8, 382, 397, 501.6, 533, 593
170.38(16)	9.5(8)	N				559
175.59(9)	8.8(8)	N				46, 108, 344
179.16(7)	38.7(27)					414
181.25(7)	21.2(19)	N				176, 520
185.88(8)	14.3(9)	N	153(19)	M1		150, 393, 439
192.84(9)	8.6(12)	N				599
193.75(20)	3.7(11)	N				242.5, 361.6
196.18(10)	17.3(10)	N	152(20)	M1(+E2)		53, 96, 310
199.01(12)	6.1(11)	N				599
210.30(8)	25.6(21)		162(14)	M1+E2		46, 105, 122, 168, 213.7, 226
212.85(19)	225(14)		128(12)	M1(+E2)		46, 75, 123.3, 168, 213.7, 242.5, 288
213.72(5)	807(58)		72.2(65)	E1	E1 [43]	53, 63, 75, 96, 105, 123.3, 196, 210, 212.8, 216, 226, 283.8, 332, 336, 345, 382, 397, 501.6, 533, 593
213.88(24)	14.6(10)	N				540, 586
215.59(6)	138.8(79)		116(10)	M1		46, 96, 168, 213.7, 310
226.21(4)	308(18)		104(10)	M1	M1 [43]	46, 168, 210, 213.7, 401
230.68(7)	28.6(18)		91(15)	M1		53, 96, 310
234.62(7)	26.3(19)	N	90(18)	M1		46, 344
234.64(25)	19.2(12)	N				520

Table 3.2: continued

E_γ (keV)	I_γ (relative)		ICC measurements $10^4\alpha_K$	Multip. of γ ray	Former results	Coincident γ rays E_γ (keV)
242.52(3)	1142(70)		93(8)	M1+E2	M1+E2 [43]	46, 63, 123.3, 150, 194, 212.8, 336, 361.6, 458, 518, 549, 555
242.82(21)	20.4(24)					145, 196, 559
246.50(18)	5.5(13)	N				283.8
251.61(16)	3.3(10)	N				565
254.76(10)	11.3(21)	N	86(34)	M1+E2		46, 344
264.43(12)	3.7(7)	N				437
271.91(16)	13.7(9)	N				520
276.60(9)	9.2(8)					525
283.47(6)	49.9(31)		57.1(52)	M1		46, 344
283.80(5)	93.5(57)		57.1(52)	M1	M1+E2 [43]	96, 168, 246, 310
286.06(7)	30.6(24)	N				468
288.43(5)	142.5(88)		30.8(71)	E1		123.3, 150, 212.8, 336, 361.6, 458, 518, 549, 555
299.94(11)	12.9(10)					53,96
300.95(24)	6.8(10)	N				414
309.78(4)	247(17)		113(10) norm.point	E2	E2 [43]	53, 216, 231, 283.8, 345, 382, 420, 530
315.02(14)	4.9(4)	N				414
318.25(7)	23.5(16)					194, 332
331.98(6)	58.2(41)		36.5(41)	M1		46, 105, 168, 194, 213.7, 318
334.08(4)	318(22)		38.6(34)	M1		46, 420
336.24(5)	125.6(81)		38.8(36)	M1		75, 242.5, 288
344.17(3)	899(56)		36.3(32)	M1	M1 [43]	46, 123.9, 126.6, 176, 234.62, 255, 283.4, 357, 416
345.19(26)	8.6(10)					46, 53, 96, 168, 213.7, 310
354.89(11)	6.1(20)	N				437
356.91(9)	14.0(14)	N				344
361.30(24)	12.2(16)	N				437

Table 3.2: continued

E_γ (keV)	I_γ (relative)		ICC measurements $10^4\alpha_K$	Multip. of γ ray	Former results	Coincident γ rays E_γ (keV)
361.64(5)	124.5(83)		30(3)	M1		46, 75, 168, 194, 213.7, 242.5, 288
379.83(11)	41.1(23)					414
379.83(18)	2.0(7)					53,96, 168
382.17(5)	80.0(47)		26(3)	M1		46, 53, 96, 168, 213.7, 310
387.56(9)	7.2(10)					414
392.72(4)	178(12)		29.4(28)	M1(+E2)		46, 63, 126.8, 181, 186, 405
397.11(5)	49.8(29)	N	22.4(37)	M1		105, 168, 213.7
401.37(7)	21.5(13)					226
404.92(9)	5.8(16)	N				393, 439
414.48(4)	592(34)		23.2(24)	M1	E1 [43]	145, 151, 170, 179, 181, 301, 315, 379.8, 388, 427
416.42(8)	18.8(12)	N				344
419.82(7)	48.3(29)		26(4)	M1+E2		46, 96, 310
420.02(8)	15.1(11)	N				334
427.06(6)	33.4(21)					414
436.59(4)	597(35)		21.1(18)	M1		46, 142, 162, 264, 355, 361.3
438.65(5)	368(21)		10.4(9)	E1		63, 123.3, 126.8, 186, 234.64, 405
440.10(12)	9.4(17)	N				
447.53(15)	5.3(9)	N				46, 344
455.35(4)	372(22)		18.9(17)	M1	M1,(E1) [43]	46, 123.3
458.39(7)	53.8(38)		19.2(47)	M1(+E2)		46, 242.5, 288
468.16(5)	351(21)		17.7(16)	M1	M1+E2 [43]	46, 111, 286
477.14(11)	5.9(8)	N				53
495.01(13)	6.3(10)					105
501.43(25)	89.2(55)	N	6.8(14)	(E1)		123.3
501.60(22)	109.2(65)		14.3(49)	(M1)		46, 168, 213.7
517.97(7)	30.8(17)	N				242.5
519.70(4)	463(27)		13.2(12)	M1	M1+E2 [43]	46, 108, 181, 234.64

Table 3.2: continued

E_γ (keV)	I_γ (relative)		ICC measurements			Coincident γ rays E_γ (keV)
			$10^4\alpha_K$	Multip. of γ ray	Former results	
525.32(4)	230(13)		13.7(13)	M1		277
530.09(9)	24.3(14)					96, 310
533.28(7)	27.0(15)		13.3(67)	M1(+E2)		168, 213.7
540.33(9)	57.3(41)		11.6(23)	M1		46, 213.9
549.11(7)	27.3(15)					46, 242.5
555.38(7)	22.5(14)	N				46, 242.5, 288
558.99(4)	110.2(68)		15.2(22)	E2		170, 242.8
565.12(4)	529(32)		10.8(11)	M1		252
578.55(5)	105.5(72)	N	12.8(17)	M1+E2		46
586.41(4)	475(28)		4.9(6)	E1		213.9
592.71(5)	74.3(52)	N				168, 213.7
598.81(4)	400(22)		9.2(9)	M1		46, 192.8, 199
604.19(8)	24.4(14)	N				46
624.55(6)	34.6(20)	N				
627.61(5)	149.2(91)		8.4(10)	M1		46, 126.6
644.90(12)	14.4(9)					
673.61(4)	168.5(97)					126.6
700.99(5)	86.2(55)					46
715.39(8)	15.4(40)	N				
729.52(5)	113.4(69)		5.7(10)	M1		
732.51(5)	120.8(73)		7.4(9)	E2		
746.86(12)	10.2(9)	N				
754.38(9)	12.9(9)	N				46
760.46(7)	22.0(14)	N				46
770.74(6)	39.8(29)	N				46
791.69(8)	20.6(13)	N				
794.26(5)	69.0(46)					
797.72(14)	16.9(10)	N				46
800.29(4)	136.1(80)					
806.39(22)	7.5(6)	N				
816.76(5)	129.2(78)	N				
841.66(6)	35.7(22)	N				
843.78(5)	125.6(79)	N				

The level spin and parity assignments are based mainly on the decay properties of levels, the measured internal conversion coefficients, the Hauser-Feshbach analysis of the relative reaction cross section for different levels, and the available γ-ray angular distribution data [41, 44, 45]. A detailed discussion of the level spin-parity assignments is given in Table 3.3.

The ^{72}As level scheme is compared with the formerly known levels in Fig. 3.5. The adopted levels of the Nuclear Data Sheets evaluation (King [48]) contain also the high-spin ($J \geq 5$) states, observed by Mariscotti et al. [45] in (α,npγ) and (α,3npγ) reactions. These were not excited in (p,nγ) reaction at $E_p \leq 6.51$ MeV energy.

The proposed ^{72}As level scheme has many common features with the former (p,nγ) results [41, 42, 43, 44]. The main differences are as follows.

a) The proposed level scheme contains 58 new transitions (mainly in coincidence relations), 38 new transition multipolarities, and many new spin-parity assignments. The 565.7, 715.3, 806.4, 816.8, 839.9, and 843.8 keV levels were introduced into the level scheme for the first time.

b) I found no experimental evidence for the existence of the 243, 333, 343 and 454 keV levels. According to Mordechai et al. [41] these levels decay only to the ground state of ^{72}As directly. I have observed the corresponding four γ rays to be in coincidence with the 45.90 keV transition. Consequently the levels were placed 45.9 keV higher, in agreement with Kimura et al. [43] and Ten Brink et al. [44].

c) My results prove that the 565.1 and 565.7 keV states are two different levels, having different parity. In the former works [43, 44] was already suspected that the 565.4 keV level is a doublet, but the available insufficient data did not allow their separation.

d) According to my measurement the 414 keV transition has M1 multipolarity, contrast with the E1 assignment of Kimura et al. [43]. As the 414 keV transition feeds the 2^- ground state, the 414 keV level must have negative parity. This is confirmed also by the fact that the 559 keV level (which has well established negative parity) decays by an M1 transition to the 414 keV state.

Table 3.3: Spin and parity (J^π) assignments to ^{72}As levels

Level energy (keV)	J^π	Basis of the J^π assignment, comments
0.0	2^-	The shape of β^+ energy spectrum corresponds to first forbidden unique β^+/E. C. decay of ^{72}As ground state [49], log $f^{1u}t$= 8.8 to ^{72}Ge 0^+_1 state [50]
45.90(2)	1^+	The ^{72}Se 0^+_1 state decays with log $ft = 4.49\pm0.05$ to this level [39, 40, 48]
213.71(5)	3^+	E1 transition to 2^-, E2 transition to 1^+ sate, γ-ray angular distribution, agreement with former results [42, 43, 44, 45, 46, 47, 48]
288.49(3)	$(2)^+$	E1 transition to 2^-, M1+E2 transition to 1^+, Hauser-Feshbach analysis, γ-ray angular distribution [44, 48]
309.75(3)	4^-	Pure E2 transition to 2^-, dipole transition to 3^+, agreement with former assignments [43, 45, 48]
318.17(7)	4^+	M1, (E1) transition to 3^+, Hauser-Feshbach analysis, Kimura et al. [43] give also 4^+
362.79(11)	5^-	Dipole transition to 4^-, Hauser-Feshbach analysis. In King's evaluation [48] $J^\pi = (5)$ is given. The 593.5 keV level decays with M1 transitions both to the 362.8 and 309.8 keV levels. As the latter has odd parity, the 362.8 keV level must have also odd parity
380.24(7)	0^+	M1 transition to 1^+, Hauser-Feshbach analysis. Kimura et al. [43] give $0^{(+)}$
390.00(3)	1^+, 2^+	M1 transition to 1^+ state, Hauser-Feshbach analysis
414.38(4)	3^-	M1 transition to 2^-, Hauser-Feshbach analysis. The 559 keV level decays with E2 transition to the ground 2^-, with M1(+E2) transition to 362.8 keV 5^- and with M1 to 414 keV 3^- states, thus all these four levels must have odd parity
438.80(6)	1^+, 2^+	E1 transition to 2^-, M1 transition to $(2)^+$, M1 (+E2) transition to 1^+ states, Hauser-Feshbach analysis
439.90(12)	3^+	M1 transitions to 3^+ and 4^+ states, Hauser-Feshbach analysis. King [48] gives $(3)^+$
482.59(4)	2^+	M1 transition to 1^+, Hauser-Feshbach analysis, γ-ray angular distribution
501.37(2)	2^+	(E1) transition to 2^-, M1 transition to 1^+, M1(+E2) transition to $(2)^+$, Hauser-Feshbach analysis, γ-ray angular distribution
514.04(12)	$(0)^+$	M1 transition to 1^+, Hauser-Feshbach analysis
525.33(3)	3^-	M1 transitions to 2^- and 4^- states, Hauser-Feshbach analysis
558.97(4)	4^-	M1 transition to 3^-, E2 transition to 2^-, M1(+E2) transition to 5^-, Hauser-Feshbach analysis
565.12(4)	1^-, 2^-	M1 transition to 2^-, Hauser-Feshbach analysis

Table 3.3: continued

Level energy (keV)	J^π	Basis of the J^π assignment, comments
565.68(4)	1^+, 2^+	M1 transition to 1^+ state, M1+E2 transition to 1^+, 2^+ level, Hauser-Feshbach analysis
586.41(3)	1^+, 2^+	E1 transition to 2^-, M1 transition to 1^+, Hauser-Feshbach analysis
593.46(4)	4^-	M1 transitions to 4^- and 5^- states, Hauser-Feshbach analysis
624.63(3)	1^+, 2^+	M1 transitions to $(2)^+$ and 1^+, 2^+ states, M1+E2 transition to 1^+, transition to $(0)^+$ state, Hauser-Feshbach analysis
644.81(4)	2^+	M1 transition to 1^+, M1+E2 transition to 1^+, 2^+ state, Hauser-Feshbach analysis, γ-ray angular distribution
650.15(6)	3^+	M1 transitions to $(2)^+$ and 4^+ states, M1+E2 transition to 3^+, Hauser-Feshbach analysis
662.73(27)	≥ 5	γ transition to 5^- state, Hauser-Feshbach analysis. Mariscotti et al. [45] give $J=(\geq 6)$
673.64(3)	2^+	M1 transitions to 1^+ and 1^+, 2^+ states, Hauser-Feshbach analysis, γ-ray angular distribution
707.98(80)	≥ 5	γ transition to 5^-, Hauser-Feshbach analysis
715.28(9)	3^+	M1 transitions to 3^+ and 4^+ states, Hauser-Feshbach analysis
729.53(3)	3^-	M1 transition to $J^\pi = 2^-$, M1+E2 transition to 4^- states, Hauser-Feshbach analysis
732.51(4)	4^-, 0^-	Pure E2 transition to 2^- state, Hauser-Feshbach analysis
742.62(13)	4	γ transition to 5^- state, Hauser-Feshbach analysis
744.96(12)	$4^- - 6^-$	M1 transition to 5^-, Hauser-Feshbach analysis
749.94(3)	2^+, 3^+	M1+E2 transitions to $(2)^+$ and 3^+ states, γ-transitions to 2^-; 1^+ and 1^+, 2^+ states, Hauser-Feshbach analysis
>794		For levels between 794.3 and 843.8 keV the spin assignments are given on the basis of the decay properties of levels (see in the level scheme of Fig. 5) and Hauser-Feshbach analysis. The parities of levels are not known, because of the absence of experimental data on the multipolarities of transitions

3.4 Hauser-Feshbach analysis

In order to determine level spins the theoretical σ_{LEV} (p,n) relative cross sections were calculated at 5.75, 6.16, and 6.21 MeV bombarding proton energies using the computer code CINDY, which was based on the Hauser-Feshbach theory. The trans-

Table 3.4: Optical-model parameters used in this work. (The V, W and V_{so} potential depths are given in MeV and the r range and a diffuseness parameters in fm).

	V	W	V_{so}	r_{re}	r_{im}	a_{re}	a_{im}	Refs.
p+^{72}Ge	58.70−0.55E	12.6	7.5	1.25	1.25	0.30	0.47	[27, 28]
n+^{72}As	47.01−0.267E	9.52	7.0	1.29	1.25	0.66	0.48	[29]
	-0.0018E^2	-0.053E						

mission coefficients were calculated using the optical model parameter sets mentioned in the section 2.1.5, except the real diffuseness parameter for protons, which was reduced in order to adjust the height of the Coulomb barrier. Such a change leads to inappreciable differences in the relative cross section at lower bombarding energies, but near the top of the Coulomb barrier (at my bombarding energies) it enabled to reach general agreement with the former spin assignments [43, 44, 48]. The parameters of the optical potential are given in Table 3.4. The experimental and theoretical cross sections were normalized using the 213.7 keV 3^+ state for positive and 309.8 keV 4^- state for negative parity states. The parities of the states were determined on the basis of transition ICCs. The obtained results are shown in Fig. 3.6.

The Hauser-Feshbach theoretical curves for states J=1 and 2 are not well separated. In order to have unique spin values I have reanalysed the available angular distribution data (measured by Ten Brink et al. [44]), using the computer code CINDY [26]. My results give unambiguous spin 2 for the 483, 501, 645 and 674 keV levels.

3.5 IBFFM calculations and discussion

In order to get an insight into the structure of the low-lying ^{72}As states, we have performed calculation using the interacting boson-fermion-fermion model (IBFFM). The hamiltonian of the model is [51, 52, 53]

$$H_{IBFFM} = H_{IBFM}(\pi) + H_{IBFM}(\nu) - H_{IBM} + H_{RES}(\pi\nu), \tag{3.1}$$

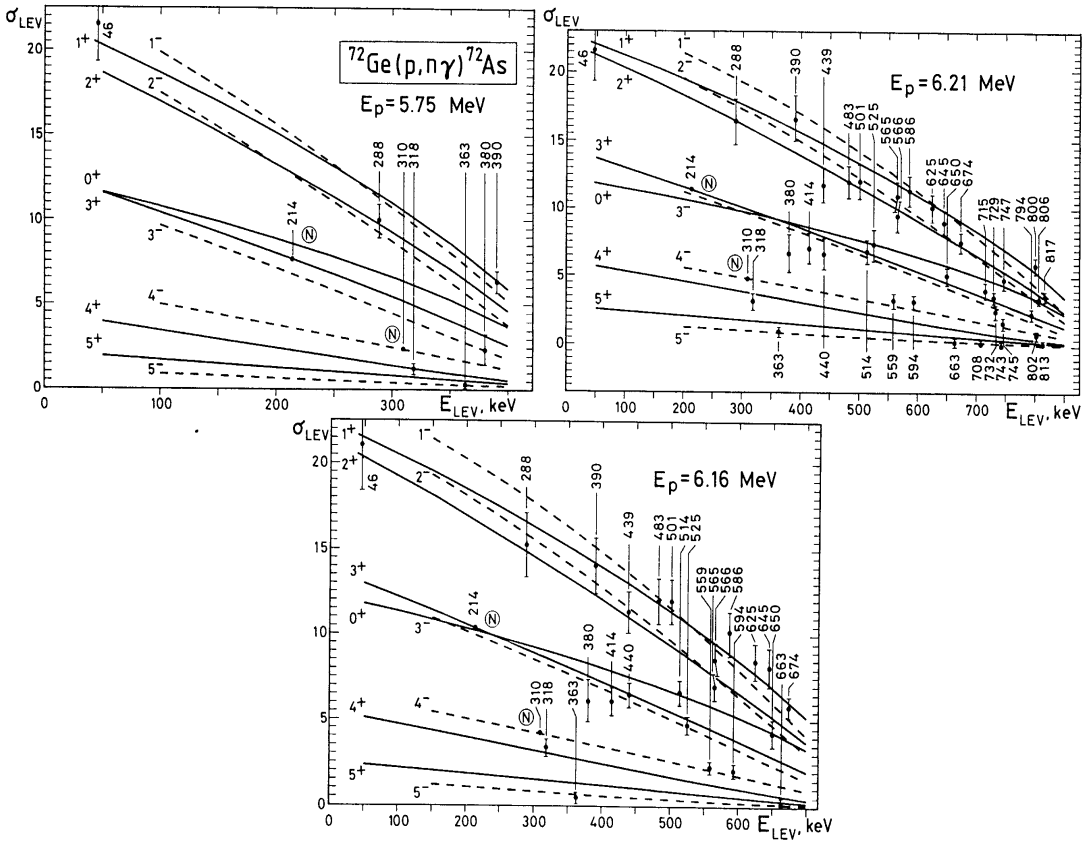

Figure 3.6: *Experimental relative cross sections (σ_{LEV}) of the $^{72}Ge(p,n\gamma)^{72}As$ reaction (dots with error bars) as a function of the ^{72}As level energy (E_{LEV}). The curves show Hauser-Feshbach theoretical results. Encircled N means normalization point. The results obtained at 5.75, 6.16, and 6.21 MeV bombarding proton energies are shown separately.*

where H_{IBM} denotes the IBM hamiltonian for the even-even core nucleus [7, 8], $H_{IBFM}(\pi)$ and $H_{IBFM}(\nu)$ are the IBFM hamiltonians for the neighbouring odd-even nuclei with an odd proton and odd neutron, respectively [9, 10, 54], and $H_{RES}(\pi,\nu)$ is the hamiltonian of the residual interaction. The IBFFM hamiltonian (3.1) was diagonalized in the proton-neutron-boson basis:

$$|\,(j_\pi, j_\nu)j_{\pi\nu}, n_d I; J\rangle,$$

where j_π and j_ν stand for the proton and neutron angular moments coupled to $j_{\pi\nu}$, n_d is the number of d bosons, I is their angular momentum, and J is the spin of the state. The computations were performed using the code IBFFM [55].

In the IBFFM description the ^{72}As nucleus consists of a boson core plus one odd proton and one odd neutron. The core parameters were fitted to the energy spectrum and electromagnetic properties of $^{70}_{32}Ge_{38}$ nucleus. The parameters are: $N = 4$, $h_1 = 0.88$ MeV, $h_2 = -0.3$ MeV, $h_3 = 0.12$ MeV,$h_{40} = 0.2$, $h_{42} = -0.4$, $h_{44} = -0.08$. This reduced boson number leads to a smaller boson space and substantially reduces the scope of calculations for odd-odd ^{72}As nucleus, without sizeably affecting the results. In the second step of calculation we have adjusted the parameters of the IBFM(π) hamiltonian to the low-energy spectrum and electromagnetic properties of $^{71}_{33}As_{38}$. In the third step of our calculation we have fitted the parameters of the IBFM(ν) hamiltonian to the energy levels and electromagnetic properties of $^{71}_{32}Ge_{39}$. For ^{70}Ge, ^{71}As and ^{71}Ge energy spectra, B(E2), B(M1) reduced transition probabilities, γ-branching ratios and electromagnetic moments were deduced. The calculated states were assigned to the experimental levels on the basis of energy, spin, parity, one-nucleon transfer reaction data, where available [56, 57, 58, 59], decay properties, and wave functions. The low-energy level spectrum of ^{70}Ge, ^{71}As and ^{71}Ge and the electromagnetic moments were reasonably reproduced by the IB(F)M calculations. The main γ-branchings were also correctly predicted in most cases. The calculated IBFM energy spectra for ^{71}As and ^{71}Ge compared with the available experimental data are presented in Fig. 3.7 and in Fig. 3.8, respectively.

In the fourth, final step of our calculation, we have calculated the low-energy level spectrum and electromagnetic properties of $^{72}_{33}As_{39}$. The quasiparticle energies (E in MeV), boson-fermion interaction parameters (A_0, Γ_0, Λ_0 in MeV) and strengths of residual interaction (V_δ, $V_{\sigma\sigma}$, V_t in MeV) have been adjusted to the level spectrum of ^{72}As. They are as follows: $E(\pi\tilde{p}_{3/2}) = 0$, $E(\pi\tilde{f}_{5/2}) = 0.41$, $E(\pi\tilde{p}_{1/2}) = 0.74$, $E(\pi\tilde{g}_{9/2}) = 2.2$, $E(\pi\tilde{d}_{5/2}) = 5.2$, $E(\nu\tilde{p}_{3/2}) = 0.95$, $E(\nu\tilde{f}_{5/2}) = 0.53$, $E(\nu\tilde{p}_{1/2}) = 0$, $E(\nu\tilde{g}_{9/2}) = 0.2$, $E(\nu\tilde{d}_{5/2}) = 3.2$, $A_0^\pi = 0.05$, $\Gamma_0^\pi = 0.5$, $\Lambda_0^\pi = 0.5$ for positive and 1.5 for negative parity states, $A_0^\nu = 0$, $\Gamma_0^\nu = 0.55$ for positive and 0.45 for negative parity states, $\Lambda_0^\nu = 1.3$ for positive and 5.5 for negative parity states. The strengths of residual interaction are $V_\delta = 0$ for positive and -0.6 for negative parity states, and $V_{\sigma\sigma} = 0$, $V_t = 0.015$. Here, in order to improve the agreement with experiment, some of the quasiparticle energies and boson-fermion interaction strengths have been

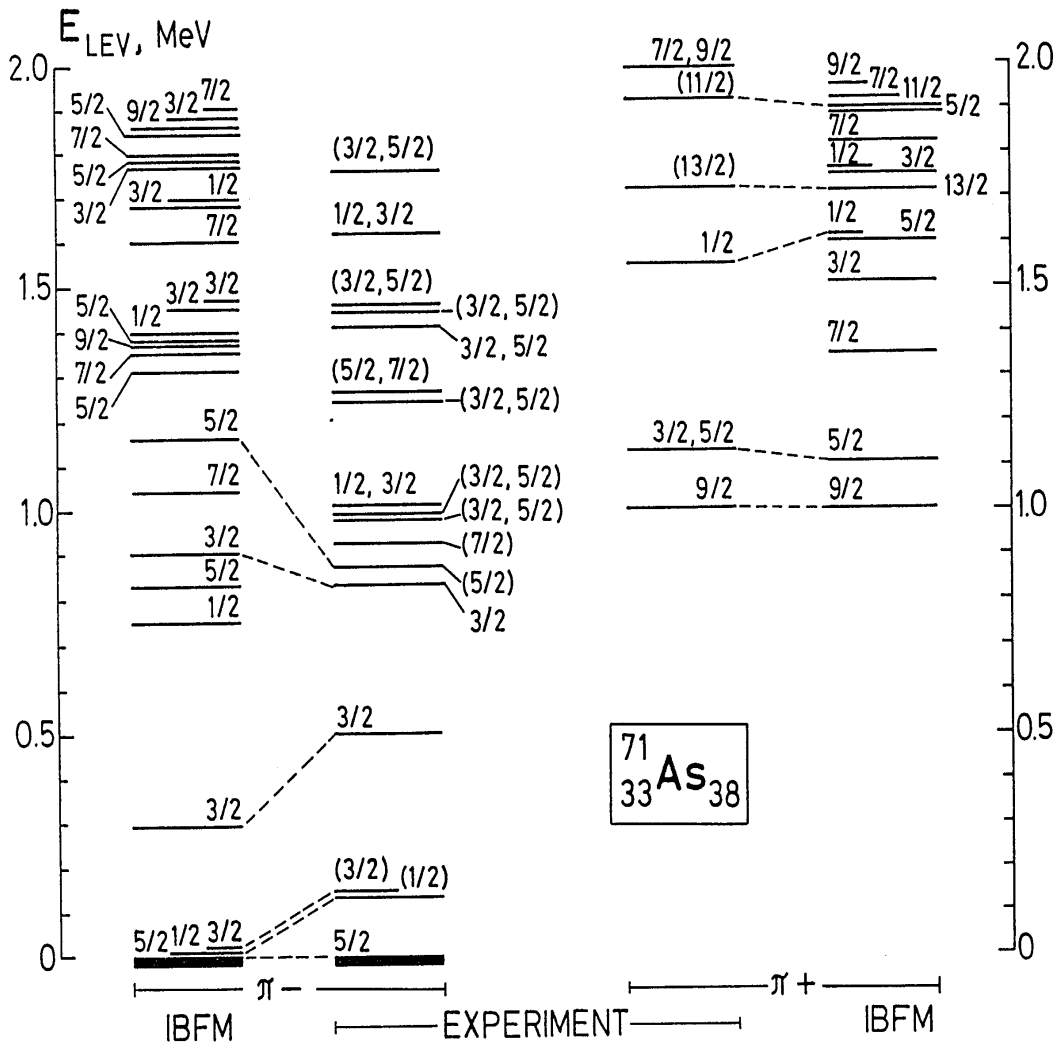

Figure 3.7: *Calculated IBFM energy spectra of the low-lying states of* ^{71}*As in comparison with experimental data [53]. The positive* (π +) *and negative* (π −) *parity states are shown separately.*

modified with respect to the values from the IBFM calculations in the second and third steps. In particular, we note the increase of the energy of $\pi\tilde{f}_{5/2}$ quasiparticle, the increase of the strengths of boson-fermion dynamical interaction Γ_0^ν for negative parity states, and the modification of the exchange interaction strengths. Such a renormalization seems to be in accordance with the general observation in the regions of soft nuclei, that the dynamical deformation can change sizeably, if one nucleon is added. This is consistent with the finding that odd-odd nuclei are in many cases

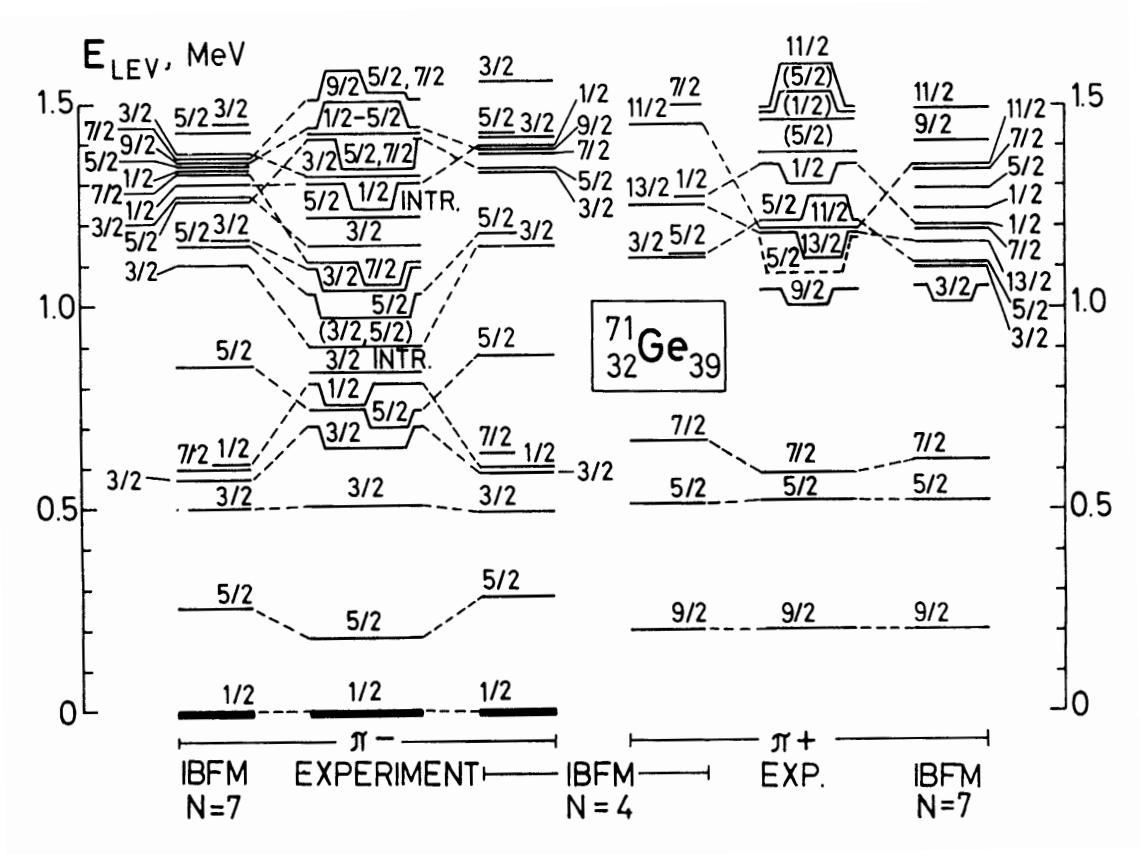

Figure 3.8: *Experimental [53] and theoretical IBFM energy spectra of the low-lying states of* ^{71}Ge.

more deformed than their odd-even neighbours. The increase of the strength of boson-fermion interaction causes overall shifts of proton-neutron multiplets, i.e. an effective renormalization of quasiparticle energies, in accordance with the parabolic rule [61].

The IBFFM energy spectrum of ^{72}As is compared with the experimental one in Fig. 3.9. The main components of the wave functions of some low-lying states are presented in Table 3.5.

Using the wave functions of ^{72}As we have calculated the electric quadropole and magnetic dipole static moments and γ-ray branching ratios (Tables 3.6 and 3.7). In these calculations the effective charges and gyromagnetic ratios were: $e^\pi = 1.5\ e$, $g_l^\pi = 1$, $g_s^\pi = 0.7 g_s^\pi(\text{free}) = 3.910$, $g_t^\pi = \frac{1}{25} < r^2 > g_s^\pi(free) = 3.34$, $e^\nu = 0.5\ e$, $g_l^\nu = 0$, $g_s^\nu = 0.7 g_s^\nu$ (free) $= -2.678$, $g_t^\nu = \frac{1}{13} < r^2 > g_s^\nu(free) = -4.40$. Here all values are in accordance with standard estimates, only g_t^ν was enchanced.

Table 3.5: Wave function of some low-lying states of ^{72}As. Only components with >10% weight are given. The basis states are $\mid (j_\pi j_\nu) j_{\pi\nu}, n_d I; J >$ (see in text).

J^π(theor.)	$(j_\pi, j_\nu) j_{\pi\nu}; n_d I$	Amplitude	J^π(theor.)	$(j_\pi, j_\nu) j_{\pi\nu}; n_d I$	Amplitude
0_1^+	(3/2,3/2)0;00	0.603	1_1^-	(5/2,9/2)2;12	0.661
	(3/2,3/2)0;20	−0.417		(5/2,9/2)2;32	−0.332
	(3/2,3/2)2;12	0.375	2_1^-	(5/2,9/2)2;00	0.740
1_1^+	(3/2,5/2)1;00	0.638		(5/2,9/2)2;20	−0.394
	(3/2,5/2)1;20	−0.424	3_1^-	(5/2,9/2)3;00	0.644
1_2^+	(3/2,1/2)1;00	0.837		(5/2,9/2)3;20	−0.349
	(3/2,1/2)1;20	−0.391		(5/2,9/2)5;12	−0.324
2_1^+	(3/2,1/2)2;00	0.659	3_2^-	(3/2,9/2)3;00	0.704
	(3/2,5/2)2;00	0.349		(3/2,9/2)3;20	−0.376
2_2^+	(3/2,1/2)2;00	−0.546	3_3^-	(3/2,9/2)5;12	−0.402
	(3/2,5/2)2;00	0.452	4_1^-	(1/2,9/2)4;00	0.521
	(3/2,5/2)1;12	−0.335		(5/2,9/2)4;00	−0.440
3_1^+	(5/2,5/2)3;00	0.396	4_2^-	(3/2,9/2)4;00	0.623
	(1/2,5/2)3;00	0.332		(3/2,9/2)4;20	−0.326
	(5/2,5/2)4;12	0.329	4_3^-	(3/2,9/2)6;12	0.433
4_1^+	(3/2,5/2)4;00	0.519		(5/2,9/2)2;12	0.364
	(3/2,5/2)4;12	0.439		(3/2,9/2)4;00	−0.352
	(3/2,5/2)4;20	−0.354	5_1^-	(1/2,9/2)5;00	−0.502
				(5/2,9/2)7;12	−0.414
			7_1^-	(5/2,9/2)7;00	0.697
				(5/2,9/2)7;20	−0.395

Table 3.6: Calculated electric quadropole and magnetic dipole static moments of ^{72}As and comparison with available experimental data (Raghavan [55], if otherwise not indicated).

Nucleus	J^π	$Q(e\cdot\mathrm{b})$		$\mu(\mu_N)$	
		Theor.	Exp.	Theor.	Exp.
^{72}As	2_1^-	−0.132	−0.082(24)	−1.809	−2.1578(22)[48]
	6_1^-	−0.147		0.874	+0.696(12)
	3_1^+	0.229		1.525	+1.581(18)[48]

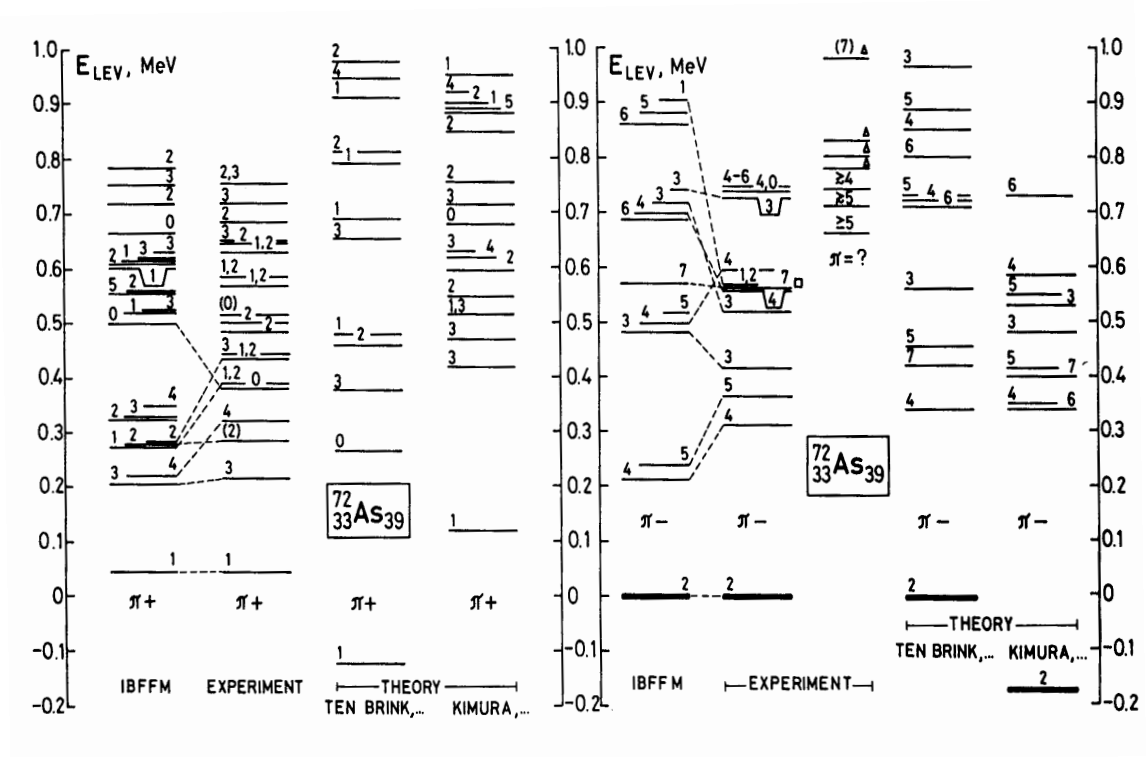

Figure 3.9: *Experimental energy spectra of ^{72}As in comparison with the present IBFFM and former theoretical calculations (Ten Brink et al. [37] and Kimura et al. [36]). For △ and □ see caption of Fig. 10.*

The IBFFM theoretical levels are assigned to the experimental ones mainly on the basis of energy, spin, parity, and decay properties. As seen in Fig. 3.9, the lowest-lying experimental levels have counterparts in the theoretical spectrum.

On the basis of magnetic dipole momentum measured by Hogervorst et al. [63], the 2^- ground state of ^{72}As has $\pi\tilde{f}_{5/2}\nu\tilde{g}_{9/2}$ configuration. The IBFFM calculations confirm these results: in the 2^-_1 ground state and the 3^-_1 and 7^-_1 excited states the dominating configuration is $\pi\tilde{f}_{5/2}\nu\tilde{g}_{9/2}$ (Table 5.3). In a recent publication Döring et al. [47] assigned to the 562.8 keV level the $7^{(-)}$ spin parity [instead of the former assignment (6)]. This state may be the 7^- member of the $\pi\tilde{f}_{5/2}\nu\tilde{g}_{9/2}$ multiplet.

The IBFFM calculations show that the 4^-_1 and 5^-_1 states have the main configuration $\pi\tilde{p}_{1/2}\nu\tilde{g}_{9/2}$, with 4^-_1 state lying below the 5^-_1. This is in agreement with the experimental results and also with the prediction of the parabolic rule.

On the basis of lifetime measurements and other considerations Hübner [40] came

Table 3.7: Calculated E2 and M1 transitions for ^{72}As in IBFFM and comparison with the experiment.

E_{lev}(MeV)	Transition	I_γ		E_{lev}(MeV)	Transition	I_γ	
J^π(exp.)	J^π(theor.)	Theor.	Exp.	J^π(exp.)	J^π(theor.)	Theor.	Exp.
0.3097	$4_1^- \to 2_1^-$	100	100	0.7295	$3_3^- \to 4_2^-$	0.3	
4^-				3^-	$\to 1_1^-$	0.002	
0.3628	$5_1^- \to 4_1^-$	100	100		$\to 4_3^-$	6.4	8(2)
5^-					$\to 3_2^-$	12	
0.4144	$3_1^- \to 5_1^-$	0.000			$\to 3_1^-$	4.2	4(1)
3^-	$\to 4_1^-$	0.3			$\to 5_1^-$	0.02	
	$\to 2_1^-$	100	100		$\to 4_1^-$	21	43(7)
0.5253	$3_2^- \to 3_1^-$	0.4			$\to 2_1^-$	100	100
3^-	$\to 5_1^-$	0.001		0.2137	$3_1^+ \to 1_1^+$	100	100
	$\to 4_1^-$	39	60(8)	3^+			
	$\to 2_1^-$	100	100	0.2885	$2_1^+ \to 3_1^+$	0.3	9(3)
0.5590	$4_3^- \to 3_2^-$	8.3		$(2)^+$	$\to 1_1^+$	100	100
4^-	$\to 3_1^-$	283	52(6)	0.3182	$4_1^+ \to 2_1^+$	0.000	
	$\to 5_1^-$	80	15(2)	4^+	$\to 3_1^+$	100	100
	$\to 4_1^-$	350		0.3802	$0_1^+ \to 2_1^+$	0.0001	
	$\to 2_1^-$	100	100	0^+	$\to 1_1^+$	100	100
0.5651	$1_1^- \to 3_2^-$	0.000		0.3900	$1_2^+ \to 0_1^+$	0.002	
$1^-, 2^-$	$\to 3_1^-$	0.001	1.3(5)	$1^+, 2^+$	$\to 2_1^+$	0.4	
	$\to 2_1^-$	100	100		$\to 3_1^+$	0.00004	
0.5935	$4_2^- \to 4_3^-$	0.1			$\to 1_1^+$	100	100
4^-	$\to 3_2^-$	14		0.4388	$2_2^+ \to 1_2^+$	0.001	
	$\to 3_1^-$	27	41(5)	$1^+, 2^+$	$\to 0_1^+$	0.000	
	$\to 5_1^-$	95	31(4)		$\to 4_1^+$	0.000	
	$\to 4_1^-$	100	100		$\to 2_1^+$	45	13(4)
	$\to 2_1^-$	0.0004			$\to 3_1^+$	3.8	
					$\to 1_1^+$	100	100

to the conclusion that the 1_1^+ state of the ^{72}As has either $\pi p_{3/2}^{-1}\nu f_{5/2}^{-1}$ or $\pi p_{3/2}^{-1}\nu p_{1/2}$ configuration. The IBFFM calculations give the $\pi\tilde{p}_{3/2}\nu\tilde{f}_{5/2}$ dominating configuration for this state. The parabolic rule predicts an open-down parabolic energy splitting for the $\pi\tilde{p}_{3/2}\nu\tilde{f}_{5/2}$ multiplet, with a minimum energy for the 1^+ state. The 4^+ member of this multiplet may be the 4_1^+ state. The 2^+ and 3^+ members of this

multiplet are in IBFFM more fragmented (e. g. into 2_1^+, 2_2^+ etc., see Table 3.5).

According to Bertschat et al. [42] the best agreement between the predicted and measured g-factors of the 3_1^+ state at 214 keV is obtained for the $\pi f_{5/2}\nu f_{5/2}^{-1}$ and $\pi f_{5/2}\nu p_{1/2}$ configurations. Our IBFFM calculation indicates a mixed configuration for this state, with $\pi \tilde{f}_{5/2}\nu \tilde{f}_{5/2}$ configuration being the strongest one. The parabolic rule predicts an open-up parabolic splitting for the $\pi \tilde{f}_{5/2}\nu \tilde{f}_{5/2}$ multiplet, with a minimum energy for the 3^+ (or 4^+) member.

The calculated branching ratios ^{72}As are in a reasonable agreement with experimental data for most transitions, but there are some pronounced discrepancies. The main branches seem to be correctly predicted for decays of 3_1^-,3_2^-, 1_1^-, 4_2^-, 3_3^-, 2_1^+, 4_1^+, 0_1^+, 1_2^+ and 2_2^+ levels. However, there is a discrepancy with decay pattern of the 4_3^- level: the strongest theoretical branch is $4_3^- \rightarrow 4_1^-$, while experimentally this transition was not observed. The calculated reduced transition probability $B(E2;3_1^+ \rightarrow 1_1^+)$ is by an order of magnitude smaller than the experimental value.

Prior to the present work, Ten Brink et al. [44] calculated the energy spectra and electromagnetic properties of ^{72}As, using a number conserving BCS quasiproton-quasineutron model. They used a Schiffer force for the effective proton-neutron interaction. It was supposed that the nuclear core is spherical and the phonon degrees of freedom were neglected. Kimura et al. [43] have also calculated the level spectra of ^{72}As using harmonic oscillator wave functions and a spin dependent δ interaction as proton-neutron residual interaction.

The experimental energy spectrum of ^{72}As is compared with the results of present and former theoretical calculations in Fig. 3.9. Below 800 keV excitation energy 36 levels were observed experimentally, while the IBFFM calculations predict 34 states compared to 21 [43] and 17 [44] ones from quasiparticle calculations.

Chapter 4

Study of the ^{73}As nucleus

4.1 Previous studies

The energy levels of ^{73}As have been studied earlier by gamma spectroscopic methods from ^{73m,g}Se β^+-decay by Marlow and Faas [64], Meeker and Tucker [65] and Ten Brink *et al.* [66], from (p,nγ) reaction by van der Merwe *et al.* [67] and Ten Brink *et al.* [66], and from (α,2n) and ^{58}Fe(^{18}O,p2n) reactions by Heits *et al.* [68]. The structure of the nucleus was investigated also by single proton transfer reactions by Ramaswamy *et al.* [69], M. Schrader *et al.* [70] and Rotbard *et al.* [71], as well as from (p,t) reaction by Vergnes *et al.* [72]. These studies extended our knowledge on the level scheme of ^{73}As considerably, nevertheless they are somewhat inconsistent, as some of the levels were observed only in one or another work, and, the level spins are different in different studies. Unambiguous spin–parity values could be assigned only to five levels in the 1993 Nuclear Data Sheets evaluation [73]. The earlier studies are summarized in Table 4.1.

4.2 Experimental results

γ-ray spectra of the ^{73}Ge(p,nγ)^{73}As reaction were measured at 1.92, 2.27, 2.45, 2.75 MeV for determination of the energies and the intensities of the transitions and for Hauser–Feshbach analysis, and at 4 MeV bombarding proton energy for obtaining of the internal conversion coefficients. The measurement of $\gamma\gamma$–coincidence events, as well as of the internal conversion electron spectra were performed also at E_p=4.0 MeV. The intensities of proton beams were between 0.1–1 μA.

Table 4.1: Summary of the former experimental studies of the structure of ^{73}As

Reference *	Reaction	Techniques, detectors	Measurements	Results
Marlow (1969) [64]	decay of ^{73g,m}Se	Ge(Li) detectors, NaI(Tl) scintillators	E_γ, I_γ, $\gamma\gamma$-coinc	50 γ rays identified and placed in the level schemes, logft values for 21 levels deduced, unambiguous J^π assignments for 3 states, γ-branching given
Meeker (1970) [65]	decay of ^{73g,m}Se	Ge(Li) detectors, NaI(Tl) scintillators	E_γ, I_γ, $\gamma\gamma$-coinc	50 γ rays identified and placed in the level schemes, $\gamma\gamma$-coincidence relations given for 7 γ rays, deduced logft values for 20 levels, J^π assignments for 3 state
Ten Brink (1980) [66]	decay of ^{73g,m}Se, ^{72}Ge(p,nγ)^{73}As, E_p=1.6-3.1 MeV, ^{72}Ge(^{3}He,d)^{73}As, $E_{^3He}$=21 MeV	in-beam techniques, Ge(Li) detectors magnetic split pole spectrograph	E_γ, I_γ, $\gamma\gamma$-coinc, E_d	124 γ rays from decay and 73 γ rays from (p,nγ) reaction identified and placed in the level schemes, logft values deduced for 31 levels, unambiguous J^π assignments for 7 states
Merwe (1975) [67]	^{73}Ge(p,n)^{73}As, ^{73}Ge(p,nγ)^{73}As, E_p=2.1-3.3 MeV	in-beam and time of flight techniques, plastic scintillator, Ge(Li) detectors	E_γ, I_γ, nγ-coinc, $\sigma(E,\theta_\gamma)$, $\sigma(E_\gamma,E_n)$	65 transitions identified and placed in the level scheme, A_2, A_4 factors deduced for 15 γ rays, mixing ratio δ given for 13 transitions, the level scheme contains, 39 states up to 1980 keV with 5 unambiguous J^π assignments, Hauser-Feshbach analysis for 7 levels
Heits (1977) [68]	^{71}Ga(α,2n)^{73}As, E_α=17-24 MeV, ^{58}Fe(^{18}O,p2n)^{73}As, $E_{^{18}O}$=40-52 MeV,	in-beam techniques, Ge(Li) detectors	E_γ, I_γ, $\gamma\gamma$-coinc $\sigma(E,E_\gamma,\theta_\gamma)$	33 transitions identified and placed in the level scheme, A_2, A_4 factors deduced for 13 transitions, the high spin level scheme constructed up to 4.1 MeV with 6 unambiguous J^π assignments

Table 4.1: continued

Reference *	Reaction	Techniques, detectors	Measurements	Results
Ramaswamy (1979) [69]	^{72}Ge(^{3}He,d)^{73}As $E_{^3He}$=20 MeV	in-beam techniques, multigap magnetic spectrograph with K2 nuclear emulsion plates	σ(E,θ)	l_p and spectroscopic factors deduced for 30 levels
Schrader (1976) [70]	^{72}Ge(^{3}He,d)^{73}As $E_{^3He}$=23 MeV	in-beam techniques, Q3D magnetic spectrograph with sensitive wire proportional counter	σ(E_d,θ)	l_p and spectroscopic factors determined for 21 levels
Rotbard (1983) [71]	^{74}Se(d,^{3}He)^{73}As E_d=25.2 MeV	in-beam techniques, split pole magnetic spectrometer with solid-state position sensitive detectors	σ(E_d,θ)	18 levels deduced, l_p and spectroscopic factors determined for them
Vergnes (1976) [72]	^{75}As(p,t)^{73}As E_p=26 MeV	in-beam techniques, split pole magnetic spectrometer with solid-state position sensitive detectors	$\sigma(\theta)$	deduced levels with 8 unambiguous J^π assignments
King, Chou (1993) [73]				compilation

* Only the first author is indicated in this column.

Identification of γ rays was based first of all on $\gamma\gamma$ coincidence relations. The strongest lines of ^{73}As were already known, what ensured the identification of the coincident γ rays. In addition to the ^{73}As lines the spectra contained peaks also from ^{73}Ge(p,p')^{73}Ge and ^{73}Ge(p,γ)^{74}As reactions and from the radioactive decay of

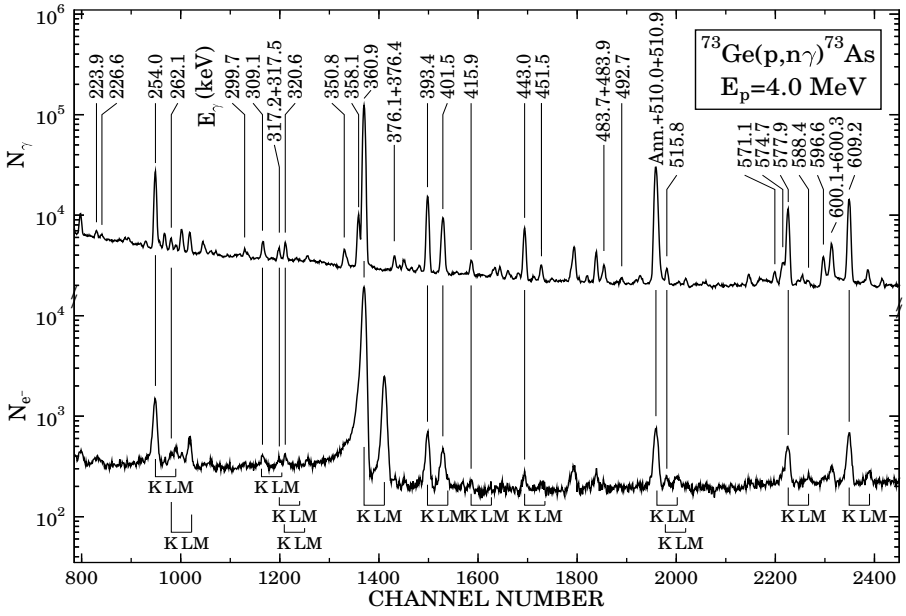

Figure 4.1: *Typical γ-ray and internal conversion electron spectra of the $^{73}Ge(p,n\gamma)^{73}As$ reaction. The energies of γ rays are given only for the strongest ^{73}As lines. Corresponding conversion electron peaks are also indicated.*

reaction products, but the level schemes of these nuclei are well-known from the previous works [73, 17] and the contaminating lines could be identified. The ∼30 million $\gamma\gamma$-coincidence events were recorded in event-by-event mode. The good statistics of the $\gamma\gamma$-coincidence measurement enabled unambiguous identification for all γ rays observed in the singles spectra. If a γ ray was unresolved or weak in singles spectra, its energy and intensity was determined from gated spectra. Typical γ-ray and internal conversion electron spectra are shown in Fig. 4.1. The energies and intensities of γ rays observed in the ^{73}Ge(p,nγ)^{73}As reaction at 2.75 MeV bombarding proton energy are listed in Table 4.2. About 70% more γ transitions could be assigned to ^{73}As as were previously known.

The $\gamma\gamma$ coincidence relations were measured at 4 MeV proton energy in order to observe also feeding transitions for all the levels below 1.5 MeV excitation energy. In Table 4.2 the coincidence relations have been summarized between those transitions, which were obtained at 2.75 MeV bombarding energy.

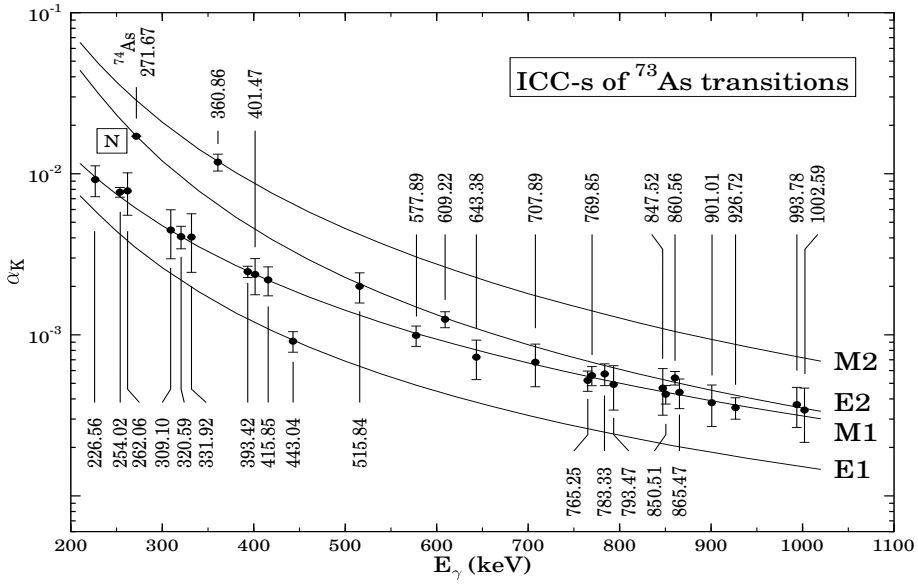

Figure 4.2: *Experimental (symbols with error bars) and theoretical (curves) internal conversion electron coefficients of ^{73}As transitions as a function of the γ-ray energy.*

Internal conversion coefficients (ICC) were determined from the internal conversion electron and γ-ray spectra. For normalization of the experimental ICCs I have used the theoretical α_K value [25] of the 271.67 keV stretched E2 ^{74}As transition [17]. The theoretical and experimental ICCs of the ^{73}As transitions are shown in Fig. 4.2. In the case of the 643, 865 and 994 keV doublets, as the intensities of the weaker components are smaller than the statistical errors of the intensities of the stronger ones, the given ICCs correspond to the stronger transitions. On the basis of ICCs and the recommended upper limits for transition probabilities [74] multipolarities were assigned to 28 transitions, from which 20 are new. The obtained ICCs, as well as the deduced and formerly known multipolarities are given in Table 4.2.

4.3 Discussion of the level scheme of ^{73}As

The construction of the level scheme was based on the $\gamma\gamma$–coincidence measurements, on the energy and intensity balance of transitions and on the results of γ-ray excitation function measurement. The proposed level scheme is shown in Figs. 4.3 (low-energy part) and 4.4 (higher-energy part). Above 1344 keV, the highest energy

Table 4.2: Energy, intensity, internal conversion coefficient, multipolarity and coincidence relations of γ rays of the ^{73}Ge(p,nγ)^{73}As reaction

E_γ (keV)	I_γ [a]) (relative)	ICC measurements $10^4\times\alpha_K$	ICC measurements Multip. of γ ray	Former results on multip. of γ rays [73]	Coincident γ rays E_γ(keV)				
67.06(3)	8672(892)			M1+E2	224	227	283	300	317
					351	358	361	416	443
					451	484	511	575	588
					600	643	689	697	703
					708	765	767	783	787
					793	814	819	865	901
					927	979	1020	1111	1154
					1232	1277			
84.36(4)	50.0(94)			[M1]	139	170	181	195	262
					309	311	317	321	358
					376	401	451	467	490
					493	503	512	516	571
					575	597	600	647	689
					694	697	725	765	767
					787	819	828	833	909
					931	951	979	994	1003
					1215				
116.59(14)	5.0(10)				393				
139.44(4)	2.9(12)			M1+E2	84	170	181	254	262
					300	332	351	358	376
					451	457	467	493	600
					647	689	694	697	725
					767	787	828	909	931
					951				
169.64(8)	2.2(4)				84	139	300	321	401
					484	516	600	647	689
					694	708	725	765	833
					931	935			
181.15(4)	1.9(9)			M1+E2	84	139	254	309	311
					332	393	503	512	725
184.44(20)	0.8(4)				84	393			
191.92(15)	0.9(6)				67	511	578		
195.07(18)	0.9(5)				67	84	254	262	393
					401	571			

Table 4.2: continued

E_γ (keV)	I_γ [a]) (relative)	ICC measurements $10^4\times\alpha_K$	ICC measurements Multip. of γ ray	Former results on multip. of γ rays [73]	Coincident γ rays E_γ(keV)				
223.93(5)	5.2(7)				67	254	351	376	393
					516	703	770		
226.56(17)	0.9(6)	92(20)	M1(+E2)		67	393	467	793	861
254.02(2)	76.9(83)	77(6)	M1	M1(+E2)	139	195	224	262	311
					317	321	324	332	351
					358	376	401	408	432
					451	457	467	493	503
					512	516	566	575	597
					600	632	644	647	689
					725	767	787	792	819
					824	833	931	935	979
					1045				
256.20(20)	4.4(6)				609				
262.06(3)	2.8(12)	78(23)	M1+E2	M1+E2	84	139	169	254	309
					358	393	432	566	647
					689				
282.66(9)	1.0(2)				67	511	578		
299.68(20)	4.3(7)				67	84	224	309	393
					416	443	484	510	511
					578	600	927	994	
309.10(5)	9.3(10)	45(15)	M1+E2	M1+E2	84	181	224	262	311
					332	351	358	376	451
					467	467	484	493	512
					575	600	647	689	694
					697	725	828	909	931
					951				
311.45(15)	0.6(2)				84	181	254	321	332
					393				
317.18(6)	2.0(8)				67	84	254	376	393
317.50(15)	3.0(25)				467	511	516	703	770
					793	861			
					793	861			
320.59(3)	6.0(7)	41(7)	M1(+E2)	M1	84	170	254	311	332
					503	512	725		
323.95(10)	1.2(6)				254				

Table 4.2: continued

E_γ (keV)	I_γ [a] (relative)	ICC measurements $10^4\times\alpha_K$	ICC measurements Multip. of γ ray	Former results on multip. of γ rays [73]	Coincident γ rays E_γ(keV)				
331.92(12)	2.8(5)	40(16)	M1+E2		67	84	139	254	309
					311	321	376	393	493
					510	632			
350.77(3)	8.5(10)				67	224	254	393	416
					443	484	510	511	516
					578	600	703	927	994
358.09(4)	1.1(3)				67	84	139	170	254
					262	309	393	401	571
					656				
360.86(2)	1000(101)	118(14)	M2	M2	67				
376.08(7)	1.0(6)				67	84	139	224	254
376.42(4)	5.1(7)				309	317	332	393	408
					443	451	510	575	787
393.42(2)	84.4(85)	25(3)	M1	M1+E2	117	181	184	195	224
					262	283	300	311	317
					332	351	358	376	408
					451	457	467	484	493
					503	512	600	647	689
					694	697	725	765	787
					792	814	819	827	909
					931	951	979		
401.47(2)	27.5(28)	24(6)	M1+E2	M1+E2	84	170	195	254	358
					432	566	644	647	689
408.19(20)	2.7(3)				67	254	376	393	516
					703	770			
415.85(5)	10.2(11)	22(5)	M1(+E2)		67	184	300	351	393
					511	578			
431.59(20)	1.0(7)				254	262	401		
441.68(20)	1.8(11)				67	793	861		
443.04(2)	41.1(41)	9.1(13)	E1		67	351	376	484	708
					765	783	792	814	819
451.45(2)	9.7(10)				67	84	254	309	376
					393	511	516	578	703
					770				
457.04(12)	1.3(2)				139	254	309	393	

Table 4.2: continued

E_γ (keV)	I_γ [a]) (relative)	ICC measurements $10^4\times\alpha_K$	Multip. of γ ray	Former results on multip. of γ rays [73]	Coincident γ rays E_γ(keV)				
467.15(5)	6.6(7)				84	139	254	309	317
					393	697			
483.72(3)	7.6(15)				67	300	351	443	467
483.94(20)	2.8(10)				510	793	861		
490.23(12)	0.6(2)				84	725			
492.71(8)	2.3(3)				84	139	254	309	332
					393				
503.39(15)	1.5(9)				84	139	181	254	321
					393				
510.03(10)	214.1(270)				376	484	708	765	783
					792	814	819		
510.86(10)	59.6(174)				67	192	283	300	351
					416	484	575	600	643
					767	787	979		
512.45(10)	1.0(7)				84	181	242	309	321
					393				
515.84(3)	9.0(10)	20(4)	E2(+M1)		84	170	224	254	317
					408	451	575	787	
565.86(20)	3.0(10)				67	84	254	393	401
					571				
571.09(6)	5.5(12)				84	195	358	432	566
					647	689			
574.72(20)	9.5(12)				67	84	254	309	376
					93	511	516	703	770
577.89(2)	83.9(98)	9.9(14)	M1(+E2)		192	283	351	416	451
					600	643	697	767	979
588.39(15)	2.3(5)				67	358	647	689	
596.57(12)	1.1(6)				254				
600.13(15)	7.9(41)				67	84	139	254	300
600.31(3)	33.0(36)				309	351	393	511	578
609.22(2)	177.6(191)	12.5(14)	E2(+M1)	[E2]	256				
632.14(11)	0.4(3)				254	332			
643.38(3)	8.2(15)	7.3(20)	M1+E2		67	511	578		
643.96(20)	0.5(3)				254	262	393	401	571

Table 4.2: continued

E_γ (keV)	I_γ [a] (relative)	ICC measurements $10^4\times\alpha_K$	ICC measurements Multip. of γ ray	Former results on multip. of γ rays [73]	Coincident γ rays E_γ(keV)				
646.82(20)	0.2(1)				84	254	262	393	401
					571	656			
655.50(11)	2.7(8)				195	358	4332	689	
689.03(3)	15.8(16)				67	84	170	254	262
					309	393	401	571	588
					655				
693.59(8)	3.2(6)				84	139	254	309	393
702.77(2)	32.2(33)				67	224	317	408	451
					575	787			
707.89(3)	5.3(10)	6.8(20)	M1,E2		67	443	510		
724.35(20)	2.5(12)								
724.69(20)	3.1(14)				84	181	254	321	393
					490				
765.25(20)	52.2(53)	5.2(8)	M1+E2		67	443	510		
766.65(20)	12.7(40)				67	511	578		
769.85(2)	54.4(62)	5.6(8)	M1+E2		224	317	408	451	575
					787				
783.33(2)	69.8(71)	5.7(9)	M1,E2		67	443	510		
792.12(20)	2.2(7)				67	443	510		
793.47(2)	90.1(92)	4.9(15)	M1,E2		67	227	317	442	484
					697				
814.06(7)	5.8(8)				67	443	510		
818.76(15)	14.0(20)				67	443	510		
823.99(8)	1.2(5)				254				
827.83(15)	3.1(20)				84	139	254	309	393
833.07(23)	6.4(32)				84	170	254		
847.52(12)	32.6(33)	4.7(15)	M1,E2						
850.51(2)	63.3(64)	4.3(6)	M1(+E2)						
860.56(2)	143.6(145)	5.4(6)	E2(+M1)		227	317	442	484	697
865.47(30)	232.6(277)	4.4(9)	M1,E2						
865.47(30)	18.1(151)								
901.01(2)	46.4(48)	3.8(11)	M1,E2						
908.86(20)	2.8(11)				84	139	254	309	393
926.72(2)	71.2(77)	3.5(6)	M1+E2		67	300	351		
930.77(4)	4.4(22)				84	139	254	309	393

Table 4.2: continued

E_γ (keV)	I_γ [a]) (relative)	ICC measurements $10^4\times\alpha_K$	ICC measurements Multip. of γ ray	Former results on multip. of γ rays [73]	Coincident γ rays E_γ(keV)				
934.82(15)	2.3(8)				84	170	254		
951.02(16)	2.1(10)				84	139	254	309	393
993.63(10)	0.7(4)				{ 84	300	351		
993.78(2)	91.1(154)	3.7(10)	E2,M1						
1002.59(7)	8.0(44)	3.4(13)	E2,M1		84				
1019.87(13)	3.0(5)				67				
1045.33(6)	0.7(5)				254				
1077.91(20)	5.3(6)								
1086.99(5)	4.4(5)								
1111.00(2)	129.2(157)				67				
1154.25(2)	83.2(85)				67				
1214.97(20)	0.5(4)				84				
1232.30(15)	0.7(5)				67				
1277.47(20)	31.0(32)				67				
1302.25(4)	11.2(13)								
1324.19(3)	7.3(9)								
1344.57(12)	2.8(5)								

[a]) Relative intensities at 2.75 MeV bombarding proton energy

given in the level scheme, an ∼150 keV energy gap follows, which is in agreement with the previous results. The γ-ray energies and relative branching ratios, given in Figs. 4.3 and 4.4, are weighted averages of values obtained at different bombarding energies. The level energies were fitted to all the energies of γ rays placed in the level scheme. The uncertainty of the level energies determined from the uncertainty of the γ energies is $\Delta E_{lev} < 0.2$ keV.

In order to obtain a complete level scheme below 1.4 MeV the nucleus has been excited to much higher energy (2.8 MeV), and the stronger γ rays were placed into the level scheme up to 2.5 MeV excitation energy. As a result of the higher excitation energy and good statistics of the coincidence measurement the position of each γ ray in the proposed level scheme is confirmed by coincidence relations, and most of the transitions were seen from above (as indicated also in Figs. 4.3 and 4.4). All

the γ rays assigned to ^{73}As below 2.8 MeV bombarding energy were placed into the level scheme.

The proposed level scheme is considered to be complete in the 1/2–15/2 spin window. Although the feeding of the lowest spin states above 1 MeV was very weak in the excitation function measurements, the deexciting transitions have enough intensities and clear coincidence patterns at 4 MeV bombarding energy, ensuring completeness even for the lowest spin states.

All the levels observed in the present experiment were already found at least in one of the previous studies. The levels proposed at 628 and 674 keV by Merwe *et al.* [67] on the basis of weak indications in the neutron time of flight spectrum of (p,n) reaction were not seen in the present study. Similarly, the level at 715 keV observed in one of the (^{3}He,d) measurements [69] is missing. The 862 keV γ ray deexciting the 928.9 keV level of Heits *et al.* was put on top of the 1178 keV level on the basis of its coincidence relations, so this level also does not exist in the deduced level scheme. The 1078 keV level seems to be single in this study contrary to some of the previous proposals [67, 70, 73]. It is weakly excited at each bombarding proton energy opposing to the result of the direct measurement of the intensity of the neutron groups of Merwe *et al.* [67]. This weak excitation value does not allow even for a single 5/2 state (see subsection 4.3.1) suggested by the $\ell_p = 1 + 3$ transferred angular momentum in one of the single proton exchange reactions, where the 1073$\pm$5 keV peak has some ^{71}As contamination [70], too.

The branching ratios deduced are in a reasonable agreement with the compiled data, except for the 1293.39 keV level, where the intensity of a previously unresolved doublet was split on the basis of the coincidence measurement.

4.3.1 Hauser-Feshbach analysis

As the low-energy ($E_{lev} \leq 1.4$ MeV), low-spin level scheme of ^{73}As can be considered complete the cross sections for the neutron groups feeding the ^{73}As levels were deduced and compared with the theoretical σ_{lev}(p,n) values. At the calculation of the transmission coefficients the optical model parameter sets mentined in the section 2.1.5 were used and they are given in Table 4.3. Besides the neutron channels all

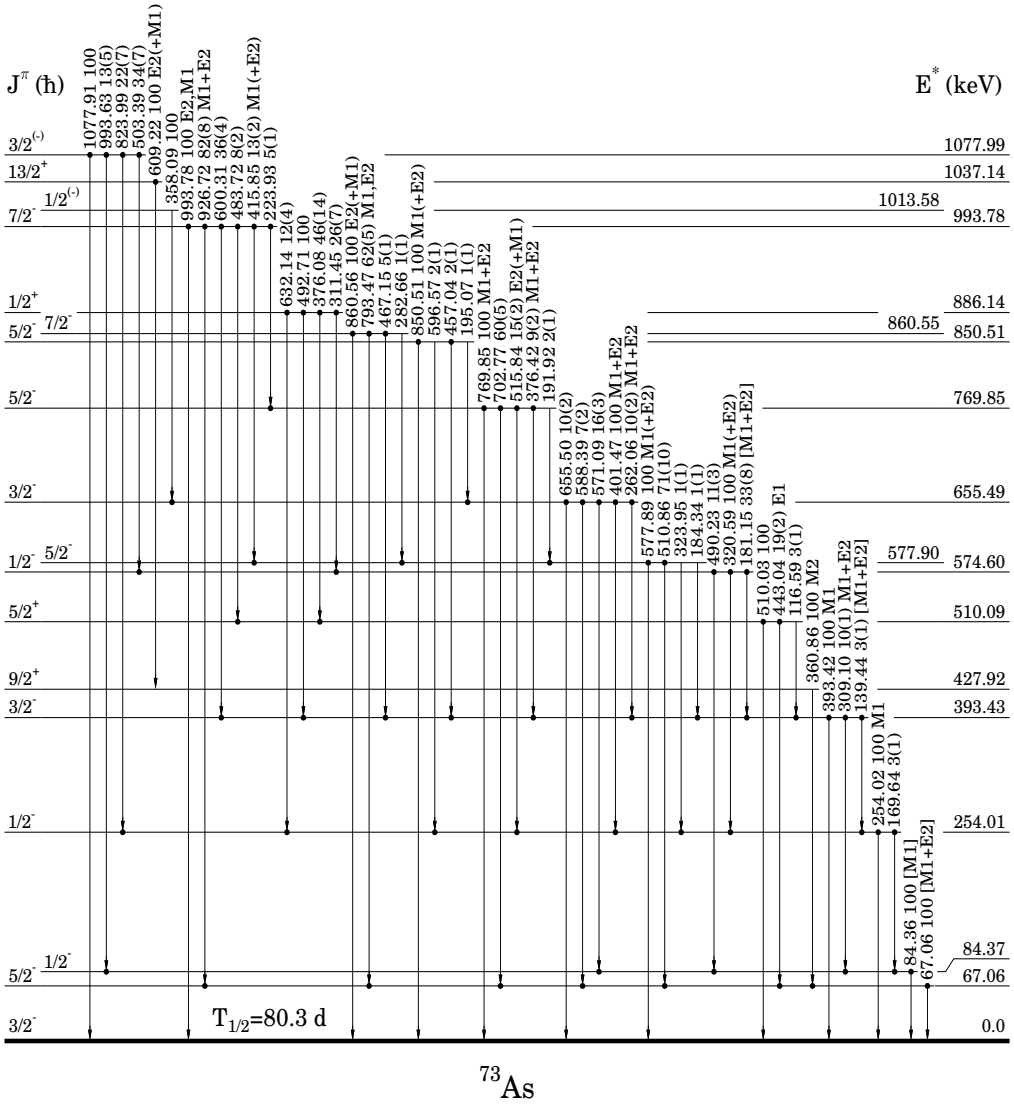

Figure 4.3: *Low-energy part of the proposed level scheme of* ^{73}*As from (p,nγ) reaction. Solid circles at the ends indicate γγ-coincidence relations. Behind the γ-ray energies, γ-branching ratios (and their errors) and multipolarities are given. The multipolarities given in square brackets are taken from the last Nuclear Data Sheets evaluation.*

known (p,p') (up to 1.2 MeV) and (p,γ) channels (up to 1.2 MeV) were also included. Moldauer width fluctuation correction [26] was also taken into account.

The experimental cross sections were deduced from transition intensities at 1.92, 2.27, 2.45 and 2.75 MeV bombarding proton energies. The experimental and theoretical cross sections were normalized at the 428 keV $9/2^+$ state [73]. The results

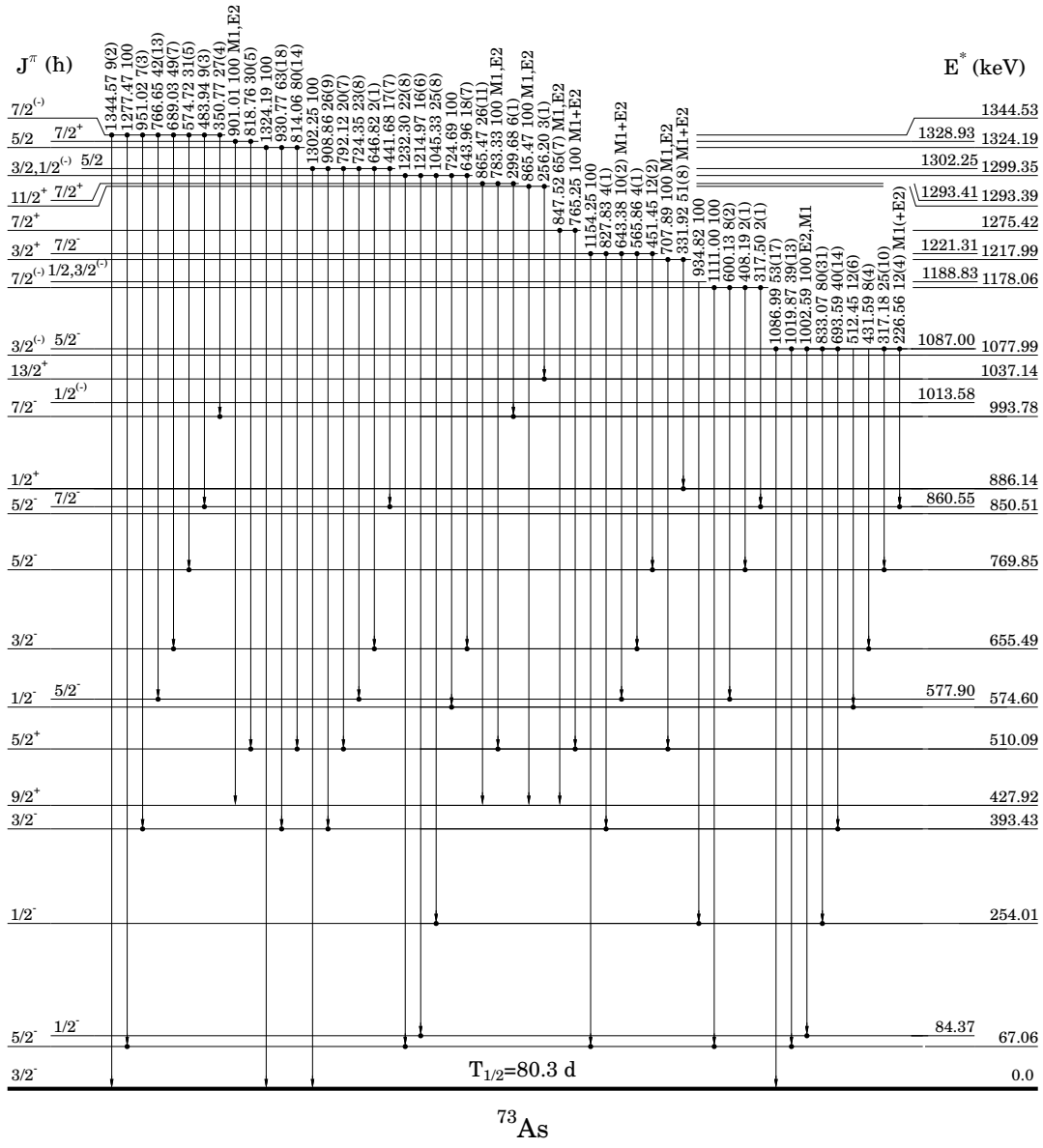

Figure 4.4: *High-energy part of the proposed level scheme of* ^{73}*As.*

Table 4.3: Optical-model parameters used in this work. (The V, W and V_{so} potential depths are given in MeV and the r range and a diffuseness parameters in fm.)

	V	W	V_{so}	r_{re}	r_{im}	a_{re}	a_{im}	Refs.
p+^{73}Ge	58.70−0.55E	13.5	7.5	1.25	1.25	0.65	0.47	[27, 28]
n+^{73}As	47.01−0.267E	9.52	6.2	1.29	1.25	0.66	0.48	[27, 29]
	-0.0018E^2	−0.053E						

obtained at 2.75 MeV and for low–spin states also at 1.92 and 2.27 MeV bombarding proton energies are shown in Fig. 4.5. As the side feeding is large at higher bombarding energy, the uncertainties of the feedings of low energy low spin states increased. Their spin values could be determined at lower proton energy as shown in the upper part of Fig. 4.5.

The theoretical curves from the compound nuclear calculations do have some uncertainty, too. This comes first of all from misidentification of the spin of states, that is a wrong estimate of the outgoing channels. It affects first of all the curves for those spins where only one outgoing channel is present, like the 13/2 state in this case. The uncertainty of the calculated curve can go up up to 35% due to adding a second 13/2 state. Fortunately, this is not the case for the normalizing 9/2 state, which is so strongly excited, that a second 9/2 state cannot be missed. For the low spin states, where the uncertainty of the theoretical curves is more critical, due to the large number of these states the uncertainty is much less, it is $\sim$5%. Although the optical model parameters are uncertain, even large changes of their values leads to small changes in the relative position of the theoretical curves, and affects only the absolute magnitude of the reaction cross sections.

The spins, given in Figs. 4.3 and 4.4, have been determined from the Hauser–Feshbach analysis, and they are in agreement with the decay properties of levels, the measured internal conversion coefficients and the results of the transfer reactions. All but two spin values are within the limits given in the recent NDS compilation. The 1302 and 1324 keV levels are a bit more excited in my case as determined by Merwe *et al.* [67] from direct measurement of the yield of neutrons from (p,n) reaction, leading to higher spin values for these states.

The parities were deduced from the multipolarities of transitions and the negative parity of the ground state. For those states which are decaying to states of only one kind of parity the same parity was tentatively assigned. The parities deduced in this way in all but one case confirm the values compiled from different sources or are determined for the first time. The only exception is the 1218 keV level, where in contrary to the previous assignment (from ℓ(d,^{3}He)=1 [71]), a positive parity has been proposed on the basis of the ICC measurement.

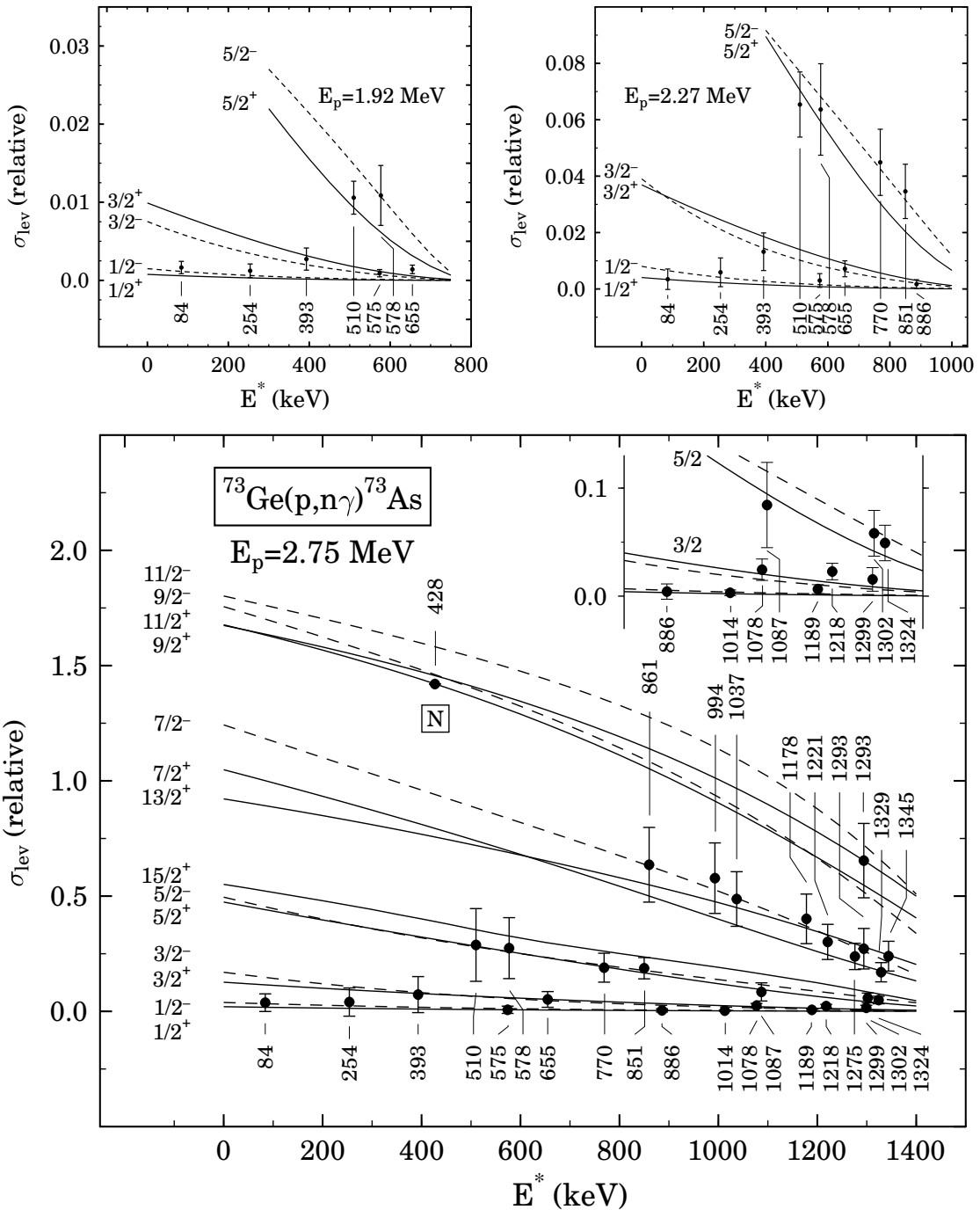

Figure 4.5: *Experimental relative cross sections (σ_{lev}) of the $^{73}Ge(p,n\gamma)^{73}As$ reaction (dots with error bars) as a function of the ^{73}As level energy (E^*) measured at different bombarding proton energies. The curves show Hauser–Feshbach theoretical results. N means normalization point.*

4.4 Theoretical description of ^{73}As

Prior to this study the low–lying states of ^{73}As were calculated by Toki *et al.* [75] and by Ten Brink *et al.* [66]. Toki *et al.* have used particle + rotor model with an asymmetric rotor having a variable moment of inertia. They calculated only the energies of the positive parity states. Ten Brink *et al.* have described the properties of the ^{73}As using the cluster–vibration model of Alaga [76]. In their approach the cluster of three protons was coupled to a harmonic vibrator, allowing up to 3 phonons in the core excitation. Both calculations gave adequate descriptions for the lowest 4–6 levels of given parity. Above these states some of the experimental and theoretical states do not have counterparts, and the quality of description of the branching ratios is quickly getting worse with increasing energy.

In the present study the structure of ^{73}As was interpreted in the framework of interacting boson fermion model (IBFM). In the calculation the boson number corresponding to half of the valence nucleons was used.

The boson core parameters have been taken from the IBM fit to the low-lying levels of ^{72}Ge as in ref. [17] (Algora et al.): $h_1 = 0.86$, $h_2 = -0.15$, $h_3 = 0.03$, $h_{40} = 0$, $h_{42} = -0.3$, $h_{44} = -0.08$ (all h_i parameters in MeV), with the boson number $N = 7$. These values correspond to a transitional boson core lying between the SU(5) and O(6) limits. It should be noted that the 692 keV 0^+ state in ^{72}Ge was excluded from the fitting procedure, because this level is of intruder type (Rester et al. [77], Ardouin et al. [78]).

For the calculation of negative-parity states we included the quasiparticle states $\tilde{p}_{3/2}$, $\tilde{f}_{5/2}$, $\tilde{p}_{1/2}$ and $\tilde{f}_{7/2}$ with quasiparticle energies $E(\pi\tilde{f}_{5/2}) - E(\pi\tilde{p}_{3/2}) = 0.21$ MeV, $E(\pi\tilde{p}_{1/2}) - E(\pi\tilde{p}_{3/2}) = 0.33$ MeV and $E(\pi\tilde{f}_{7/2}) - E(\pi\tilde{p}_{3/2}) = 2.81$ MeV. The energy of the $\tilde{f}_{5/2}$ quasiparticle was chosen to be 0.21 MeV and the energy of the $\tilde{p}_{1/2}$ quasiparticle to 0.33 MeV. The occupation probabilities $V^2(\pi\tilde{p}_{3/2}) = 0.579$, $V^2(\pi\tilde{f}_{5/2}) = 0.341$ and $V^2(\pi\tilde{p}_{1/2}) = 0.118$ have been taken from the BCS calculation using Kisslinger-Sorensen parametrization [79]. In the present calculation we included also the $\tilde{f}_{7/2}$ quasiparticle with $V^2(\pi\tilde{f}_{7/2}) = 0.968$ obtained from the BCS calculation. The boson-fermion interaction strengths have been adjusted to the low-lying levels of ^{73}As: $A_0 = 0.02$ MeV, $\Gamma_0 = 0.3$ MeV, $\Lambda_0 = 1.2$ MeV and

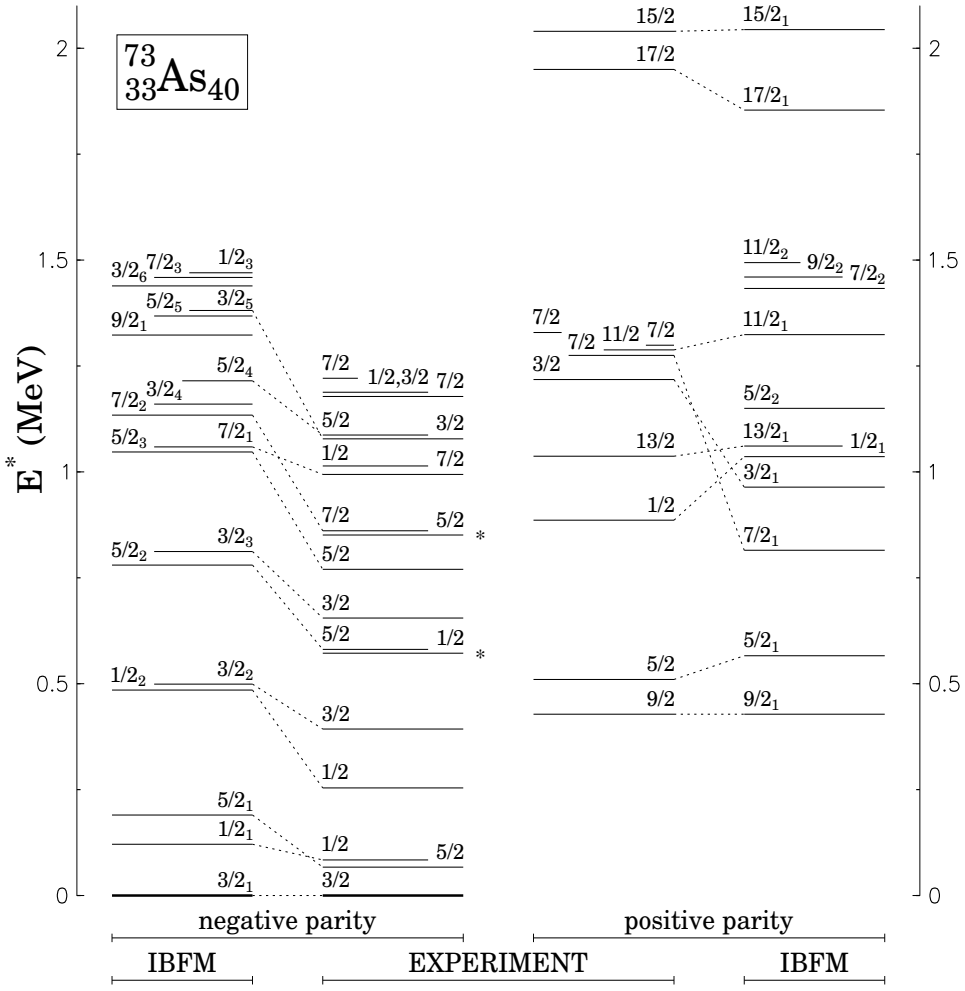

Figure 4.6: *The calculated IBFM energy spectra of the low–lying states of* ^{73}*As in comparison with experimental data. The levels marked with stars (*) might be intruder states.*

$\chi = -\sqrt{7}/2$. The high value of χ is typical in the SU(3) region, but not in the SU(5)/O(6) one. The need for it in description of this nucleus can be explained by core polarization (see ref. [80] and references therein). The resulting low-lying negative-parity spectrum is presented in Fig. 4.6 in comparison with the observed negative-parity levels below 1.4 MeV. The assignment of theoretical states to the experimental ones is based first of all on the comparison of calculated and measured branching ratios. The experimental states at 575 keV and 851 keV with spin $1/2^-$ and $5/2^-$, respectively, do not have theoretical counterparts, they might be

Table 4.4: Calculated electric quadrupole (Q in eb) and magentic dipole (μ in μ_N) moments of low-lying states in ^{73}As.

J_n^π	Q_{IBFM}	Q_{exp} [73]	μ_{IBFM}	μ_{exp} [73]
$5/2_1^-$	-0.14	$\pm$ 0.356(12)	1.05	+1.63(10)
$9/2_1^+$	-0.51		5.96	+5.234(14)

quasiparticle states coupled to the intruder 692 keV 0^+ state of ^{72}Ge core.

For the calculation of positive parity states we included the quasiparticle states $\tilde{g}_{9/2}$ and $\tilde{d}_{5/2}$ with occupation probabilities $V^2(\pi\tilde{g}_{9/2}) = 0.06$, $V^2(\pi\tilde{d}_{5/2}) = 0.01$, and quasiparticle energy $E(\pi\tilde{d}_{5/2}) - E(\pi\tilde{g}_{9/2}) = 3$ MeV. The boson-fermion interaction strengths were $A_0 = 0.10$ MeV, $\Gamma_0 = 0.38$ MeV, $\Lambda_0 = 5.0$ MeV and $\chi = -\sqrt{7}/2$. The positive parity states are compared with the present experimental data and the yrast states from compilation [73] up to 2 MeV in Fig. 4.6.

The main parts of the IBFM wave functions of the low-lying states $3/2_1^-$ and $5/2_1^-$ can be approximately presented in the form of quasiparticle–core block terms $\tilde{p}_{3/2}\otimes 0_1$ and $\tilde{f}_{5/2}\otimes 0_1$, respectively, where, 0_1 denotes the wave function of the ground state of the core. In such a block presentation the $1/2_1^-$ wave function has the largest block term $\tilde{p}_{1/2}\otimes 0_1$ with large admixture from $(\tilde{f}_{5/2}\otimes 2_1)1/2$, where 2_1 denotes the wave function of the first excited state of the IBM boson core. The $1/2_2^-$ wave function has the largest block term $(\tilde{p}_{3/2}\otimes 2_1)1/2$ with large admixture of $\tilde{p}_{1/2}\otimes 0_1$. The $3/2_2^-$ and $5/2_2^-$ wave functions have the largest block term $(\tilde{f}_{5/2}\otimes 2_1)3/2$ and $(\tilde{p}_{3/2}\otimes 2_1)5/2$, respectively. The $7/2_1^-$ wave function has the largest block component $(\tilde{p}_{3/2}\otimes 2_1)7/2$ with large admixture of $(\tilde{f}_{5/2}\otimes 2_1)7/2$. The $9/2_1^+$ and $5/2_1^+$ wave functions have the largest block components $\tilde{g}_{9/2}\otimes 0_1$ and $(\tilde{g}_{9/2}\otimes 2_1)5/2$ with admixture from $\tilde{d}_{5/2}\otimes 0_1$.

Employing the IBFM wave functions we have calculated the electromagnetic properties of the low-lying states in ^{73}As. The values of the effective proton charge, boson charge, gyromagnetic ratios and χ are the following: $e^{sp} = 1.5$, $e^{VIB} = 0.8$, $\chi = -\sqrt{7}/2$, $g_R = Z/A = 0.452, g_l = 1, g_s = 0.7 g_s^{free} = 3.91, g_T = \frac{1}{25}\langle r^2\rangle g_s^{free} = 3.372$. The calculated static moments and γ-ray branches are presented in Tables 4.4 and 4.5, respectively. We have calculated all the possible branches, and neglected

Table 4.5: Electromagnetic transitions between the low-lying ^{73}As states calculated in IBFM.

$J_i \to J_f$	I_γ^{exp}	I_γ^{IBFM}	$J_i \to J_f$	I_γ^{exp}	I_γ^{IBFM}
$5/2_1^- \to 3/2_1^-$	100	100	$7/2_1^- \to 7/2_2^-$	<1	3
$1/2_1^- \to 3/2_1^-$	100	100	$\to 5/2_3^-$	5	5
$1/2_2^- \to 1/2_1^-$	3	7	$\to 5/2_2^-$	13	100
$\to 3/2_1^-$	100	100	$\to 3/2_2^-$	36	1.4
$3/2_2^- \to 1/2_2^-$	3	12	$\to 5/2_1^-$	82	10
$\to 1/2_1^-$	10	15	$\to 3/2_1^-$	100	59
$\to 5/2_1^-$	<0.6	1	$5/2_4^- \to 7/2_2^-$	12	3
$\to 3/2_1^-$	100	100	$\to 5/2_3^-$	25	0.0
$5/2_2^- \to 3/2_2^-$	1	22	$\to 3/2_3^-$	8	55
$\to 1/2_2^-$	1	0.02	$\to 3/2_2^-$	40	100
$\to 1/2_1^-$	<0.6	1.6	$\to 1/2_1^-$	100	76
$\to 5/2_1^-$	71	49	$\to 5/2_1^-$	39	96
$\to 3/2_1^-$	100	100	$3/2_5^- \to 3/2_2^-$	<9	12
$3/2_3^- \to 5/2_2^-$	<7	15	$\to 1/2_2^-$	22	82
$\to 3/2_2^-$	10	4.5	$\to 3/2_1^-$	100	24
$\to 1/2_2^-$	100	77	$1/2_1^+ \to 5/2_1^+$	100	100
$\to 1/2_1^-$	16	100	$13/2_1^+ \to 9/2_1^+$	100	100
$\to 5/2_1^-$	7	19	$3/2_1^+ \to 1/2_1^+$	51	100
$\to 3/2_1^-$	10	64	$\to 5/2_1^+$	100	16
$5/2_3^- \to 5/2_2^-$	2	0.1	$7/2_1^+ \to 5/2_1^+$	100	100
$\to 3/2_2^-$	9	28	$\to 9/2_1^+$	65	79
$\to 1/2_2^-$	15	6	$11/2_1^+ \to 13/2_1^+$	3	11
$\to 1/2_1^-$	<1	7	$\to 9/2_1^+$	100	100
$\to 5/2_1^-$	60	100	$17/2_1^+ \to 13/2_1^+$	100	100
$\to 3/2_1^-$	100	33	$15/2_1^+ \to 11/2_1^+$	22	17
$7/2_2^- \to 5/2_2^-$	1	0.5	$\to 13/2_1^+$	100	100
$\to 3/2_2^-$	5	3			
$\to 5/2_1^-$	62	100			
$\to 3/2_1^-$	100	76			

from the table those transitions which were beyond the experimental detection limits.

The overall agreement of calculated and experimental results is reasonable, but there are number of discrepancies in both energies and electromagnetic properties.

One point is that the calculated negative-parity energy spectrum seems to show a repeating j,$j+1$ doublet structure, which is not evidenced experimentally. However, the wave functions of the states of each doublet are not of the same structure. For example, the states of $1/2^-_2$, $3/2^-_2$-doublet, $5/2^-_2$, $3/2^-_3$-doublet and $5/2^-_3$, $7/2^-_1$-doublet have rather splitted components, and the largest component is not the same.

The static moments of the $5/2^-_1$ state have too small magnitudes in comparison to the experimental data and the $B(E2)$ value for the depopulation of $5/2^-_1$ state is also too small, indicating that some collectivity is missing. The calculation fails in predicting the main branches depopulating $5/2^-_2$, $7/2^-_1$ and $3/2^-_3$ states. This is connected to the fact that these states, as well as the $3/2^-_2$ one they are decaying to, have relatively large $(\tilde{p}_{3/2} \otimes 2_1)$ components, and because of this too strong M1 and weak E2 transitions are predicted between them. The $5/2^-_3 \rightarrow 5/2^-_2$ and $5/2^-_4 \rightarrow 5/2^-_3$ transitions are predicted to be too weak. Assuming some additional transition strength of the order of magnitude of 0.01 Weisskopf unit because of some more mixing would improve the situation significantly. It should be noted that the agreement of the present IBFM calculation with experiment is less satisfactory than usually achieved for other medium-heavy nuclei. However, we have not achieved to obtain a better optimalization of the IBFM parameters. This might be caused by the presence of low lying 0^+_2 intruder state, the first excited state in the ^{72}Ge nucleus, which is not accounted for in our calculation. This might be an evidence for the influence of the IBM-2 type of correlation in the core.

In spite of the above mentioned shortcomings, the states below 1 MeV could be classified in an acceptable way, and the assignments of the lowest lying states are in correspondence with the pervious proposals of refs. [66, 75].

Chapter 5

Structure of ^{68}As from ^{12}C(^{58}Ni,pnγ) reaction

5.1 Results of earlier studies

Low-spin states of ^{68}As have previously been investigated from β decay of ^{68}Se [81]. Some of the higher spin states were excited via the ^{54}Fe(^{16}O,pn) and ^{58}Ni(^{12}C,pn) heavy ion reactions up to an isomeric state at 2158 keV [82, 83, 84]. In a recent study [6] the level scheme has been extended to an excitation energy of 3.2 MeV, and the experimental results have been described in the framework of the EXCITED VAMPIR model. The former studies are summarized in Table 5.1.

5.2 Experimental results from the present study

The total projection spectrum of the $1p1n$ matrix cleaned by using a successive subtraction technique in order to eliminate the contaminating γ lines is shown in Fig. 5.1, where only the strongest γ rays belonging to ^{68}As are labelled. The energies, intensities, angular distribution ratios and the deduced multipolarities of the transitions assigned to ^{68}As are given in Table 5.2. A total of 58 transitions were identified, 34 of which are new.

The level scheme was constructed mainly on the basis of the $\gamma\gamma$-coincidence relations, but the energy and intensity balances were also considered. The order of transitions in the γ-ray cascades was established by their intensity relations. To confirm locations of the γ transitions in the level scheme relative to the isomeric state at 2158 keV, spectra and matrices were also sorted with delays of multiples of 10 ns. The prompt and the 40 ns delayed proton and neutron gated matrices

Table 5.1: Summary of the former experimental studies of the structure of ^{68}As

Reference *	Reaction	Techniques, detectors	Measurements	Results
Baumann (1994) [81]	decay of ^{68}Se	Ge detector, Ge(Li) detector, Si detector	E_γ, I_γ, $\beta\gamma$-coinc, $\gamma\gamma$-coinc	10 γ rays identified and placed in the level scheme, which contains 6 states with 5 unambiguous J^π assignments, logft values deduced for 5 levels, γ-branching given
Pardo (1988) [82]	^{54}Fe(^{16}O,pnγ)^{68}As, ^{58}Ni(^{12}C,pnγ)^{68}As	in-beam techniques	E_γ, I_γ, $\gamma\gamma$-coinc	25 transitions identified and placed in the level scheme, deduced 15 levels without J^π assignment, $T_{1/2}$ determined for the isomeric state at 2159.1 keV
Badica (1989) [83]	^{56}Fe(^{14}Ni,2nγ)^{68}As	in-beam techniques, Ge(Li) detectors	E_γ, I_γ, $\gamma\gamma$-coinc	level scheme deduced up to the isomeric state, which contains 24 transitions and 18 levels without J^π assignment, ICC for the 158 keV γ ray
Badica (1994) [84]	^{54}Fe(^{16}O,pnγ)^{68}As, E_O=45-63 MeV, ^{58}Ni(^{12}C,pnγ)^{68}As, E_C=32-45 MeV	in-beam techniques, Ge(HP) detectors, liquid scintillator	E_γ, I_γ, nγ-coinc, $\sigma(\theta)$	21 γ rays identified and placed in the level scheme, which contains 16 levels up to the isomeric state with unambiguous J^π assignments for 3 states, A_2, A_4 factors deduced for all transitions
Petrovici (1996) [6]	^{54}Fe(^{14}N,2nγ)^{68}As, E_N=46 MeV, ^{58}Ni(^{12}C,pnγ)^{68}As, E_C=36-45 MeV, ^{46}Ti(^{25}Mg,p2nγ)^{68}As, E_{Mg}=68 MeV,	in-beam techniques, Ge(HP) detectors, Ge(Li) detectors, Ge detector-ball	E_γ, I_γ, $\gamma\gamma$-coinc	27 transitions identified and placed in the level scheme, which contains 20 levels below 3.2 MeV, unambiguous J^π assignments only for the ground state
Bhat (1995) [85]				compilation

* Only the first author is indicated in this column.

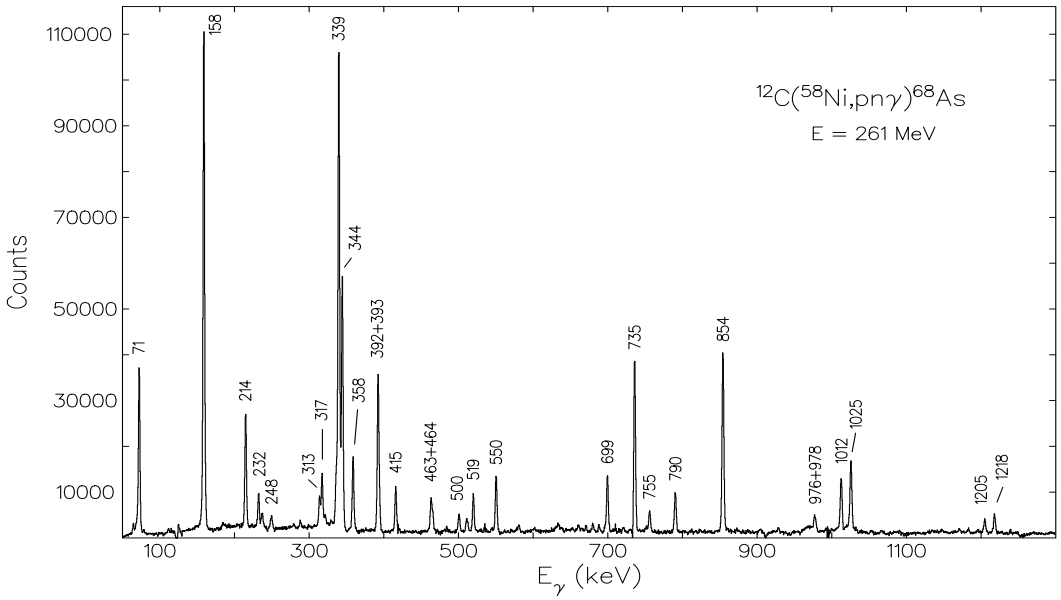

Figure 5.1: *Total projection spectrum of ^{68}As obtained from the 1p1n gated $\gamma\gamma$ matrix after subtraction of the contaminating channels.*

were analysed in detail using standard gating techniques. Typical gated spectra are shown in Fig. 5.2. The proposed level scheme is shown in Fig. 5.3.

The level scheme deduced is considerably extended compared to the results of previous studies [82, 84, 6]. New transitions were found between known levels, new states are established both below and above the 2158 keV isomeric state. The placement of already known γ rays is in agreement with at least one of the previous works. States with low spin [81, 84] were not observed in the present work, as well as the 1119 and 1757 keV levels which have no spin assignments [82]. The 2060 keV and 2935 keV states [6] were also not observed in my study, as the 631 keV and 991 keV γ rays assigned to their decay are too weak in my case to confirm the existence of these states.

The spins were determined from the angular distribution ratios and the known spin and parity value of 3^+ of the ground state [81]. The experimental intensity ratios given in Table 5.2 are average values determined by using several stronger

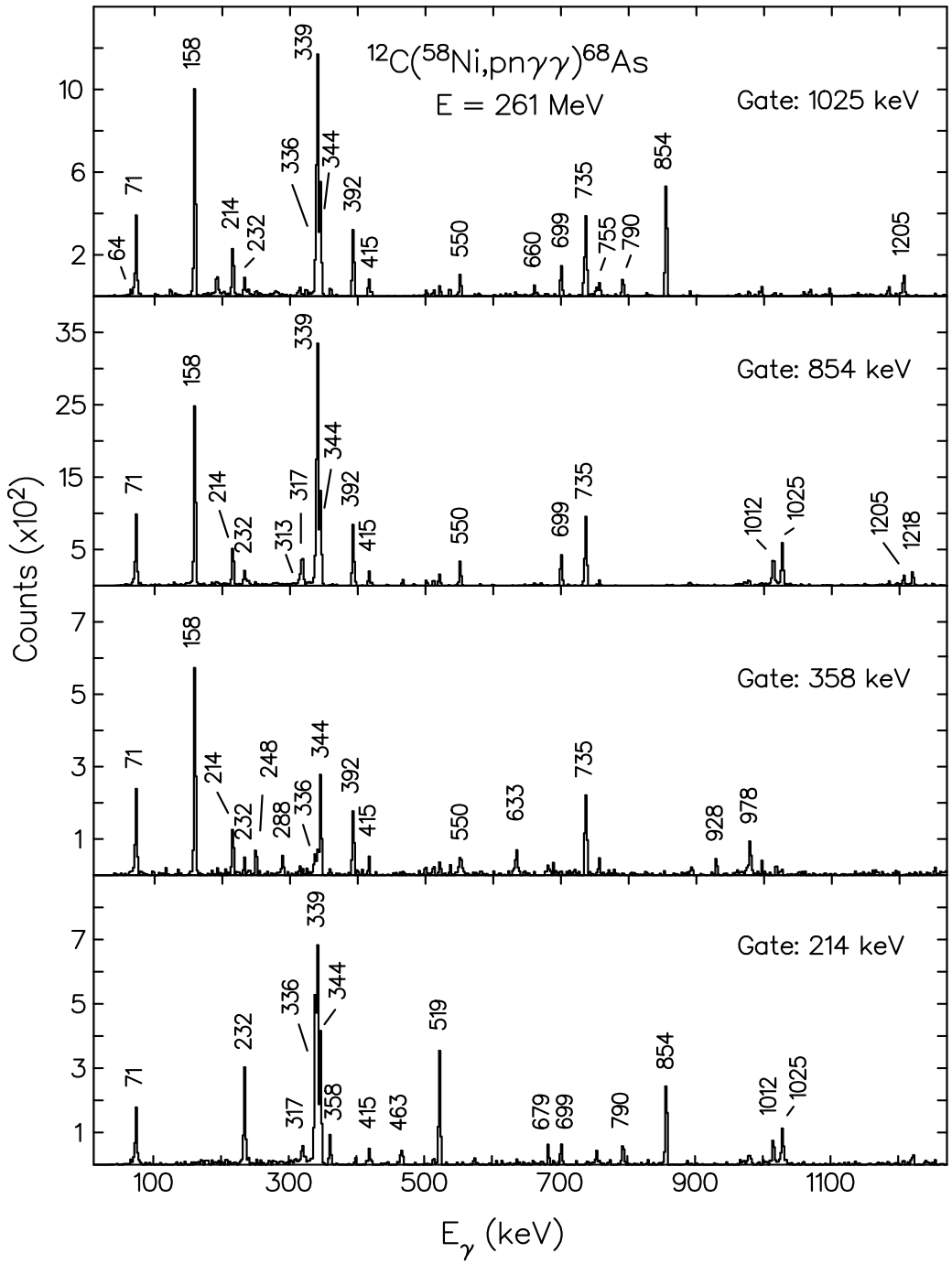

Figure 5.2: *Typical $\gamma\gamma$-coincidence spectra of ^{68}As.*

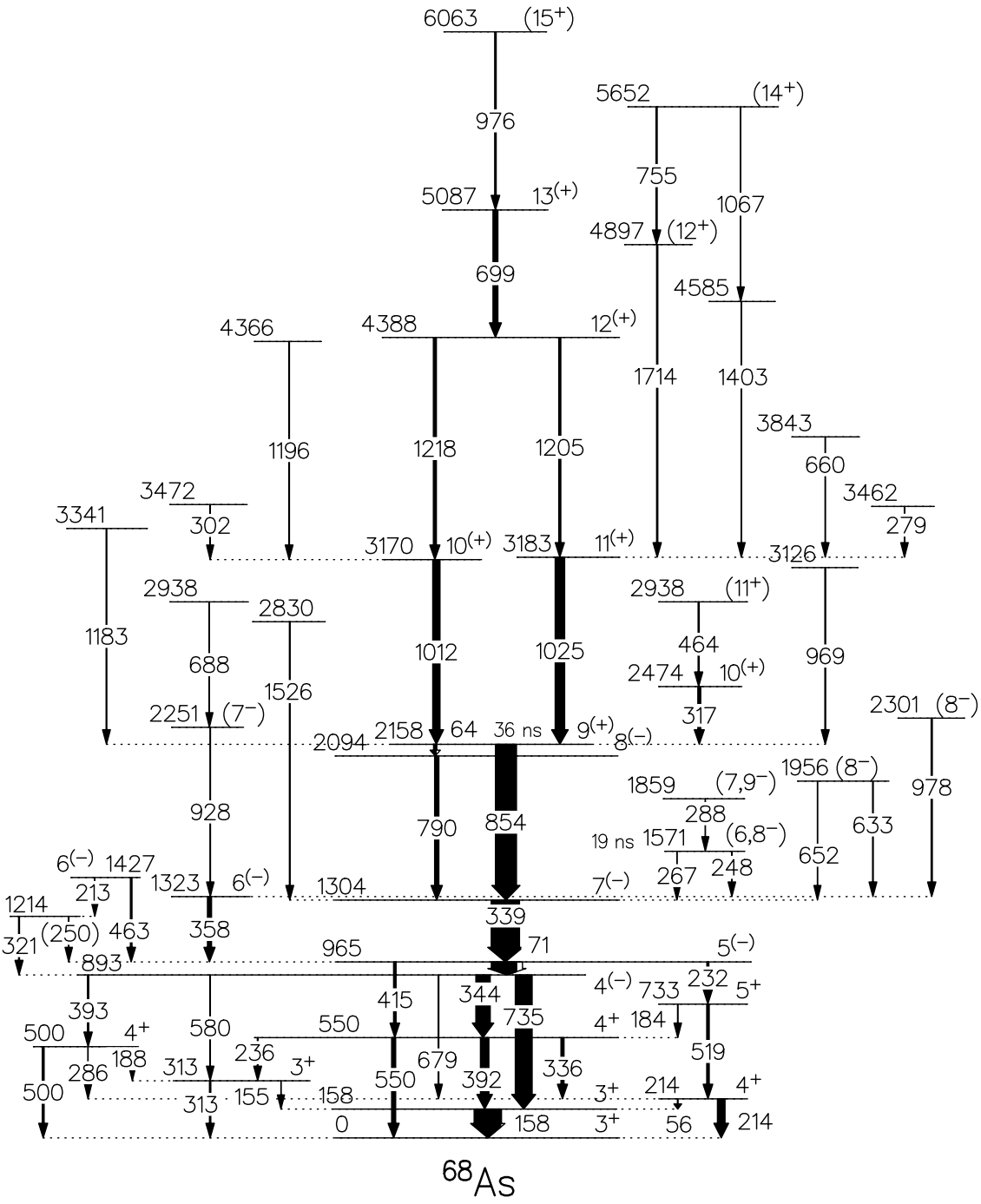

Figure 5.3: *Proposed level scheme of ^{68}As from the $^{12}C(^{58}Ni,pn\gamma)^{68}As$ reaction. The unfilled part of the 71 keV arrow represent the intensity of the conversion electrons, assuming pure M1 multipolarity.*

Table 5.2: Energies, intensities and angular distribution ratios (R=$\frac{I_\gamma(143^\circ)}{I_\gamma(79^\circ)+I_\gamma(101^\circ)}$) of γ rays from the ^{12}C(^{58}Ni,pnγ)^{68}As reaction.

E_γ (keV)	I_γ(%)	R ratio	$J_i^\pi \rightarrow J_f^\pi$	E_i(keV)
56.1(4)	1.68(48)		$4^+ \rightarrow 3^+$	214
63.9(1)	9.01(42)		$9^{(+)} \rightarrow 8^{(-)}$	2158
71.3(1)	90.46(310)	0.85(5)	$5^{(-)} \rightarrow 4^{(-)}$	965
154.8(3)	0.76(11)		$3^+ \rightarrow 3^+$	313
158.0(1)	95.24(571)	0.88(4)	$3^+ \rightarrow 3^+$	158
183.8(3)	1.52(17)		$5^+ \rightarrow 4^+$	733
187.6(33)	0.36(6)		$4^+ \rightarrow 3^+$	500
213.1(4)	0.42(11)		$6^{(-)} \rightarrow$	1427
214.1(1)	26.67(381)	1.18(6)	$4^+ \rightarrow 3^+$	214
231.6(1)	7.20(29)	1.53(13)	$5^{(-)} \rightarrow 5^+$	965
236.4(1)	2.65(14)	1.34(16)	$4^+ \rightarrow 3^+$	550
248.4(2)	1.43(11)	1.54(23)	$(6,8^-) \rightarrow 6^{(-)}$	1571
250.2(3)	1.03(14)		$\rightarrow 5^{(-)}$	1214
266.6(5)	0.32(10)		$(6,8^-) \rightarrow 7^{(-)}$	1571
278.8(2)	1.30(11)		$\rightarrow 11^{(+)}$	3462
285.9(4)	0.36(6)		$4^+ \rightarrow 4^+$	500
288.0(2)	0.67(8)	0.79(20)	$(7,9^-) \rightarrow (6,8^-)$	1859
301.9(3)	0.67(10)		$\rightarrow 10^{(+)}$	3472
313.1(1)	4.76(10)		$3^+ \rightarrow 3^+$	313
316.6(1)	10.27(38)	0.80(7)	$10^{(+)} \rightarrow 9^{(+)}$	2474
321.1(2)	3.30(23)		$\rightarrow 4^{(-)}$	1214
335.7(2)	10.84(42)	1.25(9)	$4^+ \rightarrow 4^+$	550
339.0(1)	100.00(312)	1.49(8)	$7^{(-)} \rightarrow 5^{(-)}$	1304
343.7(1)	51.24(160)	1.46(8)	$4^{(-)} \rightarrow 4^+$	893
358.1(1)	14.46(55)	0.89(7)	$6^{(-)} \rightarrow 5^{(-)}$	1323
391.7(1)	30.00(109)	1.35(14)	$4^+ \rightarrow 3^+$	550
393.3(2)	4.38(15)		$4^{(-)} \rightarrow 4^+$	893
415.1(1)	8.54(36)	0.82(7)	$5^{(-)} \rightarrow 4^+$	965
462.7(1)	5.35(29)	0.87(10)	$6^{(-)} \rightarrow 5^{(-)}$	1427
464.4(1)	3.90(19)	0.60(12)	$(11^+) \rightarrow 10^{(+)}$	2938
500.1(1)	6.67(10)	0.58(9)	$4^+ \rightarrow 3^+$	500
519.3(1)	8.99(48)	0.57(8)	$5^+ \rightarrow 4^+$	733
549.7(1)	14.44(63)	1.27(13)	$4^+ \rightarrow 3^+$	550
580.0(2)	1.37(15)		$4^{(-)} \rightarrow 3^+$	893

Table 5.2: continued

E_γ (keV)	I_γ(%)	R ratio	$J_i^\pi \rightarrow J_f^\pi$	E_i(keV)
633.0(2)	2.50(19)	1.46(35)	$(8^-)\rightarrow 6^{(-)}$	1956
652.1(3)	0.57(15)		$(8^-)\rightarrow 7^{(-)}$	1956
659.9(2)	1.64(17)		$\rightarrow 11^{(+)}$	3843
679.4(2)	1.89(17)		$4^{(-)} \rightarrow 4^+$	893
687.5(3)	0.86(14)		$\rightarrow (7^-)$	2938
699.0(1)	17.41(61)	0.97(14)	$13^{(+)} \rightarrow 12^{(+)}$	5087
735.4(1)	60.14(194)	0.92(10)	$4^{(-)} \rightarrow 3^+$	893
755.4(1)	4.21(23)	1.41(25)	$(14^+)\rightarrow (12^+)$	5652
790.1(1)	15.10(59)	1.32(14)	$8^{(-)} \rightarrow 7^{(-)}$	2094
853.9(1)	75.01(238)	1.47(10)	$9^{(+)} \rightarrow 7^{(-)}$	2158
928.1(3)	1.26(19)	0.75(27)	$(7^-)\rightarrow 6^{(-)}$	2251
968.8(2)	2.84(25)		$\rightarrow 9^{(+)}$	3126
976.3(1)	5.18(29)	1.42(28)	$(15^+)\rightarrow 13^{(+)}$	6063
978.2(1)	4.19(32)	1.47(26)	$(8^-)\rightarrow 6^{(-)}$	2301
1012.4(1)	25.81(91)	0.54(8)	$10^{(+)} \rightarrow 9^{(+)}$	3170
1025.4(1)	33.77(114)	1.52(21)	$11^{(+)} \rightarrow 9^{(+)}$	3183
1067.1(6)	0.53(15)		$(14^+)\rightarrow$	5652
1183.2(2)	2.55(25)		$\rightarrow 9^{(+)}$	3341
1196.0(2)	2.36(23)		$\rightarrow 10^{(+)}$	4366
1204.9(1)	7.31(34)	0.64(14)	$12^{(+)} \rightarrow 11^{(+)}$	4388
1218.0(1)	10.70(46)	1.48(24)	$12^{(+)} \rightarrow 10^{(+)}$	4388
1402.6(3)	1.68(21)		$\rightarrow 11^{(+)}$	4585
1526.0(2)	2.61(27)		$\rightarrow 7^{(-)}$	2830
1713.9(2)	4.29(27)	0.78(22)	$(12^+)\rightarrow 11^{(+)}$	4897

γ rays as gating transitions. In order to determine the effect of the alignment loss on the angular distribution ratios due to the finite lifetime of the isomeric state the R ratio was deduced for the 854 keV M2 transition, and compared with the R=1.5 value expected for a stretched quadrupole transition from a completely aligned state. It was found that a 5% correction to R is enough to correct for the alignment loss. In the construction of the level scheme the assumption was applied that the γ rays take away the maximal possible angular momentum. For states with several branches this often can happen only for one of the transitions,

while the others cannot be stretched. The angular distribution ratio for the 158 keV transition 0.88±0.04 allows for a stretched dipole or a highly mixed ΔJ=0 transition. The experimental conversion coefficient, α_K=0.1±0.03 [83] corresponds to $I(E2)/I(M1) = 0.8 \pm 0.2$ mixing ratio. My angular distribution ratio allows only for ΔJ=0 spin change for such a high mixing ratio.

For all but one transitions having finite quadrupole components I assigned M1+E2 multipolarity. The only exception is the 854 keV transition, which, according to the life time of the 2158 keV state it is decaying from, is excepted to be of M2 nature. The recommended upper limits (RUL) for the transition strengths [74] suggest that the 64 keV transition, decaying from the same level, is an E1 transition. On the basis of the multipolarities of the transitions I assigned positive parity to the states below 600 keV. The rest of the level scheme is connected to these states via pure dipole transitions, which may be either M1 or E1, thus all the parities above 600 keV are tentative. In the nuclei ^{70,72}As the yrast J=9 states have tentative positive parity, while the yrast J=7 states, lying about 850 keV below them, have definite negative parity in ^{72}As [86] and tentative negative parity in ^{70}As [87]. In ^{74}As the yrast J=9 state has positive parity and has been assigned a $\pi g_{9/2}\nu g_{9/2}$ configuration [88]. Thus, on the basis of systematics I assigned tentative positive parity to the J=9 state at 2158 keV, and negative parity to the J=7 state at 1304 keV. The parity change is in agreement with the M2 nature of the 854 keV transition connecting them. Negative parity was assigned to the 965 and 893 keV states on the basis of the RUL and the quadrupole and dipole character of the 339 and 71 keV transitions, respectively. As for the higher lying states, tentative negative parity was assigned to the states decaying to negative parity final states and positive parity to the states decaying to positive parity final states.

My spin values are only in partial agreement with those determined in Ref. [84]. While the spin values J=3, 4 and 3,5 for the levels at 158, 893 and 965 keV, respectively, agree with my results, my angular distribution data lead to an assigment of J=4 instead of J=1 for the level at 214 keV, J=3 instead of J=1,2 for the level at 313 keV, J=4 instead of J=3,5 for the level at 550 keV and J=7 instead of J=5,6 for the level at 1304 keV, although the possible amounts of transferred angular

momenta, which can be deduced from the A_2 and A_4 values given in Ref. [84] are consistent with my angular distribution data. A possible reason of the contradiction might be that the spin values of the states at 214 and 313 keV were adopted from a preliminary report on a decay work [89], the results of which have later been revised [81]. The use of these low spin values could lead to other inconsistencies, too.

Although the level scheme deduced in Ref. [6] is quite similar to that obtained in the present study my spin assignments are different from their tentative spin assignments. In Ref. [6] (4^+) spin parity value was proposed to the 158-keV state arguing that its lifetime is less than 100 ns. This argument requires an M1 transition allowing also for spin 2 and 3 $\hbar$ in agreement with my assignment.

The spin values determined in present work for the 550 keV and 893 keV states are less than those in Ref. [6]. The 735 keV cross-over transition was measured to be a ΔJ=1 stretched dipole transition resulting in J^π=$4^{(-)}$ for the 893 keV state. The 4^+ spin-parity assignment was the only possibility for the 550-keV state to be consistent with the angular distributions of all the γ rays feeding and depopulating it. For the 1304 and 2158-keV states Iobtained J^π=$7^{(-)}$ and $9^{(+)}$, respectively, which are close to the expectations of Ref. [6].

From the delayed γ-ray spectra the half life of the 2158 keV isomeric state was determined to be 36$\pm$2 ns, which is in agreement with the previous result [85]. In addition, the 1571 keV state, depopulated by the 248 keV γ ray, was found to have a measurable half life of 19$\pm$3 ns. All the other levels have half lives less than 5 ns.

5.3 Interpretation on the basis of IBFFM calculations

We have performed calculations for ^{68}As in the framework of interacting boson-fermion-fermion model (IBFFM) [12, 90, 91].

The core parameters were adjusted to the low-lying levels of the even-even nucleus $^{66}_{32}Ge_{34}$. The parameters obtained in this way are: $h_1 = 0.92$, $h_2 = -0.1$, $h_3 = 0$, $h_{40} = 0.1$, $h_{42} = -0.25$, $h_{44} = -0.35$ (all h_i parameters in MeV) and the total boson number is $N = 5$ corresponding to the number of valence-nucleon pairs. This parametrization is close to the IBM parametrization for the $^{64}_{30}Zn_{34}$ isotone,

which was used as the core in IBFFM calculation for ^{66}Ga [12], and corresponds to a transition between the SU(5) and O(6) dynamical symmetries, being closer to the SU(5) (vibrational) limit.

The experimental data on the neighbouring odd-proton nucleus $^{67}_{33}As_{34}$ are very scarce and the corresponding fit of the IBFM parameters can not be performed. Therefore, we have taken the energies and occupation probabilities of proton quasi-particle states from the previous calculation for ^{72}As [80], with the only difference that the $\tilde{f}_{5/2}$ quasi-particle was shifted slightly up by 0.1 MeV: $E(\pi\tilde{p}_{3/2}) = 0$ MeV, $E(\pi\tilde{f}_{5/2}) = 0.51$ MeV, $E(\pi\tilde{p}_{1/2}) = 0.74$ MeV, $E(\pi\tilde{g}_{9/2}) = 2.2$ MeV, $E(\pi\tilde{d}_{5/2}) = 5.2$ MeV and $V^2(\pi\tilde{p}_{3/2}) = 0.607$, $V^2(\pi\tilde{f}_{5/2}) = 0.309$, $V^2(\pi\tilde{p}_{1/2}) = 0.131$, $V^2(\pi\tilde{g}_{9/2}) = 0.07$, $V^2(\pi\tilde{d}_{5/2}) = 0.01$. The values of boson-fermion interaction strengths of $H_{IBFM}(\pi)$ are: $A_0^\pi = 0.05$, $\Gamma_0^\pi = 0.5$, $\Lambda_0^\pi = 0.5$ (all in MeV). The value $\chi = -1$ is used, which is roughly an average of the χ values used in previous IBFFM calculations for odd-odd Ga and As nuclei [12, 14, 17, 80].

Experimental data on the neighbouring odd-neutron nucleus $^{67}_{32}Ge_{35}$ are available for a few low-lying states only. These scarce data show a close resemblance to the low-lying spectrum in the $^{65}_{30}Zn_{35}$ isotone. For this reason we used the quasi-particle energies and occupation probabilities from the previous calculation for ^{65}Zn applied in the IBFFM calculation for $^{66}_{32}Ga_{34}$ [12]: $E(\nu\tilde{f}_{5/2}) = 0$, $E(\nu\tilde{p}_{3/2}) = 0.01$, $E(\nu\tilde{p}_{1/2}) = 0.83$,$E(\nu\tilde{g}_{9/2}) = 1.69$, $E(\nu\tilde{d}_{5/2}) = 4.69$ (all in MeV) and $V^2(\nu\tilde{f}_{5/2}) = 0.48$, $V^2(\nu\tilde{p}_{3/2}) = 0.73$, $V^2(\nu\tilde{p}_{1/2}) = 0.11$, $V^2(\nu\tilde{g}_{9/2}) = 0.08$, $V^2(\nu\tilde{d}_{5/2}) = 0.01$. Here, the energy of the $\tilde{p}_{3/2}$ quasi-particle is lowered by 0.08 MeV and the $\tilde{d}_{5/2}$ orbital from the higher-lying shell is included at an energy of 3 MeV above the $\tilde{g}_{9/2}$ quasi-particle. The values of the corresponding boson-fermion interaction strengths are taken from the previous IBFM and IBFFM calculations for positive parity states in ^{72,74}As [17, 80]: $A_0^\nu = 0.0$, $\Gamma_0^\nu = 0.55$, $\Lambda_0^\nu = 1.3$ (all in MeV). The strengths of the residual interaction $V_\delta(\pi{=}+) = 0$, $V_{\delta\sigma}(\pi{=}-) = 0$ and $V_t = 0.015$ MeV are taken to be the same as in the previous calculation for ^{72,74}As [17, 80]. The values $V_\delta(\pi{=}-) = -0.3$ MeV, $V_{\delta\sigma}(\pi{=}+) = 0.12$ MeV are adjusted to the low energy spectrum of ^{68}As; the corresponding values used in the previous calculations for ^{72,74}As have been -0.6 MeV and 0 MeV, respectively.

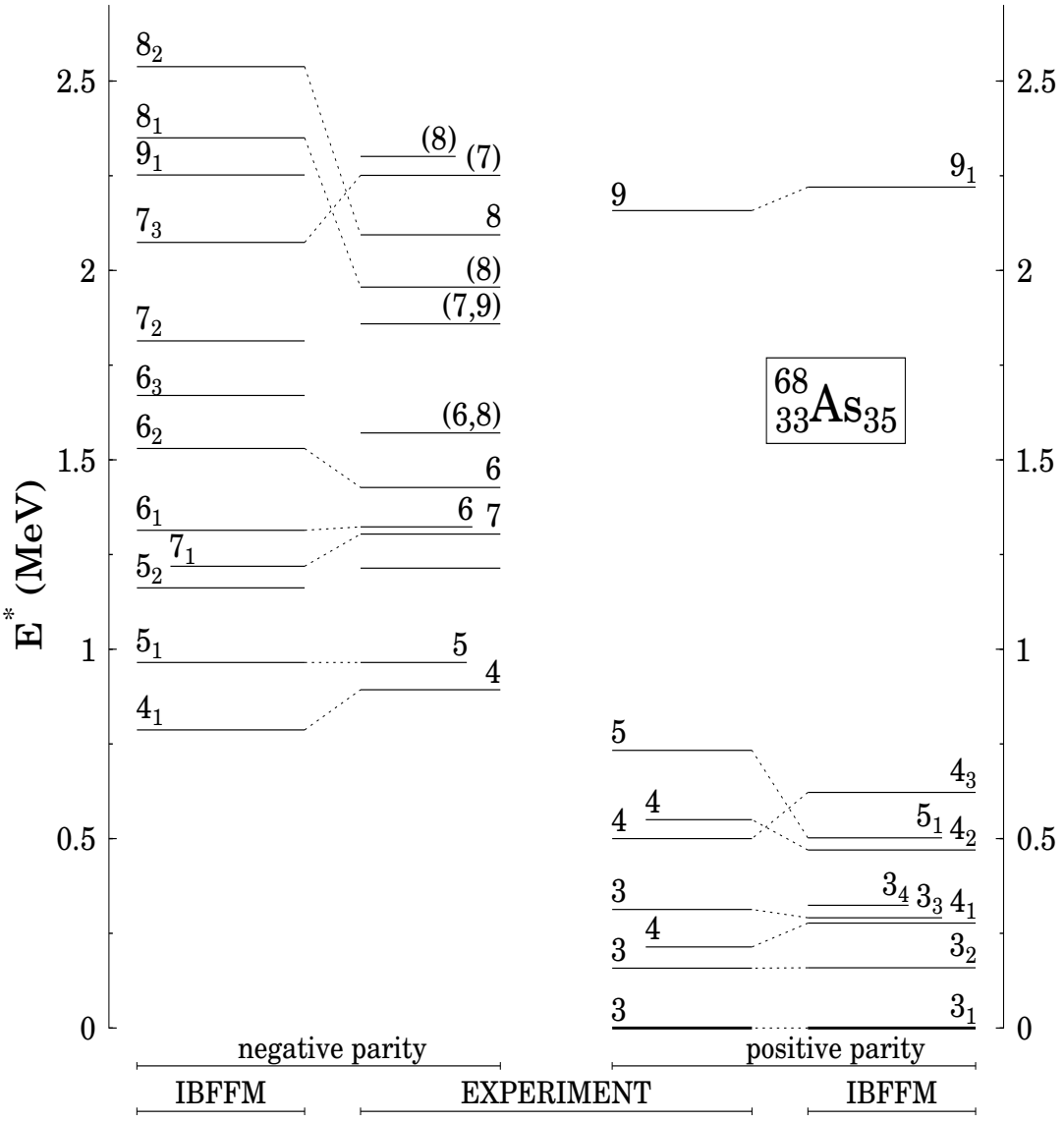

Figure 5.4: *Experimental and theoretical IBFFM energy spectra of the low-lying states in ^{68}As. Up to 0.6 MeV the positive parity levels 3^+, 4^+, 5^+ are shown. In addition, the high spin isomer 9_1^+ is shown. For negative parity the calculated states with $J^\pi = 4_1^-$, 5_1^-, 5_2^-, 6_1^-, 6_2^-, 6_3^-, 7_1^-, 7_2^-, 7_3^-, 8_1^-, 8_2^-, 9_1^- are shown.*

The IBFFM energy spectrum for $J^\pi \geq 4^-$ and $J^\pi \geq 3^+$ is compared to the results of the present experiment in Fig. 5.4. The assignment of the calculated states to the experimental levels is performed taking into account both the energy spectrum and electromagnetic properties. We note that some assignments are only tentative.

Table 5.3: Wave function of some states of ^{68}As shown in Fig. 5.4. Only components with a weight >10% are displayed. The basis states are $\mid (j_\pi j_\nu) j_{\pi\nu}, n_d I; J >$. For the components listed in the table the additional quantum number v is not needed and therefore it is omitted. The notation of the states corresponds to the calculated IBFFM states.

J^π(theor.)	$(j_\pi, j_\nu)j_{\pi\nu}$,$n_d I$	Amplitude	J^π(theor.)	$(j_\pi, j_\nu)j_{\pi\nu}$;$n_d I$	Amplitude
3_1^+	(3/2,3/2)3,00	0.81	5_2^-	(3/2,9/2)5,00	0.68
	(3/2,3/2)3,12	0.37		(3/2,9/2)5,12	−0.34
3_2^+	(3/2,5/2)3,00	0.76	6_1^-	(3/2,9/2)6,00	0.67
3_3^+	(3/2,5/2)3,00	−0.33		(3/2,9/2)6,12	−0.37
	(5/2,3/2)3,00	0.67	6_2^-	(5/2,9/2)6,00	−0.53
3_4^+	(1/2,5/2)3,00	0.55	6_3^-	(9/2,5/2)6,00	−0.61
	(5/2,5/2)5,12	0.47		(9/2,5/2)6,12	−0.35
4_1^+	(3/2,5/2)4,00	0.89	7_1^-	(5/2,9/2)7,00	0.63
4_2^+	(5/2,5/2)4,00	−0.63		(5/2,9/2)7,12	−0.41
	(5/2,3/2)4,00	0.49	7_2^-	(9/2,5/2)7,00	0.72
4_3^+	(5/2,3/2)3,12	−0.33		(9/2,5/2)7,12	−0.38
	(5/2,5/2)4,00	0.47		(9/2,5/2)7,20	−0.32
	(5/2,3/2)4,00	0.59	7_3^-	(3/2,9/2)5,12	0.68
5_1^+	(5/2,5/2)5,00	0.87	8_1^-	(3/2,9/2)6,12	0.69
4_1^-	(1/2,9/2)4,00	0.44	8_2^-	(3/2,9/2)6,12	−0.34
5_1^-	(5/2,9/2)5,00	−0.40		(5/2,9/2)6,12	−0.58
	(1/2,9/2)5,00	−0.43	9_1^-	(5/2,9/2)7,12	0.70
	(5/2,9/2)7,12	−0.33			

The IBFFM wave functions of the calculated states contain hundreds of components, for example 972 components for 3^+ states, 1058 components for 4^+ states etc. However, in the wave function of each low-lying state there are only a few sizeable components, as shown in Table 5.3. Around 65% of the 3_1^+ ground state wave function is given by the $\mid (\pi p_{3/2}, \nu p_{3/2})3, 00; 3\rangle$ two-quasi-particle component. The other members arising from the $(\pi p_{3/2}, \nu p_{3/2})j_{\pi\nu}$ multiplet are the 0_1^+, 1_2^+ and 2_2^+ states. Their calculated energies are 0.044, 0.068 and 0.165 MeV, respectively. The $(\pi p_{3/2}, \nu p_{3/2})j_{\pi\nu}$ components in these states have the amplitudes 0.72, 0.68 and 0.63, respectively. According to the parabolic rule [92], in the lowest perturbation

Table 5.4: Calculated in IBFFM branching ratios for ^{68}As compared with the experimental data.

E^*_{exp}	J^π_{exp}	$J^\pi_i \to J^\pi_f$	I_γ		E^*_{exp}	J^π_{exp}	$J^\pi_i \to J^\pi_f$	I_γ	
(MeV)	($\hbar$)	(theor.)	Exp.	Theor.	(MeV)	($\hbar$)	(theor.)	Exp.	Theor.
0.158	3^+	$3^+_2 \to 3^+_1$	100	100	0.965	$5^{(-)}$	$5^-_1 \to 4^-_1$	100	100
0.214	4^+	$4^+_1 \to 3^+_2$	6	5	1.304	$7^{(-)}$	$7^-_1 \to 5^-_1$	100	100
		$\to 3^+_1$	100	100	1.323	$6^{(-)}$	$6^-_1 \to 5^-_1$	100	100
0.313	3^+	$3^+_3 \to 4^+_1$	<2	4			$\to 4^-_1$	<3	4
		$\to 3^+_2$	16	86	1.427	$6^{(-)}$	$6^-_2 \to 5^-_2$	8	2
		$\to 3^+_1$	100	100			$\to 5^-_1$	100	100
0.500	4^+	$4^+_3 \to 3^+_3$	5	12	1.956	(8^-)	$8^-_1 \to 6^-_1$	100	100
		$\to 4^+_1$	5	5	2.094	$8^{(-)}$	$8^-_2 \to 7^-_1$	100	100
		$\to 3^+_1$	100	100	2.251	(7^-)	$7^-_3 \to 6^-_2$	<55	75
0.550	4^+	$4^+_2 \to 3^+_3$	9	220			$\to 6^-_1$	100	100
		$\to 4^+_1$	36	36			$\to 5^-_2$	<40	45
		$\to 3^+_2$	100	19					
		$\to 3^+_1$	48	23					
0.733	5^+	$5^+_1 \to 4^+_2$	17	3					
		$\to 4^+_3$	<6	26					
		$\to 4^+_1$	100	100					
3.183	$11^{(+)}$	$11^+_1 \to 9^+_1$	100	100					

order the states 0^+_1, 1^+_2, 2^+_2, 3^+_1 should lie on an open down parabola, with the 3^+_1 state being the lowest one, since the occupation probabilities are $V^2(\pi p_{3/2})$>0.5, $V^2(\nu p_{3/2})$>0.5 and the Nordheim number is $N = j_\pi - l_\pi + j_\nu - l_\nu = \frac{3}{2} - 1 + \frac{3}{2} - 1 = 1$. We note that an attempt to apply the parabolic rule to ^{68}As was made previously in Ref. [84], by taking a different set of quasi-particle energies with $\pi f_{5/2}$ and $\nu p_{1/2}$ being the lowest quasi-proton and quasi-neutron states. Using the corresponding parabolic pattern, it was predicted [84] that the $(\pi f_{5/2}, \nu p_{1/2})j_{\pi\nu} = 2^-, 3^-$ doublet is the lowest-lying multiplet, with the 3^- member of the doublet being the ground state. However, for such a quasi-particle classification there appear too few 3^+ and 4^+ states below 0.6 MeV in ^{68}As.

We note that the levels at 1.571 MeV with J^π=(6,8$^-$) and at 1.859 MeV J^π=(7,9$^-$) have properties that suggest a distinct configuration. The level at 1.571 MeV level has a half-life of 19±3 ns. In this region the calculation predicts 6^-_3, 6^-_4 and 7^-_2

states with configuration $\pi\tilde{g}_{9/2}\nu\tilde{f}_{5/2}$ (in contrast to other negative parity states with a neutron in $\nu\tilde{g}_{9/2}$). The transitions from 7^-_2 to either 6^-_3 or 6^-_4 are in agreement with the experimental data, but the decay of the 6^- states to other states is not. The calculated half-lives for 6^-_3 and 6^-_4 are 0.021 ns and 0.094 ns, respectively. The present calculation predicts stronger admixtures of other configurations than is needed, but we think that the dominant component is predicted correctly.

Using the IBFFM wave functions we have calculated the electromagnetic properties of the low-lying states of ^{68}As. The effective charges and electromagnetic ratios used are as follows: $e^\pi = 1.5\ e$, $g_l^\pi = 1.0$, $g_s^\pi = 0.4 g_s^\pi(free) = 2.234$, $g_t^\pi = \frac{1}{25} < r^2 > g_s^\pi(free) = 3.22$, $g_R = \frac{Z}{A} = 0.485$, $e^\nu = 0.5\ e$, $g_l^\nu = 0$, $g_s^\nu = g_s^\nu(free) = -3.826$, $g_t^\nu = \frac{1}{13} < r^2 > g_s^\nu(free) = -4.24$, $e_{vib} = 0.8\ e$. The values of the gyromagnetic ratios given above are taken in accordance with Ref. [17], except for g_s^π. The g_s gyromagnetic ratios in nuclear systematics lie in the range between $0.4 g_s(free)$ and $g_s(free)$. The experimental absolute value of the magnetic dipole moment deduced from the gyromagnetic factor $|g| = 0.23(2)$ [62] and the $9^{(+)}$ spin and parity of the 2158 keV state, determined in the present work, is $|\mu_{exp}(9^+_1)| = 2.07(0.18)\mu_N$, which is rather small. This value could be reproduced only by taking an unusually small value of g_s^π and a large absolute value of g_s^ν. For example, choosing g_s^ν without any quenching, the quenching of g_s^π should be smaller than 0.4 to reproduce $|\mu_{exp}(9^+_1)|$. In spite of this discrepancy, we took for the quenching $g_s^\pi = 0.4 g_s^\pi(free)$, according to the limiting value in nuclear systematics. The value of $\mu(9^+_1) = 3.19\ \mu_N$ calculated in this way is still too large. This may indicate that other components are admixed in the $9/2^+_1$ wave functions (for example those involving broken pairs), which would decrease the amplitudes of the present IBFFM components, leading to a decrease of the theoretical magnetic dipole moment.

The calculated γ-ray branching ratios are compared with the experimental ones in Table 5.4. Adopting the tentative assignment shown in Fig. 5.4, a reasonable agreement between theory and experiment was obtained for most transitions, with leading branches being reproduced. However, there are some problems and discrepancies. The main discrepancy appears for the $4^+_2 \rightarrow 3^+_3$ transition, which is much too large in the calculation. (In Table 5.4 this calculated branch is normalized to the

$4_2^+ \rightarrow 4_1^+$ transition.) This problem arises because of a rather large calculated value $B(\mathrm{M1})(4_2^+ \rightarrow 3_3^+) = 0.59\ \mu_N^2$, which basically corresponds to an internal transition within the $\pi f_{5/2}\nu p_{3/2}$ multiplet, while the value $B(\mathrm{M1})(4_2^+ \rightarrow 3_2^+) = 0.01\ \mu_N^2$ is hindered, because the main component of the 3_2^+ state is $\pi p_{3/2}\nu f_{5/2}$, and the calculated mixing of the two states is too small.

We note that in the IBFFM calculation we obtained a rather large number of low spin levels: up to 0.9 MeV there are three 0^+, nine 1^+, ten 2^+ and eight 3^+ states. The calculated branch from the 3_3^+ state to a 2^+ one is sizeable but it was not found experimentally. For high spin states with $J^\pi \geq 10^+$ the important role of configurations, which lie outside of the model space of the present calculation is expected, as for example broken pairs in the boson core and intruder states.

In the theoretical description of the present experimental results we concentrated on the structure of the low-lying states, which have well defined spin values. The EXCITED VAMPIR calculations in Ref. [6] were focused on predictions of the band structure and the analysis of shape coexistence in this nucleus. As we did not observed well developed bands, and in Ref. [6] only a few low lying states, which may serve as band heads, are mentioned, the present classification of the states cannot be directly compared with the theoretical results of the VAMPIR calculations.

Chapter 6

Spectroscopy of the neutron deficient ^{65}Ge

6.1 Earlier investigations

Using the ^{12}C(^{58}Ni,αn)^{65}Ge reaction excited states in ^{65}Ge were studied. Previously only 10 γ rays were assigned to this nucleus, forming a high energy cascade with some branchings at low energy [93]. The former studies are summarized in Table 6.1.

Table 6.1: Summary of the former experimental studies of the structure of ^{65}Ge.

Reference *	Reaction	Techniques, detectors	Measurements	Results
Görres (1987) [93]	^{40}Ca(^{28}Si,2pn)^{65}Ge, E_{Si}= 60-100 MeV	in-beam techniques, Ge(HP) detectors, 4π multisegment charged-particle detector of phoswich scintillator telescopes	E_γ, I_γ, $\gamma\gamma$-coinc, particle-γ coinc, $T_{1/2}$, $\sigma(\theta_\gamma)$	11 γ rays identified and placed in the level scheme, which contains 10 states, unambiguous J^π assignments for 4 states, $T_{1/2}$ determined for the isomeric state

* Only the first author is indicated in this column.

6.2 Experimental results

The level scheme of ^{65}Ge was established mainly on the basis of coincidence relations. The order of the transitions in the γ-ray sequences was deduced from the intensity relations. The level scheme obtained is shown in Fig. 6.1. The main branch of γ rays in the level scheme is in agreement with the previous study [93] but the 462 keV transition was relocated. Several weaker branches were found between the known levels, and short cascades of γ rays feeding both the low- and the high-lying states were added.

The spins were determined from the angular distribution ratios, $I_\gamma(143^\circ)/[I_\gamma(79^\circ)+I_\gamma(101^\circ)]$, and from the known $3/2^-$ spin-parity value of the ground state [93] assuming that the γ rays take away the maximum possible angular momenta. Definite parities were assigned to the excited states, if one of their deexciting transitions were stretched E2 or mixed M1/E2 transitions, while in the case of pure dipole transitions only tentative parities were ascribed. The 1105 keV stretched quadrupole transition, decaying from the 1215 keV isomeric state, was accepted to have M2 multipolarity on the basis of the recommended upper limits for the transition strength in agreement with Ref. [93].

6.3 Theoretical description of ^{65}Ge on the basis of IBFM calculations

The states below 3 MeV were described in the interacting boson-fermion model (IBFM) [94]. The interacting boson model (IBM) [8] parameters of the ^{64}Ge core were fitted to the energies of its excited states. The parameters obtained are h_1=0.87, h_2=$-$0.1, h_3=0, h_{40}=0.1, h_{42}=$-$0.25, h_{44}=0.35 (all in MeV). The total boson number was N=4, which is equal to the number of nucleon pairs in the valence shells. This parametrization is close to the vibrational limit of the IBM, slightly shifted towards the γ-soft direction.

For the $\tilde{p}_{3/2}$, $\tilde{f}_{5/2}$, $\tilde{p}_{1/2}$ and $\tilde{g}_{9/2}$ states, quasi-particle energies = 0, 0.05, 1.25 and 2.18 MeV with respect to $\tilde{p}_{3/2}$, and occupation probabilities = 0.64, 0.31, 0.06

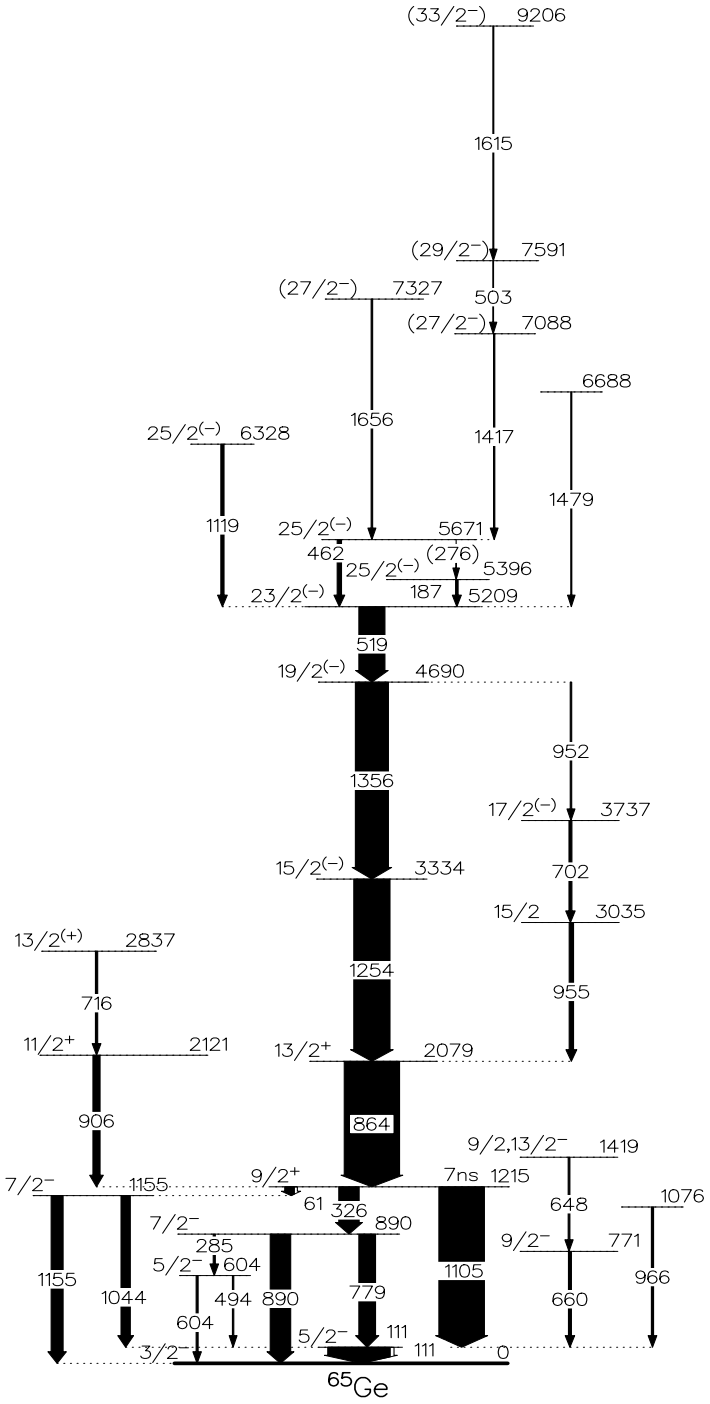

Figure 6.1: *Proposed level scheme for* ^{65}*Ge.*

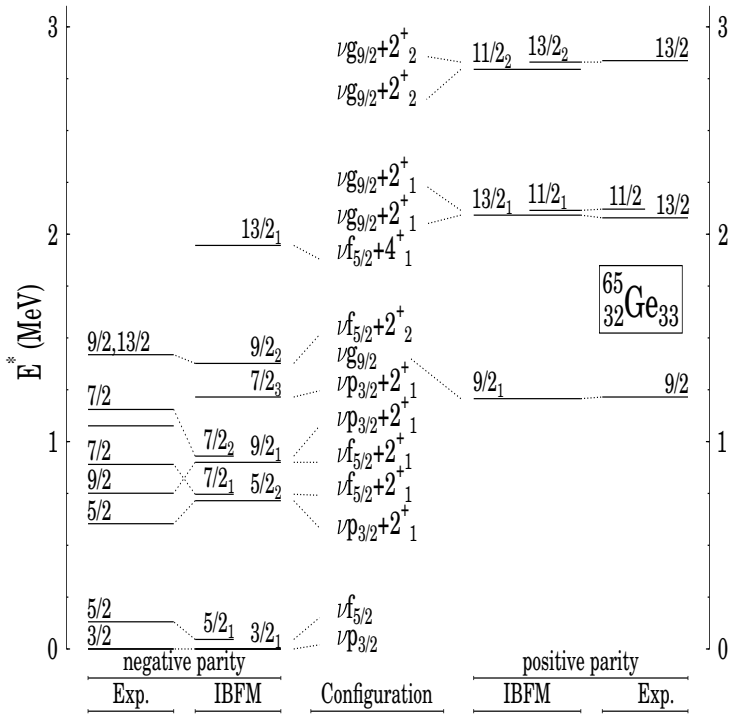

Figure 6.2: *Calculated low-lying states of ^{65}Ge compared to experimental data.*

and 0.03, respectively, were obtained from BCS calculations using single-particle energies from Ref. [95] and G=0.32 MeV. The boson-fermion interaction strengths used in the calculation are Γ_0=0.02 MeV, Λ_0=0.5 MeV,χ=$-$1.0, A_0=0.1 MeV for negative parity and 0 MeV for positive parity states. The IBFM energy spectrum is compared with the experimental data in Fig. 6.2.

The IBFM wave functions were used to calculate E2 and M1 transition probabilities, using $e^{\nu} = 0.5\ e$value for neutron effective charge and g_R = Z/A = 0.492, $g_l = 0$, $g_s = 0\ .5g_s(free) = -1.913$ values for gyromagnetic ratios. The boson charge $e^{VIB} = 1.35\ e$ and the tensor gyromagnetic ratio g_T=$-$1.07 are taken from a previous calculation for ^{66}Ga [12]. The main calculated γ-branches depopulating the levels are in agreement with the experiment for the assigned states, except for the $7/2^-_1$ state, where the ordering of the two largest branches in the calculation was reversed with respect to experiment. The level at 1.419 MeV was assigned to the $9/2^-_2$ theoretical state due to its rather small distance from $9/2^-_1$. The expected energy difference between $9/2^-_1$ and $13/2^-_1$ is about the phonon energy, $\sim$1 MeV. The

IBFM predicts the continuation of the vibrational bands, as well as additional multiphonon states at higher energies, but above 3.1 MeV a parity change takes place in the yrast sequence, which prevents the population of these states, and indicates some kind of structural change.

A detailed description of high spin states in ^{67}Ge in the IBFM + broken pair model is presented in Ref. [96]. Applying these results qualitatively to ^{65}Ge, a very pronounced competition of different broken pair states is expected for the negative parity levels with $J^{\pi} \geq 15/2^{-}$, resulting in a random order of broken proton and neutron pair states along the yrast sequence.

Chapter 7

SUMMARY

In the present dissertation I have reported on the results of investigation of the structure of ^{65}Ge and ^{68,72,73}As nuclei. The aim of my work was to study the competition between the collective and single-particle degrees of freedom in these nuclei. For this purpose I have studied the structure of Ge and As nuclei by means of in-beam γ and e^- spectroscopic methods.

7.1 Methods

The states of ^{72,73}As nuclei were excited via $(p, n\gamma)$ reaction. Single γ, $\gamma\gamma$-coincidence and internal conversion electron spectra were measured. The energies and intensities of the γ lines were determined by analysing the single spectra. The level schemes were constructed on the basis of the $\gamma\gamma$-coincidence relations, as well as energy and intensity balances.

The parities of the levels of these nuclei were determined by using the conversion coefficients deduced from the intensity ratios of the corresponding conversion electron and γ lines. The spin values were determined from comparison of the relative excitation cross sections of the levels measured at several bombarding energies with Hauser-Feshbach nuclear reaction cross section calculations. The multipolarities of the transitions and the reanalysed former angular distribution data provided further information to make the spin assignments unambiguous or more accurate.

The ^{65}Ge and ^{68}As nuclei were studied via the ^{12}C+^{58}Ni heavy-ion induced reaction at the NORDBALL multi-detector array equipped with 15 BGO-shielded Ge(HP) detectors and a γ-ray calorimeter of BaF_2 crystals. For reaction channel selection a Si ball consisting of 21 ΔE type Si detectors and a neutron wall of 11 liquid scintillators were used.

For identification of the γ rays several particle-gated spectra and matrices were sorted, and than subtracted from each other to eliminate the contaminating γ lines. The level schemes of ^{65}Ge and ^{68}As were constructed on the basis of $\gamma\gamma$-coincidence matrices. The spin values of the excited states were deduced using the results of the simplified $\gamma\gamma$ correlation analysis, which is sensitive for the angular momentum transferred by the γ rays.

7.2 Results

1. I have measured the energies and intensities of 112 transitions assigned to ^{72}As, of which 57 were new. I have also determined the internal conversion coefficients for more than 50 (among them 38 new) transitions, and deduced their multipolarities. I proposed a more complete level scheme for ^{72}As up to 850 keV, which contains 6 new states and more accurate spin-parity assignments for more than 30 states.

2. I have measured the energies and intensities of the γ rays assigned to ^{73}As. I have also determined the multipolarities. For 20 transitions belonging to ^{73}As they were unknown earlier. I have deduced more accurate or unambiguous spin and parity values for 22 states the first time.

3. I have significantly extended the level scheme of ^{68}As up to the excitation energy of 6 MeV and $J^\pi = (15^+)$, containing 33 new transitions and 18 new states. I have deduced the multipole character of more than 30 transitions from the angular distribution ratios. I have found a new isomeric state at 1571 keV with a half life of 19$\pm$3 ns.

4. I have assigned 21 new transitions to the ^{65}Ge and proposed a new, more complete level scheme up to excitation energy 9 MeV with 17 new states from the total 25 ones. I have determined the spin values of the excited states up to $(33/2^-)$.

As a part of the program interacting boson-fermion(-fermion) model (IBF(F)M) calculations were performed for more than twenty nuclei in the Zn-As region by S. Brant, Lj. Šimičić and V. Paar (Unversity of Zagreb) and by T. Fényes (ATOMKI, Debrecen). The results of the IBF(F)M nuclear structure calculations were in reasonable agreement with the experimental level schemes, as well as electromagnetic moments and reduced transition probabilities. The low-lying states of ^{68,72}As have many components, but in several cases the one-quasiparticle component was dominating. Many quasiparticle-plus-phonon states were also identified, especially in ^{65}Ge and ^{73}As.

Although intruder states have been found in the neighbouring even-even Ge nuclei, all observed states could be assigned to normal core configurations in the odd-odd As and ^{65}Ge nuclei. Only in ^{73}As there are candidates for intruder states, and indication of the presence of shape coexistence already at quite low energy.

In the studied Ge and As isotopes I did not found any band structure. The level schemes obtained resemble more to that of spherical nuclei. Even the IBF(F)M calculations show less collectivity than it was predicted on the basis of the Hartree-Fock-Bogoliubov calculations.

Chapter 8

ÖSSZEFOGLALÁS

Az A≈60-80 tömegszám tartományban több magszerkezeti problémát is vizsgáltunk. A könnyű As és Ge atommagok 4-5 valencia protont és 5-10 valencia neutront tartalmaznak. Ilyen nagyszámú valencia nukleon már elég ahhoz, hogy deformált magalak alakulhasson ki. Ezenfelül a páratlan proton vagy neutron polarizáció útján tovább deformálhatja a magtörzset. A deformált magok szerkezete a folyadékcsepp-modell fogalomrendszerét felhasználva írható le. Ezt az elképzelést támasztja alá, hogy a páros-páros Ge atommagok kvadrupól momentuma 0.8-0.9 eb között változik, valamint, hogy ezekben az izotópokban sávszerkezetet figyeltek meg. Szintén ebben a magtartományban megnyúlt és belapult magalakot találtak ugyanazon mag különböző gerjesztési energiáinál. Az EXCITED VAMPIR modellel végzett számolások alapján hasonló szerkezeti sajátságok megjelenését jósolták a könnyű Ge és As izotópoknál.

A héjmodell szemszögéből elemezve az adott atommagok szerkezetét viszont nem várunk számottevő deformációt ebben a magtartományban, mivel a valencia pályák ($2p_{1/2}$, $2p_{3/2}$, $1f_{5/2}$) rövidek, kis impulzus momentumuk miatt nem képesek jelentős deformációt létrehozni, és ezeken a pályákon levő nukleonok csak gyengén tudják polarizálni a magtörzset. Ezt az elgondolást erősíti, hogy a páros-páros Ge izotópokban a 2_1^+ állapot energiája $\sim$1 MeV, ami elég nagy a deformált magokban előforduló értékekhez képest, és hogy ezen atommagok szerkezete kvázivibrációs jelleget mutat.

Az A≈60-80 tartományba eső atommagoknak ezt az érdekes, kettős viselkedését az egyrészecskés és kollektív állapotok erős versengése indokolhatja, amit magszerkezeti számolásokkal támaszthatunk alá. Erre a célra a kölcsönható bozon-fermion(-fermion) modellt (IBF(F)M) választottuk, mivel ez a modell különösen alkalmas az átmeneti magok leírására.

Az adott atommagok szerkezetének vizsgálatát még az is motiválta, hogy a Ge-Se tartományban az U(6/12) szuperszimmetria SU(5)-ös határesetének megjelenését várhatjuk.

A leírt jelenségek jobb megértése érdekében az MTA Atommagkutató Intézetének magspektroszkópiai csoportja átfogó programba kezdett, aminek a célja a Ga-As izotópok magszerkezeti vizsgálata volt. A kísérleti munkát az a tény indokolta, hogy az adott atommagok nívósémáira vonatkozó ismeretek rendkívül hiányosak voltak, így bármely elméleti vizsgálat előtt új, teljesebb kísérleti adatokra volt szükség. A kutatási programhoz az ATOMKI-ban rendelkezésre álltak a megfelelő eszközök, a könnyű ionok gyorsítására alkalmas izokrón ciklotron, a nagytisztaságú félvezető Ge és Si detektorok, elektronikus egységek és az intézetben kifejlesztett szupravezető mágneses elektron spektrométer.

Az említett program keretében én a ^{65}Ge és a ^{68,72,73}As atommagok szerkezetét tanulmányoztam in-beam γ- és elektronspektroszkópiai módszerekkel. A jelen értekezésben ezekről a kutatási eredményeimről számolok be.

8.1 Módszerek

A ^{72,73}As atommagok kisenergiás gerjesztett állapotait $(p, n\gamma)$ reakcióban vizsgáltam Debrecenben. A mérések során egydimenziós γ-, kétdimenziós $\gamma\gamma$-koincidencia- és belső konverziós elektronspektrumokat vettem fel. A γ-átmenetek pontos energiáját és relatív intenzitását az egydimenziós γ-spektrumokból határoztam meg. A vizsgált atommagok nívósémáit $\gamma\gamma$-koincidencia kapcsolatok, energia- és intenzitásmérleg alapján építettem fel.

A megfelelő konverziós elektron és γ-sugárzások intenzitásának hányadosaiból származtattam a belső konverziós együtthatókat és ezeket felhasználva határoztam meg az átmenetek multipolaritását és a gerjesztett állapotok paritását. Különböző bombázó energiákon mértem a nívók gerjeszési hatáskeresztmetszetét. A kapott hatáskeresztmetszetek Hauser-Feshbach analízise, valamint az átmenetek multipolaritása és a korábbi szögeloszlás mérési adatok feldolgozása során kapott eredmények alapján egyértelmű spin értékeket tudtam rendelni a ^{72,73}As magok gerjesztett állapotaihoz.

A stabilitási sávtól távoleső ^{65}Ge és a ^{68}As atommagokat a ^{12}C+^{58}Ni nehézion-reakcióban állítottam elő. A mérések során a 15 BGO árnyékolással ellátott Ge(HP) detektorból álló NORDBALL detekrorrendszert használtuk. Ezenkívül a detektorrendszer 30 BaF_2 kristályból álló γ-kaloriméterrel is fel volt szerelve. A reakció csatornák kiválasztására a 21 ΔE típusú Si detektorból álló töltöttrészecske-detektorrendszer és a 11 folyadék szcintillátorból álló neutron-detektorfal szolgált. A szükséges kísérletet a dániai Niels Bohr Intézetben végeztük a stockholmi Műszaki Egyetemhez tartozó magfizikai csoporttal együttműködve.

A γ-sugárzások azonosításához spektrumokba és mátrixokba gyűjtöttem azokat az eseményeket, amelyek eleget tettek az egyes reakció csatornák előállításához szükséges, megfelelő számú töltöttrészecske és neutron egyidejű detektálásának. A spektrumokban és mátrixokban megjelenő szennyező γ vonalakat egy többlépéses kivonásos módszerrel küszöböltem ki. A ^{65}Ge és a ^{68}As atommagok nívósémáit $\gamma\gamma$-koincidencia adatok alapján építettem fel. A gerjesztett állapotok spin értékeinek meghatározásánál egy egyszerűsített $\gamma\gamma$ korrelációs analízis eredményeit használtam fel.

8.2 Eredmények

1. Azonosítottam a ^{72}As atommag 57 új γ-sugárzását. Meghatároztam ezen sugárzások és a korábban ismert 55 γ-sugárzás pontos energiáját és relatív intenzitását. Továbbá meghatároztam több mint 50 átmenet belső konverziós együtthatóját, amelyek közül 38 nem volt ismert korábban, és ezen átmenetek multipolaritásait. A mért kísérleti adatokra alapozva felépítettem a ^{72}As atommag nívósémáját 850 keV gerjesztési energiáig, az eredményül kapott nívóséma 6 új nívót tartalmaz. Egyértelműen meghatároztam több mint 30 állapot spin, paritás értékét.

2. Meghatároztam a ^{73}As maghoz rendelt γ-sugárzások energia és relatív intenzitás értékét. Szintén meghatároztam 28, a ^{73}As atommaghoz tartozó átmenet belső konverziós együtthatóját és multipolaritását; ezek közül 20 nem volt ismert korábban. A ^{73}As atommag 22 gerjesztett állapotához rendeltem egyértelmű spin, paritás értéket.

3. Felépítettem a ^{68}As atommag nívósémáját 6 MeV gerjesztési energiáig és (15^+) spin értékig. Az új, jelentősen kiterjesztett nívóséma 33 új átmenetet és 18 új állapotot tartalmaz. Több mint 30 átmenet multipolaritását határoztam meg szögkorrelációs adatokból. Találtam egy új, 19±3 ns-os felezési idővel rendelekző izomer állapotot 1571 keV gerjesztési energiánál.

4. 21 új átmenetet azonosítottam a ^{65}Ge atommaghoz és felépítettem egy, az eddiginél teljesebb nívósémát 9 MeV gerjesztési energiáig, amely 17 új állapotot tartalmaz az eddig ismert 8 mellett. $(33/2^-)$ értékig meghatároztam a nívók spin értékeit.

A vizsgált atommagok és szomszédjaik nívórendszerét és elektromágneses sajátságait IBF(F) modell segítségével számoltuk. A számolásokat nemzetközi együttműködés keretében S. Brant, Lj. Šimičić és V. Paar végezte Zágrábban, és Fényes Tibor Debrecenben. Az IBF(F)M számolások eredményei elfogadható egyezést mutattak a kísérleti adatokkal, mind a nívósémákat, mind az elektromágneses sajátságokat illetően. A ^{68,72}As atommagok kisenergiás állapotai sok komponenst tartalmaznak, de bizonyos állapotokban az egykvázirészecske komponens a legerősebb. Más esetekben, különösen a ^{65}Ge és a ^{73}As magoknál kvázirészecske-plusz-fonon jellegű állapotokat is azonosítottunk.

Bár a páros-páros Ge izotópokban intruder állapotokat és alakkoegzisztenciára utaló sajátságokat is megfigyeltek, az általam vizsgált ^{68,72}As és ^{65}Ge atommagokban valamennyi állapothoz normál szerkezetet lehetett rendelni. Egyedül a ^{73}As atommagban találtunk olyan nívókat, melyek lehetséges, hogy intruder állapotok. Ebből az eredményből az alakkoegzisztencia létére következtethetünk a ^{73}As-nál már egészen alacsony energián is.

A vizsgált Ge és As izotópokban nem figyeltem meg sávszerkezetet. A kapott nívósémák gömbszerű, héjmodellel leírható szerkezetű atommagokra utalnak. Ugyanakkor az IBF(F)M számolások eredményei kevesebb kollektivitást mutatnak a vizsgált atommagoknál, mint amennyi a Hartree-Fock-Bogoljubov számolások alapján várható.

Megjegyzés: A ^{72}As atommagnál az összes mérés, a ^{73}As atommagnál az egydimenziós γ- és az elektronmérések megtervezésében, végrehajtásában, a ^{65}Ge és a ^{68,72,73}As atommagokra vonatkozó adatok feldolgozásában, valamint a fentebb felsorolt eredmények elérésében meghatározó szerepem volt. A ^{73}As magra vonatkozó kutatásokat Podolyák Zsolttal közösen végeztem, de míg ő főleg a $\gamma\gamma$-koincidenciaméréssel kapcsolatos problémákkal foglalkozott, én a γ-sugárzások energia- és intenzitásmeghatározására, a konverziós elektronmérésekre, a spin- és paritásmeghatározásra (multipolaritásmeghatározás, Hauser-Feshbach-analízis) helyeztem a hangsúlyt. A kollektív munkát igénylő méréseket a társszerzők segítségével végeztem. Résztvettem továbbá a kísérleti és az elméleti eredmények összevetésében.

Bibliography

[1] R. F. Casten, Nuclear Structure from a Simple Perspective, (Oxford University Press, New York, 1990).

[2] Table of Isotopes, ed. R. B. Firestone, V. Shirley, C. M. Baglin, S. Y. F. Chu and J. Zipkin (Wiley, New York, 1996).

[3] J. H. Hamilton, in Treatise on Heavy-Ion Science, vol. 8, ed. D. A. Bromley (Plenum, New York, 1989), p. 3.

[4] L. Chatuvedi et al., Phys. Rev. C. 43 (1991) 2541.

[5] A. Petrovici, K. W. Schmid and A. Faessler, Nucl. Phys. A 571 (1994) 77.

[6] A. Petrovici, K. W. Schmid, A. Faessler, D. Pantelica, F. Negoita, B. R. S. Babu, A. V. Ramayya, J. H. Hamilton, J. Kormicki, L. Chaturvedi, W. C. Ma, S. J. Zhu, N. R. Johnson, I. Y. Lee, C. Baktash, F. K. McGowan, M. L. Halbert, M. Riley and J. D. Cole, Phys. Rev. C 53 (1996) 2134.

[7] A. Arima and F. Iachello, Phys. Rev. Lett. 35 (1975) 157; Ann. of phys. 99 (1976) 253; 111 (1978) 201; 123 (1979) 468.

[8] F. Iachello, and A. Arima, The interacting boson model (Cambridge Univ. Press, Cambridge, 1987).

[9] F. Iachello and O. Scholten, Phys. Rev. Lett. 43 (1979) 679.

[10] O. Scholten, Progr. Part. Nucl. Phys. 14 (1985) 189; Ph. D. Thesis, Univ. of Groningen (1980).

[11] V. Paar, in Capture gamma ray spectroscopy, AIP Conf. Proc. 125 (Am. Inst. of Physics, N.Y., 1985), p.70 ; S. Brant, V. Paar and D. Vretenar, Z. Physik A319 (1984) 355; V. Paar, D. K. Sunko and D. Vretenar, Z. Physik A327 (1987) 291.

[12] J. Timár, T. X. Quang, T. Fényes, Zs. Dombrádi, A. Krasznahorkay, J. Kumpulainen, R. Julin, S. Brant, V. Paar and Lj. Šimičić, Nucl. Phys. A 573 (1994) 61.

[13] J. Timár, T. X. Quang, T. Fényes, Zs. Dombrádi, A. Krasznahorkay, J. Kumpulainen, R. Julin, Nucl. Phys. A 552 (1993) 149.

[14] J. Timár, T. X. Quang, Zs. Dombrádi, T. Fényes, A. Krasznahorkay, S. Brant, V. Paar, Lj. Simičič, Nucl. Phys. A 552 (1993) 170.

[15] T. Fényes, J. Gulyás, T. Kibédi , A. Krasznahorkay, J. Timár, S. Brant, V. Paar, Nucl. Phys. A 419 (1984) 557.

[16] Zs. Podolyák, T. Fényes, J. Timár, Nucl. Phys. A 584 (1995) 60.

[17] A. Algora, D. Sohler, T. Fényes, Z. Gácsi, S. Brant and V. Paar, Nucl. Phys. A 588 (1995) 399.

[18] Z. Gácsi, J. Gulyás, T. Kibédi , E. Koltai, A. Krasznahorkay, T. Fényes, Izv. A. N. SSSR 47 (1983) 45.

[19] M. R. Bhat, Nucl. Data Sheets 68 (1993) 117.

[20] M. M. King and W.-T. Chou, Nucl. Data Sheets 69 (1993) 865.

[21] G. Székely, Comput. Phys. Commun. **34** (1985) 313.

[22] M. Jääskeläinen, University of Jyväskylä, JYFL Rep. 3/84.

[23] T. Lönnroth and P. Jaulo, Nucl. Instr. Meth. A261 (1984) 549.

[24] Z. Árvay, T. Fényes, K. Füle, T. Kibédi, S. László, Z. Máté, Gy. Mórik, D. Novák, and F. Tárkányi, Nucl. Instr. Meth. 178 (1980) 85; T. Kibédi, Z. Gácsi, A. Krasznahorkay, and S. Nagy, ATOMKI Ann. Rep., Debrecen (1986), p. 55; T. Kibédi, Z. Gácsi, and A. Krasznahorkay, ATOMKI Ann. Rep., Debrecen (1987), p. 100.

[25] F. Rösel, H. M. Fries, K. Alder and H. C. Pauli, At. Data Nucl. Data Tables 21 (1978) 91.

[26] E. Sheldon, and V. C. Rogers, Comput. Phys. Commun. 6, (1973) 99.

[27] C. M. Perey and F. G. Perey, At. Data Nucl. Data Tables bf 17 (1976) 1.

[28] F. G. Perey, Phys. Rev. 131 (1963) 745.

[29] D. Wilmore and P. E. Hodgson, Nucl. Phys. 55 (1964) 673.

[30] B. Herskind, Nucl. Phys. A 447 (1995) 395.

[31] G. Sletten, Proc. Int. Seminar on Frontiers of Nuclear Spectroscopy, Tokyo, Japan (1992), (World Scientific, Singapore, 1993) p. 129.

[32] T. Kuroyanagi, S. Mitarai, S. Suematsu, B. J. Min, H. Tomura, J. Mukai, T. Maeda, R. Nakatani, G. Sletten, J. Nyberg, D. Jerrestam, Nucl. Instrum. Methods A 316 (1992) 289.

[33] S. E. Arnell, H. A. Roth, Ö. Skeppstedt, J. Bialkowski, M. Moszýnski, D. Wolski and J. Nyberg, Nucl. Instrum. Methods A 300 (1991) 303.

[34] D. Wolski, M. Moszýnski, T. Ludziejewski, A. Johnson, W. Klamra and Ö. Skeppstedt, Nucl. Instrum. Methods A 360 (1995) 584.

[35] A. Johnson *et al.*, Nucl. Phys. A 557 (1993) 401c.

[36] Zs. Dombrádi, B. M. Nyakó and M. Józsa, ATOMKI Ann. Rep., Debrecen (1994), p. 11.

[37] D . Radford, Nucl. Instrum. Methods A 361 (1995) 297 and 306.

[38] M. Palacz *et al.*, to be published

[39] J. B. Cumming and N. R. Johnson, Phys. Rev. 110 (1958) 1104.

[40] A. Hübner, Z. Phys. 183 (1965) 25.

[41] S. Mordechai, E. Friedman, A. A. Jaffe, D. Nir and M. Paul, Nucl. Phys. A 230 (1974) 343.

[42] H. Bertschat, H. Kluge, U. Leithäuser, E. Recknagel and B. Spellmeyer, Nucl. Phys. A 249 (1975) 93.

[43] K. Kimura, N. Takagi and M. Tanaka, Nucl. Phys. A 272 (1976) 381.

[44] B. O. Ten Brink, J. Akkermans, P. Van Nes and H. Verheul, Nucl. Phys. A 330 (1979) 409.

[45] M. J. Mariscotti, M. Behar, A. Filevich, G. Garcia Bermudez, A. M. Hernandez and C. Kohan, Nucl. Phys. A 260 (1976) 109.

[46] P. Raghavan, R. S. Raghavan and D. E. Murnick, Phys. Rev. C 15 (1977) 1583.

[47] J. Döring, S. T. Tabor, J. W. Holcomb, T. D. Johnson, M. A. Riley and P. C. Womble, Phys. Rev. C 49 (1994) 2419.

[48] M. M. King, Nucl. Data Sheets 56 (1989) 1; updated in W.-T. Chou and M. M. King, Nucl. Data Sheets 73 (1994) 215.

[49] J. Y. Mei, A. C. G. Mitchell and C. M. Huddleston, Phys. Rev. C 79 (1950) 19.

[50] E. Brun, J. J. Kraushaar and W. E. Meyerhof, Phys. Rev. C 102 (1956) 808.

[51] V. Paar, in In-beam nuclear spectroscopy, vol. 2, eds. Zs. Dombrádi and T. Fényes (Akadémiai Kiadó, Budapest, 1984), p. 675; in Capture gamma-ray spectroscopy, Proc. AIP Conf. 125 (American Inst. of Physics, New York, 1985) p. 70.

[52] S. Brant, V. Paar and D. Vretenar, Z. Phys. A 327 (1987) 291.

[53] T. Kibédi, Zs. Dombrádi, T. Fényes, A. Krasznahorkay, J. Timár, Z. Gácsi, A. Passoja, V. Paar and D. Vretenar, Phys. Rev. C 37 (1988) 2391.

[54] D. Bonatsos, Interacting boson models of nuclear structure (Clarendon, Oxford, 1988).

[55] S. Brant, V. Paar and D. Vretenar, Computer code IBFFM/OTQM, IKP Jülich (1985), unpublished.

[56] L. H. Goldman, Phys. Rev. 165 (1968) 1203.

[57] R. Fournier, J. Kroon, T. H. Hsu, B. Hird and G. C. Ball, Nucl. Phys. A 202 (1973) 1.

[58] W. A. Yoh, S. E. Darden and S. Sen, Nucl. Phys. A 263 (1976) 419.

[59] J. A. Bieszk, L. Montestruque and S. E. Darden, Phys. Rev. C 16 (1977) 1333.

[60] M. R. Bhat, Nucl. Data Sheets 68 (1993) 579.

[61] V. Paar, Nucl. Phys. A 331 (1979) 16.

[62] P. Raghavan, At. Data and Nucl. Data Tables 42 (1989) 189.

[63] W. Hogervorst, H. A. Helms, G. J. Zaal, J. Bouma and J. Blok, Z. Phys. A 294 (1980) 1.

[64] K. W. Marlow and A. Faas, Nucl. Phys. A 132 (1969) 339.

[65] R. D. Meeker and A. B. Tucker, Nucl. Phys. A 157 (1970) 337.

[66] B. O. ten Brink, P. van Nes, C. Hoetmer and H. Verheul, Nucl. Phys. A 338 (1980) 24.

[67] P. van der Merwe, E. Barnard, J. A. M. de Villiers and J. G. Malan, Nucl. Phys. A 240 (1975) 273.

[68] B. Heits, H.–G. Friederichs, A. Rademacher, K. O. Zell, P. von Brentano and C. Protop, Phys. Rev. C 15 (1977) 1742.

[69] C. R. Ramasvamy, N. G. Puttaswamy and N. Sarma, Phys. Rev. C 19 (1979) 1236.

[70] M. Schrader, H. Reiss, G. Rosner and H. V. Klapdor, Nucl. Phys. A 263 (1976) 193.

[71] G. Rotbard, M. Vergnes, J. Vernotte, G. Berrier–Ronsin, J. Kalifa and R. Tamisier, Nucl. Phys. A 401 (1983) 41.

[72] M. N. Vergnes, G. Rotbard, R. Seltz, F. Guilbaut, D. Ardouin, R. Tamisier and P. Avignon, Phys. Rev. C 14 (1976) 58.

[73] M. M. King and W.–T. Chou, Nucl. Data Sheets 69 (1993) 857.

[74] P. M. Endt, At. Data Nucl. Data Tables 23 (1979) 547.

[75] H. Toki and A. Faessler, Phys. Lett. 63B (1976) 121.

[76] G. Alaga, Bull. Am. Phys. Soc. 4 (1959) 359.

[77] A. C. Rester, J. H. Hamilton, A. V. Ramaya and N. R. Johnson, Nucl. Phys. A 162 (1971) 481.

[78] D. Ardouin, R. Tamisier, G. Berrier, J. Kalifa, G. Rotbard and M. Vergnes, Phys. Rev. C 11 (1975) 1649.

[79] L. S. Kisslinger and R. A. Sorensen, Rev. Mod. Phys. 35 (1963) 853.

[80] D. Sohler, A. Algora, T. Fényes, J. Gulyás, S. Brant and V. Paar, Nucl. Phys. A 604 (1996) 25.

[81] P. Baumann, M. Bounajma, A. Huck, G. Klotz, A. Knipper, G. Walter, G. Marguier, C. Richard-Serre, H. Ravn, E. Hagebo, P. Hoff and K. Steffensen, Phys. Rev. C 50 (1994) 1180.

[82] R. C. Pardo, Ph.D. Thesis, Univ. Texas, Austin (1976), referred by M. R. Bath, Nucl. Data Sheets 55 (1988) 1.

[83] T. Badica and I. Popescu, Bull. Acad. Sci. USSR, Phys. Ser. 53 (1989) 137.

[84] T. Badica and I. Popescu, Bull. Russ. Acad. Sci. Phys. 58 (1994) 856.

[85] M. R. Bhat, Nucl. Data Sheets 76 (1995) 343.

[86] D. Pantelica, A. Pantelica, F. Negoita, A. V. Ramayya, J. H. Hamilton, L. Chaturvedi, J. Kormicki, B. R. S. Babu, A. Petrovici, K. W. Schmid, A. Faessler, N. R. Johnson, I. Y. Lee, C. Baktash, F. K. McGowan, J. D. Cole, E. F. Zganjar, T. M. Cormier, J. Phys. G 22 (1996) 22.

[87] T. Bădică, V. Cojocaru, D. Pantelică, I. Popescu, N. Scintei, Nucl. Phys. A 535 (1991) 425.

[88] B. Rosner, S. Mordechai, D. J. Pullen, Nucl. Phys. A 206 (1973) 76.

[89] P. Baumann, M. Bounajma et al., Rapport d'Activite CRN. Strasbourg (1983) p. 80.

[90] V. Paar, in In-beam nuclear spectroscopy, vol. 2, eds. Zs. Dombrádi and T. Fényes (Akadémiai Kiadó, Budapest, 1984), p. 675; in Capture gamma-ray spectroscopy, AIP Conf. Proc. 125 (American Inst. of Physics, New York, 1985) p. 70.

[91] S. Brant, V. Paar and D. Vretenar, Z. Phys. A 319 (1984) 355, V. Paar, D. K. Sunko and D. Vretenar, Z. Phys. A 327 (1987) 291; S. Brant and V. Paar, Z. Phys. A 329 (1988) 151.

[92] V. Paar, Nucl. Phys. A 331 (1979) 16.

[93] J. Görres, T. Chapuran, D. P. Balamuth and J. W. Arrison, Phys. Rev. Lett. 58 (1987) 662.

[94] F. Iachello and P. Van Isacker, The Interacting Boson-Fermion Model (Cambridge Univ. Press, Cambridge, 1991).

[95] A. van Egmond et al., Z. Phys. A 300 (1981) 323.

[96] D. Sohler, Zs. Dombrádi, S. Brant, J. Cederkäll, M. Lipoglavsek, M. Palacz, V. Paar, J. Persson, A. Atac, C. Fahlander, H. Grawe, A. Johnson, A. Kerek, W. Klamra, J. Kownacki, A. Likar, L.-O. Norlin, J. Nyberg, R. Schubart, D. Seweryniak, G. de Angelis, P. Bednarczyk, D. Foltescu, D. Jerrestam, S. Juutinen, E. Mäkelä, B. M. Nyakó, M. de Poli, H. A. Roth, T. Shizuma, Ö. Skeppstedt, G. Sletten, S. Törmänen, to be published.

Appendix A

Acknowledgements

It is my pleasure to express my gratitude to all the people who helped me during my PhD studies. Without their skills, knowledge and friendship this work would have never been completed.

I would like to thank my supervisor Tibor Fényes, who made possible this work creating the necessary conditions for performing it, as well as for his contribution in the IBFFM calculations. His support and guidance are fully acknowledged. For his continuous help I wold like to thank Zsolt Dombrádi, who introduced me to the field of experimental nuclear spectroscopy and who directed me during the last two years.

Most of the experiments I have participated in, have been difficult requiring many people to take part. First of all, I would like to thank Zoltán Gácsi and János Gulyás for introducing me to the techniques of the experimental work. I am grateful to Attila Krasznahorkay and János Timár for their help in the measurements.

I will always remember pleasant cooperation and nice company of Alejandro Algora and Zsolt Podolyák, who participated in this work and without whom the "Arsenic Group" would have not be the same. Many thanks to István Dankó, Mohammed Fayez-Hassan and Lóránt Félegyházi.

I am also obliged to Vladimir Paar and Slobodan Brant for their contribution in the IBFFM calculations.

I would like to thank also the cyclotron staff and the cryogenics laboratory for their help and support in the measurements.

I am indebted to the members of the group from the Royal Institute of Technology in Stockholm under the conduct of Arne Johnson. I am very grateful to András Kerek, who was my supervisor during my scholarship in Stockholm and was my guide in Sweden. Many thanks to Lars-Olof Norlin, Joakim Cederkäll, Bosse

Cederwall, Wlodzimierz Klamra, Dezső Novák and Ramon Wyss. I will not never forget my stay in Stockholm.

The financial support from The Hungarian Fund for Scientific Research (OTKA Contract No. 3004/1991, T7481 and T20655) is gratefully acknowledged.

Finally, I wish to thank my husband, Fecus Kun for his continuous help, encouragement and patience.

Appendix B

Publications

This thesis is based on the following papers:

1. **D. Sohler**, A. Algora, T. Fényes, J. Gulyás, S. Brant and V. Paar:
   Structure of ^{72}As nucleus,
   Nucl. Phys. **A** 604 (1996) 25.

2. **D. Sohler**, Zs. Podolyák, J. Gulyás, T. Fényes, A. Algora, Zs. Dombrádi, S. Brant and V. Paar:
   Structure of ^{73}As nucleus,
   accepted for Nucl. Phys. **A**, ATOMKI Preprint 1-1996-P.

3. **D. Sohler**, Zs. Dombrádi, S. Brant, J. Cederkäll, M. Lipoglavsek, M. Palacz, V. Paar, J. Persson, A. Atac, C. Fahlander, H. Grawe, A. Johnson, A. Kerek, W. Klamra, J. Kownacki, A. Likar, L.-O. Norlin, J. Nyberg, R. Schubart, D. Seweryniak, G. de Angelis, P. Bednarczyk, D. Foltescu, D. Jerrestam, S. Juutinen, E. Mäkelä, B. M. Nyakó, M. de Poli, H. A. Roth, T. Shizuma, Ö. Skeppstedt, G. Sletten, S. Törmänen:
   Structure of ^{68}As studied via $^{12}C(^{58}Ni,pn)$ reaction,
   submitted to Nucl. Phys. **A**, ATOMKI Preprint 2-1997-P.

4. **D. Sohler**, Zs. Dombrádi, S. Brant, J. Cederkäll, M. Lipoglavsek, M. Palacz, V. Paar, J. Persson, A. Atac, C. Fahlander, H. Grawe, A. Johnson, A. Kerek, W. Klamra, J. Kownacki, A. Likar, L.-O. Norlin, J. Nyberg, R. Schubart, D. Seweryniak, G. de Angelis, P. Bednarczyk, D. Foltescu, M. Fayez-Hassan, D. Jerrestam, S. Juutinen, E. Mäkelä, B. M. Nyakó, M. de Poli, H. A. Roth, T. Shizuma, Ö. Skeppstedt, G. Sletten, S. Törmänen:
   Spectroscopy of neutron deficient ^{65}Ge
   accepted for publication in Zeitschrift für Physik **A**, ATOMKI Preprint 1-1997-P.

5. T. Fényes, A. Algora, Zs. Podolyák, **D. Sohler**, J. Timár, V. Paar, S. Brant and Lj. Šimičić:
   Structure of odd-odd Ga and As nuclei, dynamical and supersymmetries,
   Physics of Elementary Particles and Atomic Nuclei 26, No 4 (1995) 831.

6. T. Fényes, A. Algora, Zs. Podolyák, **D. Sohler**, J. Timár, V. Paar, S. Brant and Lj. Šimičić:
   Structure of odd-odd Ga and As nuclei, dynamical and supersymmetries,
   in Perspectives for the Interacting Boson Model, ed. by R. F. Casten et al. (World Scientific, Singapore, 1994) p.673.

7. **D. Sohler**, A. Algora, Zs. Podolyák, J. Gulyás, Zs. Dombrádi, S. Brant, V. Paar, J. Kern and P. Cejnar:
   Nearly complete level schemes of $^{72,73,74}As$,
   in Proc. 9^{th} Int. Symp. on Capture Gamma-Ray Spectroscopy, ed. by G. Molnár and T. Belgya (Springer, Budapest, 1996) in print.

8. **D. Sohler**, Zs. Dombrádi, J. Cederkäll, M. Lipoglavsek, M. Palacz, J. Persson, A. Atac, C. Fahlander, H. Grawe, A. Johnson, A. Kerek, W. Klamra, J. Kownacki, A. Likar, L.-O. Norlin, J. Nyberg, R. Schubart, D. Seweryniak, G. de Angelis, P. Bednarczyk, D. Foltescu, D. Jerrestam, S. Juutinen, E. Mäkelä, M. de Poli, H. A. Roth, T. Shizuma, Ö. Skeppstedt, G. Sletten, S. Törmänen, B. M. Nyakó:
   Structure of ^{68}As,
   in Proc. 9^{th} Int. Symp. on Capture Gamma-Ray Spectroscopy, ed. by G. Molnár and T. Belgya (Springer, Budapest, 1996) in print.

9. **D. Sohler**, Zs. Dombrádi, J. Cederkäll, M. Lipoglavsek, M. Palacz, J. Persson, A. Atac, C. Fahlander, H. Grawe, A. Johnson, A. Kerek, W. Klamra, J. Kownacki, A. Likar, L.-O. Norlin, J. Nyberg, R. Schubart, D. Seweryniak, G. de Angelis, P. Bednarczyk, D. Foltescu, D. Jerrestam, S. Juutinen, E. Mäkelä, M. de Poli, H. A. Roth, T. Shizuma, Ö. Skeppstedt, G. Sletten, S. Törmänen, B. M. Nyakó:
   Structure of neutron deficient $^{65,67}Ga$ *and* $^{65,67}Ge$ *nuclei*,
   in Proc. 9^{th} Int. Symp. on Capture Gamma-Ray Spectroscopy, ed. by G. Molnár and T. Belgya (Springer, Budapest, 1996) in print.